University of Zurich[UZH]

Small Scale Investigation of Debris Flow Dynamics in an Arctic Environment: A Case Study on Disko Island, Greenland

GEO 511 Master's Thesis

Author
Manuel Studer
14-122-253

Supervised by
Prof. Dr. Andreas Vieli
Dr. Brian McArdell (brian.mcardell@wsl.ch)

Faculty representative
Prof. Dr. Andreas Vieli

23.04.2021
Department of Geography, University of Zurich

Small Scale Investigation of Debris Flow Dynamics in an Arctic Environment:

A Case Study on Disko Island, Greenland

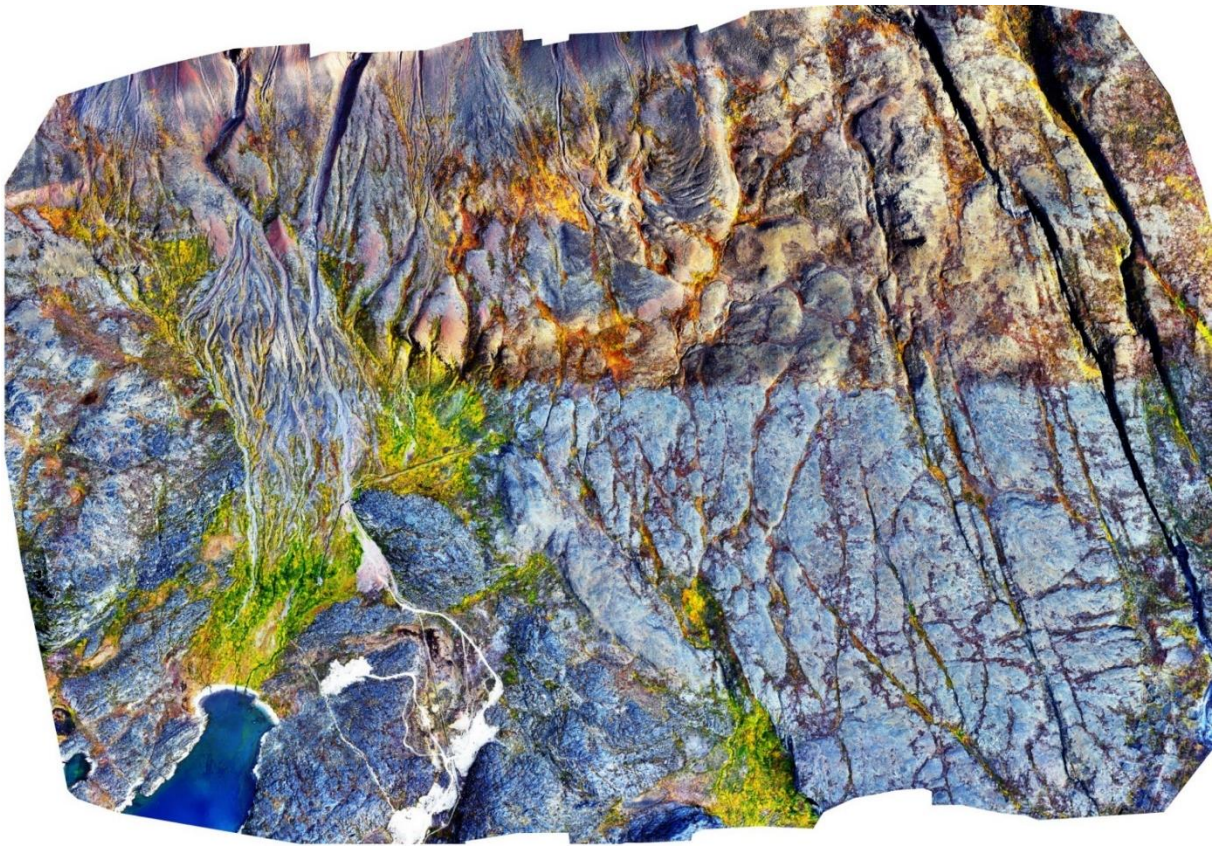

Author	Manuel Studer 14-122-253	manuel.studer@uzh.ch
Supervisor and Faculty Representative	Prof. Dr. Andreas Vieli	andreas.vieli@geo.uzh.ch
Supervisor	Dr. Brian McArdell	brian.mcardell@wsl.ch

Master's Thesis
Department of Geography 23.04.2021

University of Zurich[UZH]

Image on title page: Orthophoto north of Qeqertarsuaq, including the study area of this thesis (Vieli, 2019).

Abstract

Debris flows can occur in many parts of the world with steep reliefs, and they can endanger inhabited areas and infrastructure. Along the debris flow paths, erosion and deposition of debris material are two main processes. Additionally, zones can be present where none to very low erosion occur and material mainly is transported through. In these zones vegetation is sometimes just partly destroyed. The spatial patterns of these debris flow processes have only been sparsely investigated, especially in arctic regions and with the use of numerical models. Hence, this study aims to investigate the spatial patterns of erosion, transportation, and deposition of rather small debris flows in an arctic environment. This goal is addressed with different methods: (i) mapping of debris flow features and categorisation in *erosion*, *transport*, and *deposition zone*s with high resolution geodata; (ii) analysis of the channels topography, geometry, and maximum discharge; (iii) numerical modelling of debris flows with RAMMS using its erosion module.

Within this thesis, it was possible to successfully categorize the debris flow features on Disko Island (Greenland) into *erosion*, *transport*, and *deposition zones*. The channel geometry shows local minimums of channel depth at *transport zones* location. Also, the modelling results of the RAMMS erosion module supports the pattern of erosion and transportation, with locally lower erosion values at *transport zones*. In conclusion, the methods used generally display the pattern of the classified *erosion*, *transport,* and *deposition zones*. Furthermore, combining these methods allowed to gain detailed insights into the interaction between geometry and debris flow behaviour as well as current capabilities of debris flow models.

The presented results help to understand different debris flow zones and their characteristics. These understandings can be used, to improve future debris flow models and hazard assessment.

Table of Content

List of Abbreviations

WSL	Swiss Federal Institute for Forest, Snow and Landscape Research
SLF	WSL Institute for Snow and Avalanche Research
GIS	Geographic Information System
DEM	Digital Elevation Model
DSM	Digital Surface Model
DTM	Digital Terrain Model
RAMMS	Rapid Mass Movements Simulation
Qmax	Maximum Discharge
Vmax	Maximum Velocity
Amax	Maximum Wetted Area
Pmax	Maximum Wetted Perimeter

List of Figures

List of Tables

1 Introduction

1.1 Context and State of the Art

Fan-shaped deposits can be recognized all over the world in different climates. Accumulation of debris flow material produce such fan-shaped depositions called "alluvial fans". In many regions of the world there are large numbers of studies about debris flows and alluvial fans, however, in periglacial arctic regions such studies are rare (Bernhardt et al., 2017; De Haas et al., 2015 a). The studies of Bernhardt et al. (2017) and De Haas et al. (2015 a) are a few examples of research in the periglacial arctic region. Both are carried out on Svalbard and they look at debris flow recurrence periods and alluvial fan evolution. As well as the control and processes of the surface morphology of fans respectively, which also includes debris flows. Furthermore research has been done about landslide mapping on Greenland (e.g. Svennevig, 2019), submarine debris flows at the Greenland continental margin (e.g. Wilken & Mienert, 2006) and investigations of debris flows release processes with multi-temporal LiDAR data in Iceland (Morino et al., 2019). When it comes to research about debris flows in Greenland there are also studies linking and comparing high-arctic debris flows in Greenland to debris flows on mars (cf. Costard et al., 2001; Costard et al., 2009; De Haas et al., 2015 b; De Haas et al., 2019).

Debris flows have the potential to endanger humans, destroy structures and denude vegetation (e.g. Iverson, 1997; Jakob & Hungr, 2005; Regmi et al., 2015). Therefore, it is crucial to determine, whether a debris flow can reach infrastructure and inhabited areas. Parameters that have great influence on debris flow behaviour and runout distance are the volume of the debris flow, the material composition, and the topography, which consists mainly of surface slope and lateral channel confinement. With decreasing confinement and slope angle the runout decreases and deposition increases (Corominas, 1996; Fannin & Wise, 2001; Hungr, 2005). Thus, the definition of where deposition starts and occurs is crucial and described and discussed very diverse in research. Hungr et al. (2005), Rickenmann (2005) and VanDine (1996) show the large variations and uncertainties for this question with overviews of deposition slope angles from various authors, ranging from 0.5° to 40°. From the various suggestions of slope angles for deposition and the lack of establishment of general valid slope parameters "where substantial erosion ends, … and the slope where deposition begins" (Hungr et al., 2005). This thesis shall

try to contribute to this question in combination with other debris flow parameters. Further, a potential zone, where the debris flow material is mainly transported through and none to very low erosion occurs, will also be analysed, and can possibly be situated at the transition from erosion to deposition.

To protect and manage inhabited areas and infrastructure from debris flows, mitigation measures and hazard maps are important instruments (FOEN, 2016). Hence, modelling of debris flows can provide important estimations for such applications of hazard analysis (Bartelt et al., 2017) and can be used for post-event analysis (Frank et al., 2015). There is a wide range of different models for debris flows available as listed for example in Schraml et al. (2015). RAMMS::DEBRIS FLOW (**RA**pid **M**ass **M**ovements **S**imulation) is one possible numerical debris flow model and is used in this study. In the existing RAMMS model, an erosion module has recently been included to simulate the entrainment of material. The entrainment model is based on field data from the Illgraben catchment in Switzerland and has been tested on three other debris flow sites. The volumes and release types used in these studies, are summarized in Table 1. According to that and to the best of the current knowledge, systematic modelling applications including erosion are largely missing for cases with smaller debris flows and particularly for cases set in arctic environments.

Table 1: Volumes and release types of the studies in Switzerland, where the RAMMS entrainment module was applied.

Location	Spreitgraben		Mertschibach	Bondasca
Estimated debris flow volumes [m³]	1.	90 000	8000 – 10 000	90 000 (in two events)
	2.	130 000		
Initiation volume modelled [m³]	1.	45 000	1 – 100	10 – 1000
	2.	65 000		
Erosion volume modelled [m³]	Both events summed: 168 000		0.7 – 10 000	3 – 40 000
Release type	Input hydrograph		Block release	Block release
Source	Frank et al. (2015)		Frank et al. (2017)	Frank et al. (2017)

1.2 Aims and Research Questions

In summary, this Master Thesis aims to systematically analyze and characterize the debris flows in the case of Disko Island in western Greenland to contribute to the few existing case studies of such processes in arctic environments. The identified debris flow features shall be categorized into *erosion zones*, *transport zones,* and *deposition zones*. Further, the goal is to explore the patterns of these zones with different topographic parameter, geometric channel parameter, and the channel capacity. Finally, the applicability of the RAMMS entrainment module on rather small debris flows in arctic environment shall be tested. The aim will be addressed by the following research questions, which can be divided in three research subtopics and one main overall research question:

Disko Island Debris Flow Zones

MRQ: How can the erosion, transport, and deposition patterns of Disko Island debris flows be characterized, described, and differentiated, according to their spatial distribution, channel geometry, and modelling outputs?

Spatial Distribution Analysis

RQ 1: What debris flow features, debris flow zones, and vegetation cover classes can be found in the study area? How are they spatially distributed and how do they relate to each other?

Channel Analysis

RQ 2: What is the mutual relationship between the spatial pattern of debris flow *erosion*, *transport*, and *deposition zones* and the maximum channel capacity and topographic and geometric channel parameter along the debris flow paths?

Numerical Modelling

RQ 3: What parameter settings are needed, to model some of the debris flows and their spatial patterns of erosion and transport adequately with the RAMMS debris flow and entrainment model?

2 Theoretical Background

This chapter shall give an overview over the theoretical background which is used for this thesis. Different processes, methods, and models will be explained theoretically.

2.1 Debris Flows

Debris flows occur in all regions of the world, with at least some amount of rainfall and steep reliefs. A debris flow can be defined as a "very rapid to extremely rapid flow of saturated non-plastic debris in a steep channel" (Hungr, 2005). They consist of a combination of water, fine and coarse material. Their relative ratio influences the characteristics and rheology of the flow (Hungr, 2005; Weber, 2004). Often also some organic matter like trees and sometimes even anthropogenic material (e.g. hey bale, chopped wood) are transported. Debris flows can occur in one or several surges, with possible "watery interflow" in between. The reason for this surging behaviour is very diverse and the temporal distance between surges can range from seconds to hours. Surges can also have very different volumes and vary from one to many tens (Hungr, 2005).

Typically, debris flow paths can be divided into three zones. While Hungr (2005) defines the zones as initiation, transport, and deposition, VanDine (1996) describes the three zones as initiation, transportation and erosion, and deposition, as shown in Figure 1. These different zones are explained in the following subchapters.

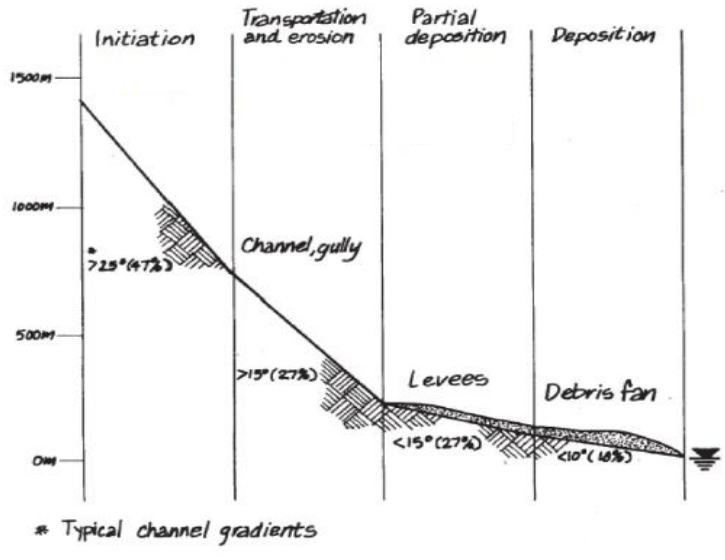

Figure 1: Zone differentiation of channelized debris flows after VanDine (1996).

2.1.1 Initiation

The initiation of debris flows can be explained with the disposition model developed by Kienholz (1995). It contains a ground disposition, a variable disposition and a triggering event and these elements describe the condition of a system.

As ground dispositions enough debris must be available and its geotechnical characteristics are thereby important. Additionally the topography has great influence on the ground disposition (Zimmermann et al., 1997). Typically, the slopes of the initiation zones range between 20° – 45° (Hungr, 2005; Sidle & Ochiai, 2006) or 26° - 45° (Bierman & Montgomery, 2014).

The variable disposition describes a mid-term variability of a system and is influenced by the accumulated sediment parameter and the pre-event condition of the hydrogeology (Zimmermann et al., 1997).

Finally, a triggering event is needed to initiate a debris flow. Short thunderstorms, long-lasting rainfall periods, intense snow and ice melt or the breakout of glacier and moraine dammed lakes, can be such triggering events. But in some catchments, if the variable disposition is not developed enough (supply-limited cases), e.g. not enough material available, not every possible triggering event leads to a debris flow initiation. On the other hand, the occurrence of debris flows is regulated by the frequency of the triggering events if there is an unlimited amount of debris available (Zimmermann et al., 1997). With the differences in the disposition among diverse catchments it becomes clear that debris flow composition is greatly influenced by the source material and the hydrogeological conditions (Haas et al., 2015 c).

Often, the debris flow initiation is related to slope failure of a side slope or the headwall. It can also be triggered in the bed of a channel if it gets instable, or by a breach of previously deposited material in the channel (Hungr, 2005).

2.1.2 Transport and Erosion

In the second and middle zone, the debris flow often is transported in established stream channels or gullies and often entrains material. Thus, a relatively small initiation volume can grow to a big debris flow and the total volume therefore is dependent on the erosion volume. The loose material is eroded from the banks and the often saturated bed of a debris flow channel. This process can consequently also change the saturation level of the debris flow and thereby change its behaviour. This middle part of the debris flow path can also contain cascades and non-erodible bedrock (Hungr, 2005).

In confined reaches erosion can take place on slopes down to 10°, with a transitional zone which is at least 10° wide. Whereby the occurrence of erosion and deposition seems to be quite randomly for small event magnitudes (Hungr et al., 2005). Fannin & Wise (2001) combined slope angles and confinement, and suggested that unconfined reaches, with slope angles between 19° and 24°, and confined reaches, with slope angles between 10° - 22° can have both, erosion and deposition in this zone.

Debris flow speeds in this zone are of the order of 10 m/s but can be faster for extreme events (Turnbull et al., 2015). De Haas et al. (2015 c) show with their laboratory experiments, that the flow velocity increases with increasing event volume.

2.1.3 Deposition

Debris flows often build up alluvial or debris fans in the deposition zones. The depositions can be heavily reworked by water directly afterwards (Hungr, 2005). The morphology and geometry of the debris flow fan and its different depositions are dependent on past debris flows and other active or inactive geomorphological processes (e.g. rock glaciers) (VanDine, 1996).

Deposition of a debris flow can occur at different locations on the debris fan and thus three forms can be distinguished according to VanDine (1996), shown on Figure 2:

- **Debris lobes:** Are usually an areal cover of parts of the debris fan and are often characterised by several arms with a snout at each ending.
- **Debris plugs:** Fill the channel partially or completely and often end in a snout or as lobe. Thus, subsequent debris flows are often forced to form a new channel and thereby change the flow direction abruptly.
- **Debris levees:** Are steep-sided and elongated ridges, which lie above and outside the flow channel. They can be tens of meters long, up to several meter high, and are often higher in the outside bend of a curve than on the inside.

At channel widenings, sometimes boulder pockets and short, eventually temporary, levees can be observed on and above the debris fan (Hungr, 2005).

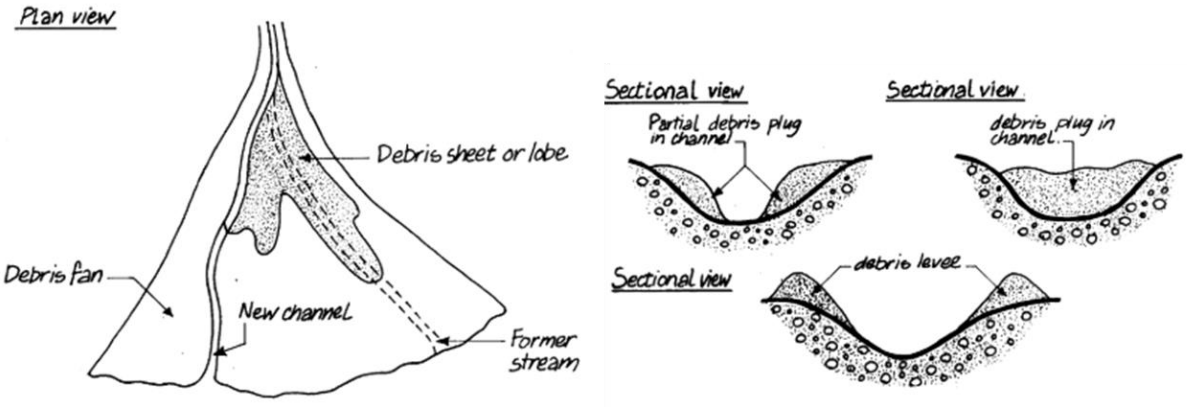

Figure 2: Debris flow fan evolution and different possible deposition forms (VanDine, 1996).

Deposition of debris flows is caused due to the separation of the debris mass and the water part (VanDine, 1996). This occurs often through a combination of slope reduction and loss of confinement (Corominas, 1996; Fannin & Wise, 2001; Hungr, 2005), but can also be caused from any natural and artificial impediments (VanDine, 1996). In general, smaller debris flows can deposit on steeper slopes and have short runout distances, while larger debris flows have smaller travel angles and therefore longer runouts (Chevalier et al., 2013; Corominas, 1996; Hungr et al., 2005). Some debris flows may even reach the stream channels in the main valleys (Hungr, 2005). De Haas et al. (2015 c) point in their laboratory experiments out that also the composition of debris flows influences the runout, which is also noted by Hungr et al. (2005). With increased coarse-material concentration the runout of debris flows get longer, while at the same time they are very sensitive to their water content (De Haas et al., 2015 c).

A wide range of slope angles can be found where debris flows start to deposit. When comparing several propositions from different authors listed in Hungr et al. (2005), Rickenmann (2005) and VanDine (1996) most of these works suggests mean values between 8° and 14°.

2.1.4 Influence by Permafrost

The presence of permafrost can influence the occurrence of debris flows. The permafrost underneath the active layer limits the infiltration of water (French, 1988). Thus, the saturated active layer can be positively influencing the variable disposition (cf. chapter 2.1.1) and therefore support debris flow triggering. But the permafrost table can also act as a slip plane for slope failures which can develop into debris flows (Larsson, 1982). However, the erosion depth and therefore the available debris volume can be restricted by limited active layer depths. Thus, larger

debris flows are primarily triggered in the second half of the summer period, when the active layer is thicker (De Haas et al., 2015 a).

2.1.5 Velocity and Discharge Calculation

Several formulas from various authors can be found to calculate velocities and discharges of debris flows. A collection of different formulas is described in Rickenmann (1999).

One method for calculating the flow velocities and flow discharges at any location in a debris flow channel, is the Manning-Stickler-equation after Henderson (1966). In this method, the flow velocity depends on the slope, the cross-sectional hydraulic radius and the Strickler coefficient:

$$v = k_s * R^{2/3} * S^{1/2} \qquad \textit{(Eq. 1)}$$

Whereby the hydraulic radius is calculated as follows:

$$R = \frac{A}{P} \qquad \textit{(Eq. 2)}$$

v	flow velocity of debris flow [m/s]	R	hydraulic radius [m]
k_s	Strickler coefficient [$m^{1/3}/s$]	A	wetted area [m^2]
S	slope gradient [-]	P	wetted perimeter [m]

With knowledge of the velocity, the discharge at that specific location can be derived:

$$Q = v * A \qquad \textit{(Eq. 3)}$$

Q	debris flow discharge [m^3/s]

2.2 Geomorphological Mapping

Geomorphological mapping is a fundamental, important, and widely used method to generate data for different purpose. It can be used for land management, hazard assessment, and risk mitigation. “The spatial distribution and mutual relationship” (Dramis et al., 2011) of different data can thereby be investigated and highlighted.

But manual mapping relays upon the experience and the expertise of the mapper and is therefore a subjective process (Cooke & Doornkamp, 1990). In geomorphological maps, landforms are identified, interpreted, and represented according to their formational process and morphology (Hubbard & Glasser, 2005). It is also possible to focus only on certain landforms or features (Smith, 2011). In geomorphological maps other data like vegetation cover, anthropogenic features, as well as activity states of geomorphological processes can be represented (Dramis et al., 2011).

Mapping is mostly conducted in GIS and validated with field mapping (Knight et al., 2011; Smith, 2011). The combination of both remote and field mapping gives the best results and therefore should be done in combination, if possible (Knight et al., 2011).

2.3 RAMMS::DEBRIS FLOW

With the RAMMS software package, the gravitational driven natural hazards such as snow avalanches, debris flows, and rockfalls can be modelled (Christen et al., 2012). RAMMS was developed by SLF (Institute for Snow and Avalanche Research) to originally provide a practical tool for avalanche simulation (Christen et al., 2010).

RAMMS::DEBRIS FLOW uses a single phase model, and therefore the material is not divided in its solid and fluid phase (Bartelt et al., 2017). RAMMS solves depth-averaged equations and the two-parameter Voellmy-fluid model to calculate the motion of the movement on a three-dimensional terrain (Christen et al., 2012). The Voellmy friction law is used, which divides the frictional resistance in Coulomb friction μ and a velocity-squared drag or viscous-turbulent friction ξ (Bartelt et al., 2017). The frictional resistance S [Pa] then is calculated as:

$$S = \mu * \rho * h * g * \cos(\Phi) + \frac{\rho g u^2}{\xi} \qquad \textit{(Eq. 4)}$$

ρ	density [kg/m^3]	u	flow velocity [m/s]
g	gravitational acceleration [m/s^2]	μ	Coulomb friction [-]
Φ	slope angle [°]	ξ	turbulent friction [m/s^2]
h	flow heigth [m]		

The friction coefficient ξ dominates when the flow is running quickly while μ dominates when the flow is close to stopping. Therefore, they are mainly responsible for the behaviour of the debris flow. This means also, that the calibration of them, must be carried out very carefully and it is one of the most important steps to get reliable results. Hence, the friction parameters should be varied to match the observed flow behaviour.

2.3.1 Input

As input for a RAMMS simulation different data, values, and settings are required or possible. Some important settings used in this thesis are shortly explained below (all from Bartelt et al., 2017):

Geospatial input: A DEM, orthophoto, and topographic map can be inserted in the simulation. But thereof only the DEM is crucial, and its quality and resolution has a high influence on the simulation results (cf. Wehrli, 2019).

Simulation resolution: Can be defined independently of the input DEM resolution. A higher simulation resolution extends the calculation time greatly.

Calculation domain: Is used to narrow down the area where calculations are executed. The smaller the calculation domain, the shorter the calculation time.

Obstacle file: Polygons can be drawn to indicate, where no flow should pass and therefore will be deflected.

Release parameter: There are two possibilities to initiate debris flows in a RAMMS simulation:

1. A **release area** can be used to define the location of debris flow release. For this a polygon with a specific release depth is defined.
2. If the initiation area is not known, or to simulate canalized debris flows an **input hydrograph** can be used. Thus, an estimated flow volume is necessary as input. From the relation between total volume and maximum discharge described by Rickenmann (1999), the discharge is automatically calculated but can be adapted manually. With it, a three-point input hydrograph is calculated at a defined initiation point in the channel.

Stopping criteria: In RAMMS the stopping criteria is based on the flow momentum. If the momentum drops below a certain threshold the simulation will stop. As thresholds, values between 1 – 10 % are reasonable. This criterion is implemented

to reduce possible numerical diffusion, very slow creeping, and velocity oscillations.

2.3.2 Output

As output of RAMMS, several parameters like flow height, velocity, erosion, volume, and shear stress are provided as spatial data and different plots can be generated. This data can be displayed in RAMMS itself in 2D or 3D view or can be exported as shapefile or ASCII-File. Some of these output values are shown in chapter 6.3.

2.3.3 Erosion module

In newer versions of RAMMS an erosion module has been implemented. With this module, more realistic debris flow simulations can be carried out. It calculates the erosion depth, and thereby the volume gain of the debris flow in the channel can be simulated (Bartelt et al., 2017). The erosion module does neither consider lateral bank collapse nor change the topography during the simulation, but this can be done afterwards separately in RAMMS (Frank et al., 2015). Because the final volume is not known before the simulation initiation, several model runs might be done to get the desired total volume (Bartelt et al., 2017).

The erosion module was constructed on generalisations of repeated terrestrial laser scans from the Illgraben in Switzerland and has been tested successfully on three other debris flow sites with mostly large flow volumes (Frank et al., 2015; Frank et al., 2017). The field data show, that increased flow strength increases the depth of erosion, and small debris flows do not always erode sediment (Schürch et al., 2011). Therefore, a critical shear stress threshold was incorporated, where the computed basal shear stress is a function to the maximum potential depth of erosion e_m for every raster cell (Bartelt et al., 2017):

$$e_m = 0 \text{ for } \tau < \tau_c \qquad \textit{(Eq. 5)}$$

$$e_m = \frac{dz}{d\tau}(\tau - \tau_c) \text{ for } \tau \geq \tau_c \qquad \textit{(Eq. 6)}$$

e_m	maximum potential erosion depth [m]	e_t	actual erosion depth [m]
τ	basal shear stress [Pa]	τ_c	critical shear stress [Pa]

If the actual erosion depth is smaller than the maximum potential erosion depth a defined erosion rate is applied:

$$\frac{dz}{dt} = -0.025 \text{ for } e_t \leq e_m \qquad \textit{(Eq. 7)}$$

$\frac{dz}{dt}$ specific erosion rate [m/s] e_t actual erosion depth [m]

The used value of 0.025 m/s is based on field measurements in the Illgraben from Berger et al. (2011).

With the implementation of the above equations (Eq. 5 – Eq. 7) in RAMMS the parameter erosion rate, potential erosion depth and critical shear stress must be defined. Additionally, a maximum erosion depth can be applied if the depth of the available material is known (Bartelt et al., 2017).

To use the erosion module, one to several polygons with possibly different parameter settings can be drawn. These define where erosion can take place on the 3D terrain (Bartelt et al., 2017).

3 Study Area

The study area for this thesis lies north of the village Qeqertarsuaq (69°14’50”N 53°32’00”W) on Disko Island, at the west coast of Greenland (Figure 3). Disko Island has a size of 8 578 km^2 and the highest elevation reaches 1 919 m (Frederiksen et al., 2014). West of Qeqertarsuaq lies the Arctic Station, which is run by the University of Copenhagen. Here, various research about the arctic is done (University of Copenhagen, 2021).

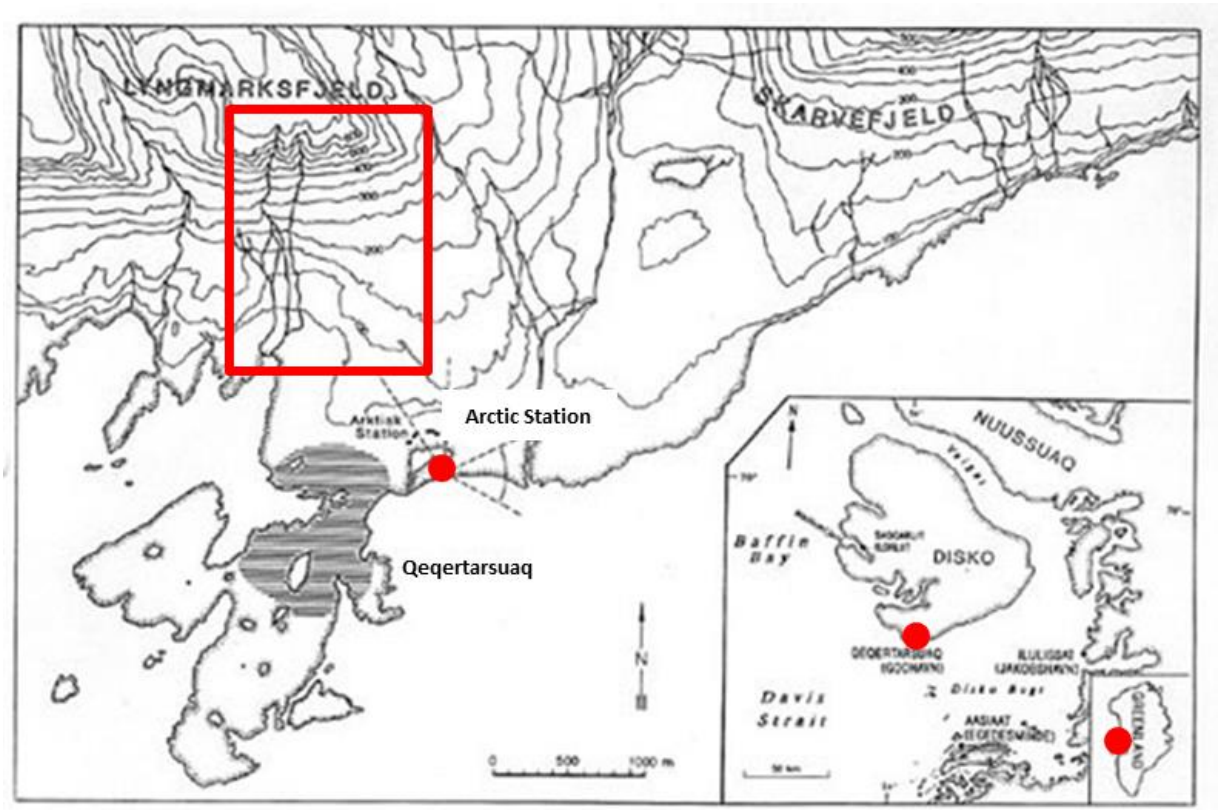

Figure 3: The study area lies in western Greenland in the south of Disko Island. The study area (red rectangle) is north of Qeqertarsuaq and the Arctic Station and includes the southern part of the mountain called Lingmarksfjeld (adapted from University of Copenhagen, 2021).

The investigated elements of the study area are several debris flow channels and a complex debris flow fan underneath the same, steep south-facing headwall of Lingmarksfjeld (Figure 3 and Figure 4). A rock glacier is part of the study area, on which some debris flows are deposited.

Figure 4: View from Qequertarsuaq towards the study area after the debris flow events in 2014 (cf. Chapter 3.3). The investigated debris flow paths are indicated with white lines. (Photo: Andreas Vieli, August 2014)

3.1 Geology

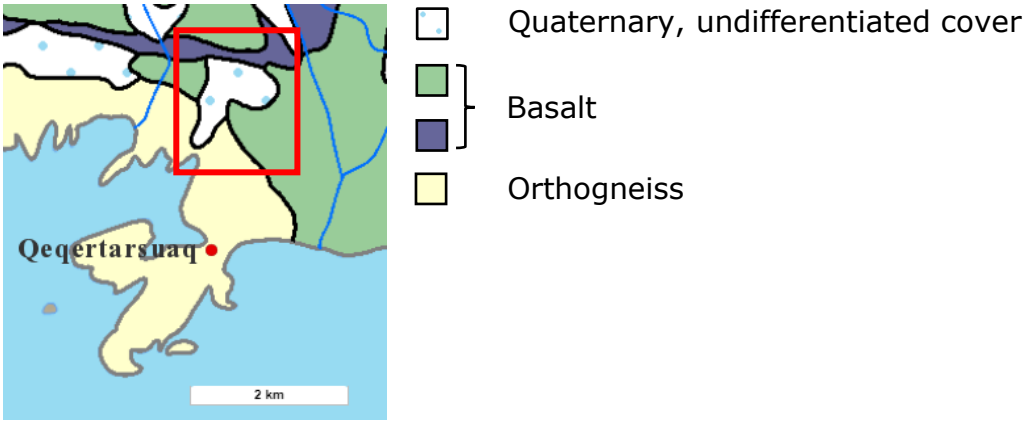

Figure 5: Geological map 1:500'000 of the study area (GEUS, 2021).

In and around the study area there are two major geological units present (Figure 5). The yellow unit is the bedrock and consist of orthogneisses from the Archaean. North and east of it, the green and violet colours indicate plateau basalts with various stratum thicknesses (cf. Figure 4). In these units, the initiation zones of the debris flows are found and therefore their rocks dominate the debris flow material. Parts of the geological units in the study area, are overlain with undifferentiated quaternary deposits, which consist of scree slopes, periglacial landforms, debris flows and fluvial deposits (GEUS, 2021). Examples of the debris flow material in the study area is shown in Figure 6.

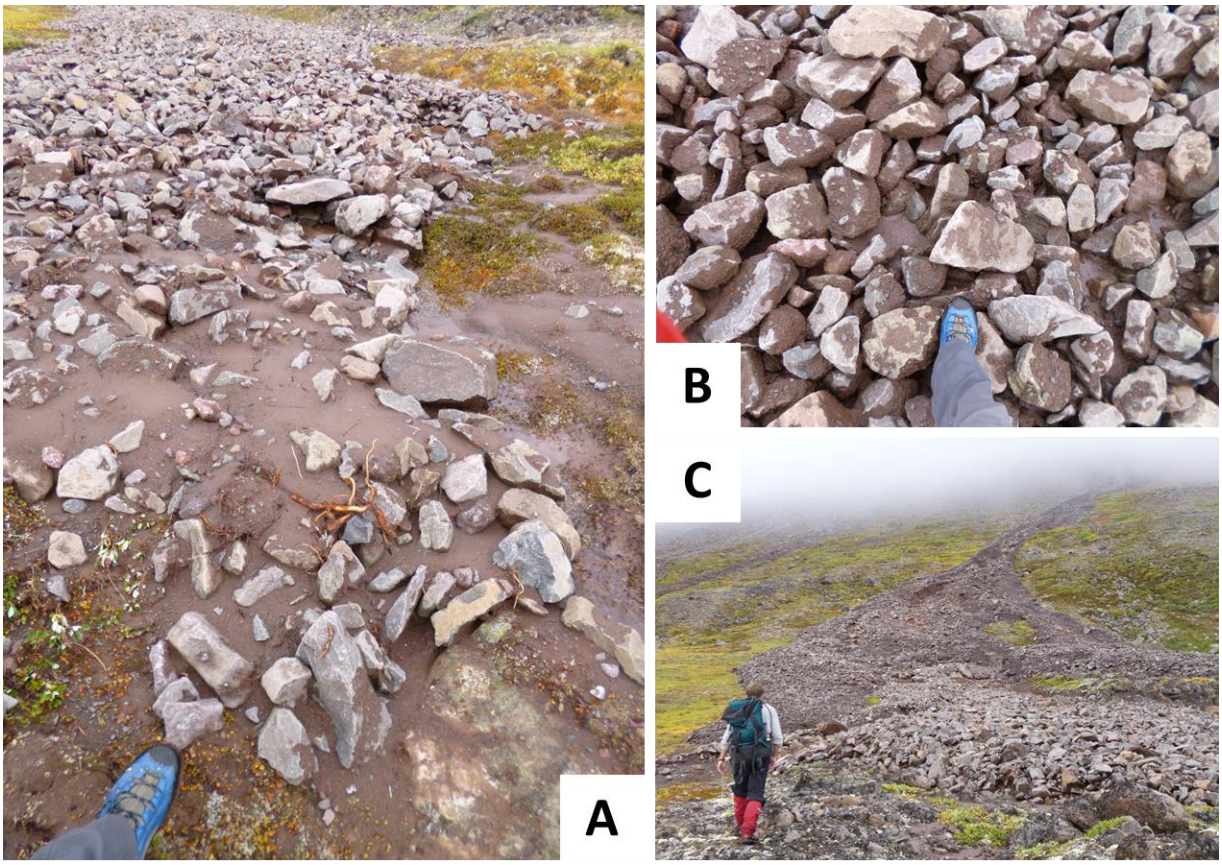

Figure 6: Debris flow depositions of DF1 after the event in August 2014. (A) End of the terminal deposition lobe at 493 m travel distance. (B) Overview over the size of coarse debris material. (C) Upper deposition lobes of DF1 and in uphill the debris flow channel. (Photos: Andreas Vieli, August 2014)

3.2 Vegetation

While the areas around the depositions of the investigated debris flows are often well vegetated, the complex debris flow fan and the scree slopes above are less overgrown (cf. Figure 4 and Figure 21). Different examples of the vegetation in the study area are shown in Figure 7.

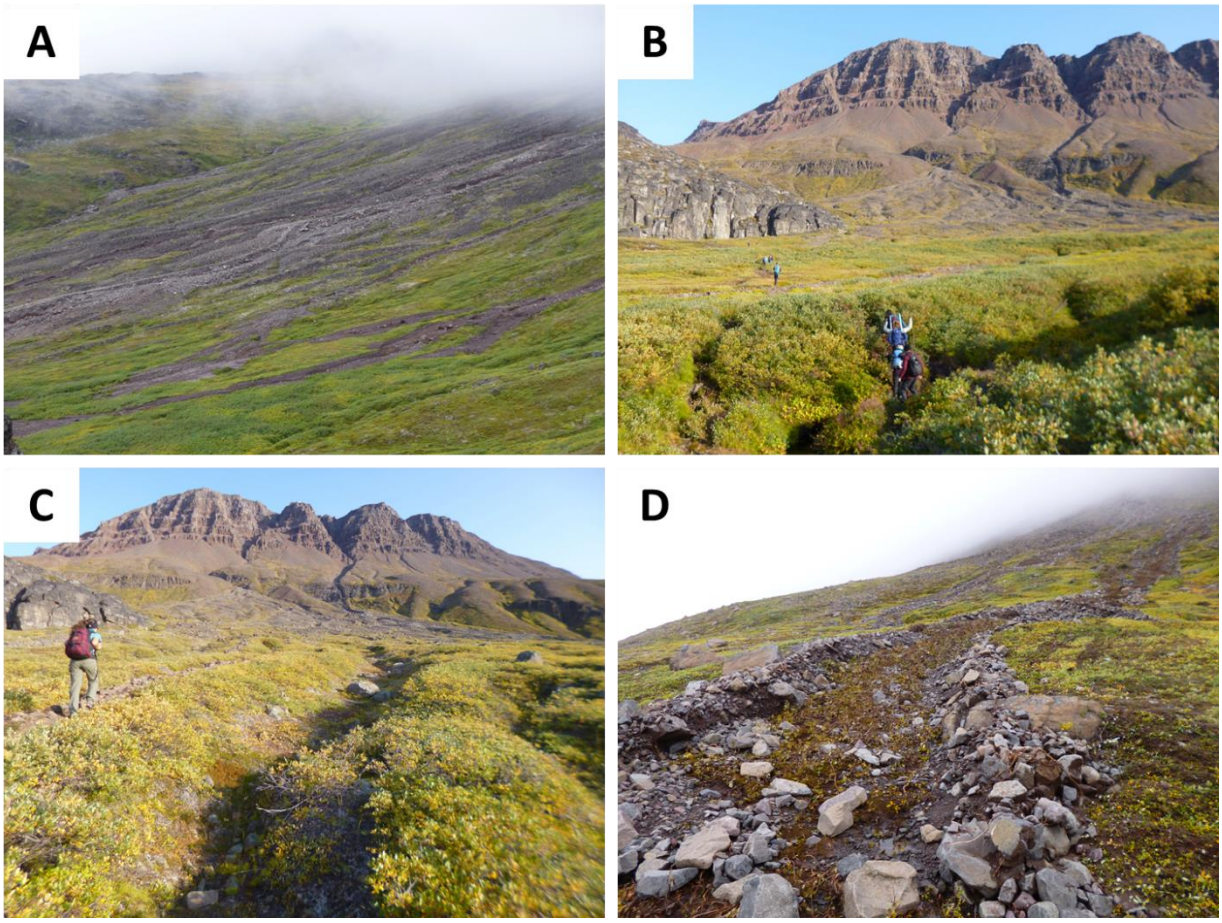

Figure 7: Different examples of the vegetation in the study area. (A) Photo taken east of the big debris flow fan. Different channels and depositions of DF4, DF6, and DF8_2 are clearly visible. (B) Higher vegetation in the lower part of the big debris flow fan. (C) Well vegetated old debris flow channel and levees. (D) Remaining vegetation inside the channel of DF2_1 after the debris flow passed through. (Photos A & D: Andreas Vieli, August 2014; Photos B & C: Andreas Vieli, July 2018)

According to the arctic vegetation map generated by Walker et al. (2005) the southern part of Disko Island lies in the low arctic zone. The vegetation on Disko Island is dominated by dwarf shrubs, mosses, and herbs. Due to the short growing season and low temperatures the vegetation is mostly short with 5 – 30 cm height (Frederiksen et al., 2014). Walker et al. (2005) define the dwarf shrub layer quite generally with heights of 10 – 40 cm. But as visible in Figure 7B, the vegetation can grow as high as one meter at some places (Frederiksen et al., 2014).

3.3 Climate

Due to the geographic location of Disko Island north of the Arctic Circle, the sun does not appear from November 29th to January 11th. On the other hand, in summer there is a lot of incoming radiation melting the snow and heating the soil (Hansen, 2011).

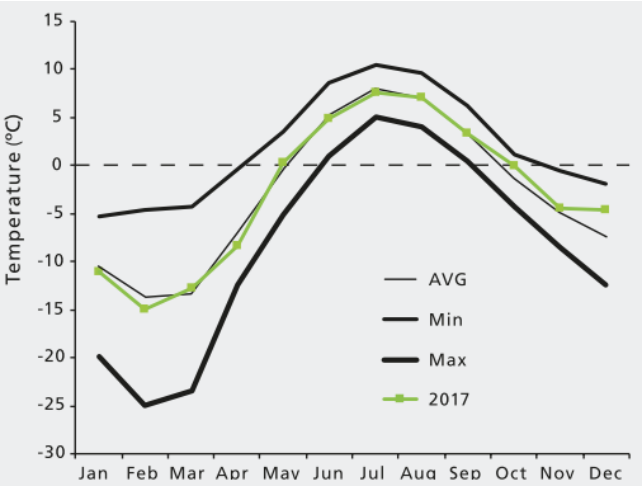

Figure 8: Average, min, and max monthly air temperature values over the period of 1992 – 2017 at the Arctic Station (Kroon & Sigsgaard, 2017).

The air temperature is the main controlling meteorological parameter of the climate in Qequertarsuaq (Hansen, 2011). Figure 8 shows the annual changes in temperature by the average, minimum and maximum values for the period 1992 – 2017. There is a high amplitude of winter and summer temperatures visible and almost reaching between 5° and 10° in summer.

Coherent with the low temperatures on Disko Island is the presence of permafrost. According to the permafrost map of Brown et al. (1997), Disko Island is located just in the continuous or at the border of continuous and discontinuous permafrost.

Big parts of Greenland's precipitation is correlated with low-pressure fronts which depend on the polar front. Especially during summer and autumn, these low-pressure zones are very dominant at Disko Island. Hence, around 58% of the yearly 585 mm precipitation falls during the summer months at the Arctic Station (Frederiksen et al., 2014). The distribution of precipitation over the summer months for the years 1990 – 2017 is shown in Figure 9.

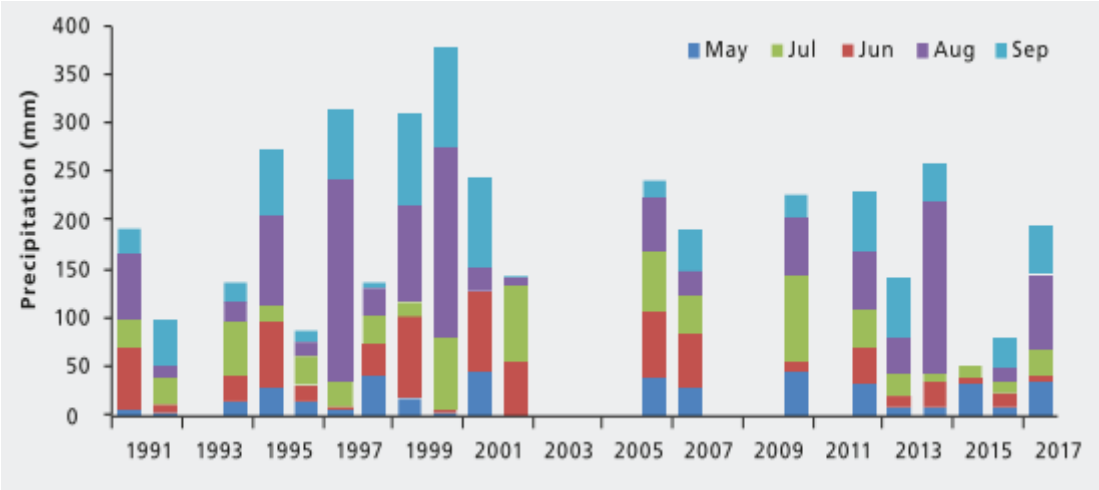

Figure 9: Distribution of stacked monthly liquid precipitation from May to September for the period of 1990 to 2017 measured at the Arctic Station (Kroon & Sigsgaard, 2017).

3.4 Precipitation Event August 2014

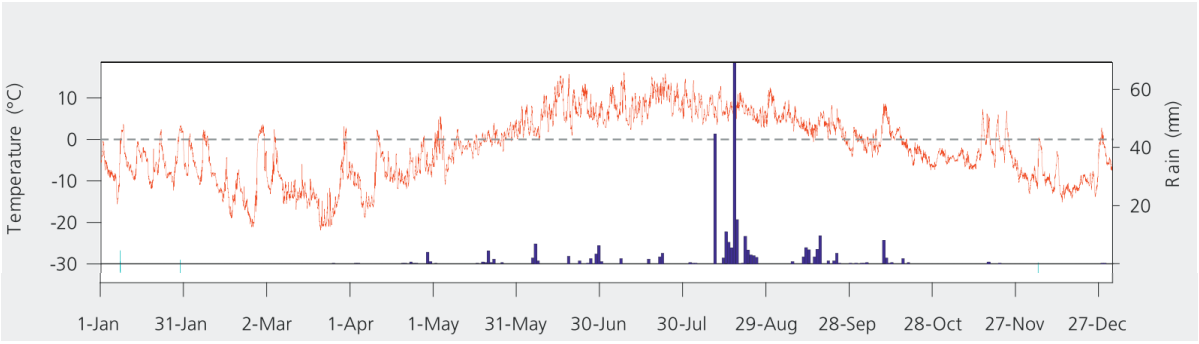

Figure 10: Temperature and rain of the year 2014, measured with an automatic weather station at the Arctic Station. The two peaks in August display two heavy rain events. (Kroon & Sigsgaard, 2014).

280 mm rain of was measured overall, in the whole year of 2014, whereof 177 mm occurred in August 2014 (Figure 9). On August 9th and August 16th 50 mm respectively 70 mm rain were registered at the Arctic Station (Kroon & Sigsgaard, 2014). As visible in Figure 10, in between these days additional minor rain was measured and showed that the ground saturation stayed high. The heavy rainfalls generated high discharges with large flooding and a lot of erosion. In and outside the study area several debris flows were triggered. The water supply of Qeqertarsuaq was disabled for days, as one debris flow damaged the water pipeline (cf. Figure 21) in the study area (Kroon & Sigsgaard, 2014).

4 Data

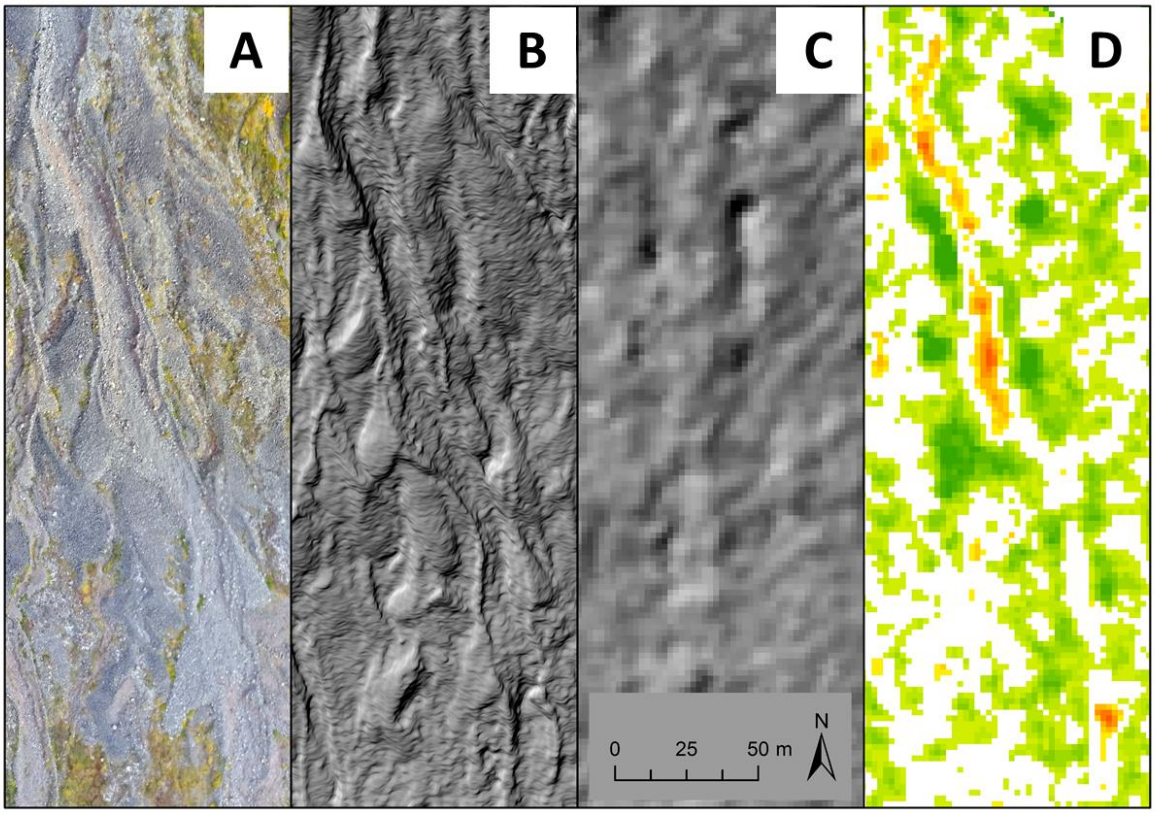

Figure 11: Study area snippet of the flow path of DF6 from 500 m to 775m travel distance. (A) High resolution orthophoto and (B) shaded DEM produced from UAV imagery (Vieli, 2019). (C) ArcticDEM of 2012, generated from satellite imagery (Porter et al., 2018). (D) Elevation-difference of two ArcticDEM datasets from 2012 and 2016. Indications of channel erosion (yellow – red colours) in the northern part of the snippet.

To answer the research questions in this thesis, various datasets from different sources are used. An overview of the used geodata, can be found in Table 2. All the datasets in the table are raster data with different spatial resolutions. A small comparison of four of the major datasets used, is shown in Figure 11.

Table 2: Overview over the used geodata.

Dataset	Spatial resolution	Year	Source
Drone orthophoto	0.07 m	2019	Vieli (2019)
Drone DEM	0.07 m	2019	Vieli (2019)
ArcticDEM	2 m	2012, 2014, 2016	Porter et al. (2018)
Google Earth screenshots	0.22 – 0.44 m	2013, 2015	Google Earth (2013) Google Earth (2015)

4.1 Drone Data

The used drone data, was collected during a drone flight in August 2019 by Vieli (2019). The drone flight was conducted with an eBee drone, produced by senseFly. Out of the 462 drone pictures, a DEM and an orthophoto was created by using the software Pix4D, using their structure from motion method. No ground control points (GCP) were used for georeferencing. Hence, the absolute accuracy of the drone data is dependent on the internal GPS of the drone and the uncertainties are shown in Table 3. The drone data does not cover the whole study area (cf. Figure 21) and at the marginal parts are less accurate due to lower quantity of pictures (cf. Figure 12) and therefore got cut off.

Table 3: Absolute (upper) and relative (lower) camera position and orientation uncertainties (Vieli, 2019).

	X[m]	Y[m]	Z[m]	Omega [degree]	Phi [degree]	Kappa [degree]
Mean	0.040	0.037	0.044	0.008	0.008	0.003
Sigma	0.007	0.007	0.009	0.001	0.002	0.001

	X[m]	Y[m]	Z[m]	Omega [degree]	Phi [degree]	Kappa [degree]
Mean	0.037	0.033	0.044	0.008	0.011	0.003
Sigma	0.008	0.007	0.018	0.002	0.003	0.001

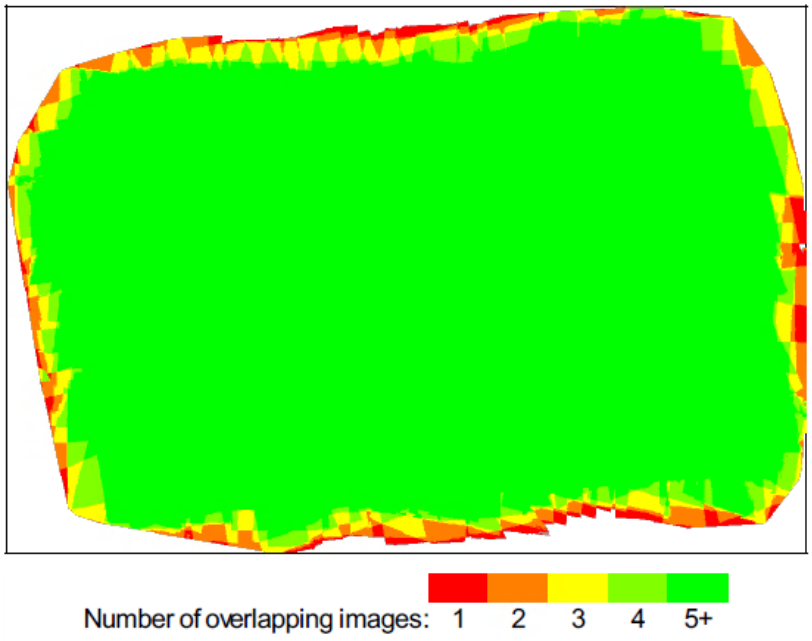

Figure 12: Number of the overlapping pictures of each pixel within the drone data coverage (Vieli, 2019).

4.1.1 Drone DEM

The drone DEM needed to be corrected in height due to missing GCP. It was corrected according to the level of the ArcticDEMs, which themselves were corrected

before (cf. chapter 4.2). Thus 6.2 m have been subtracted from every pixel value of the drone DEM. This 6.2 m difference is a mean value conducted from comparing the heights along several profile lines.

Based on the drone DEM, a hillshade dataset and a contour line layer with equi-distance of 1 m were created in ArcMap. These two products are the main data bases for the analysis in this thesis.

At this point it is important to mention that the drone DEM is a digital surface model (DSM). Hence, all obstacles and vegetation represent the surface of the drone DEM. Therefore, the drone DEM needs to be used carefully in the vegetated areas. An example of the influence of vegetation in the drone DEM is visible in

Figure 13. Here, just from the shaded drone DEM one could imagine a very deep debris flow channel, whereas in reality it just shows the high vegetation.

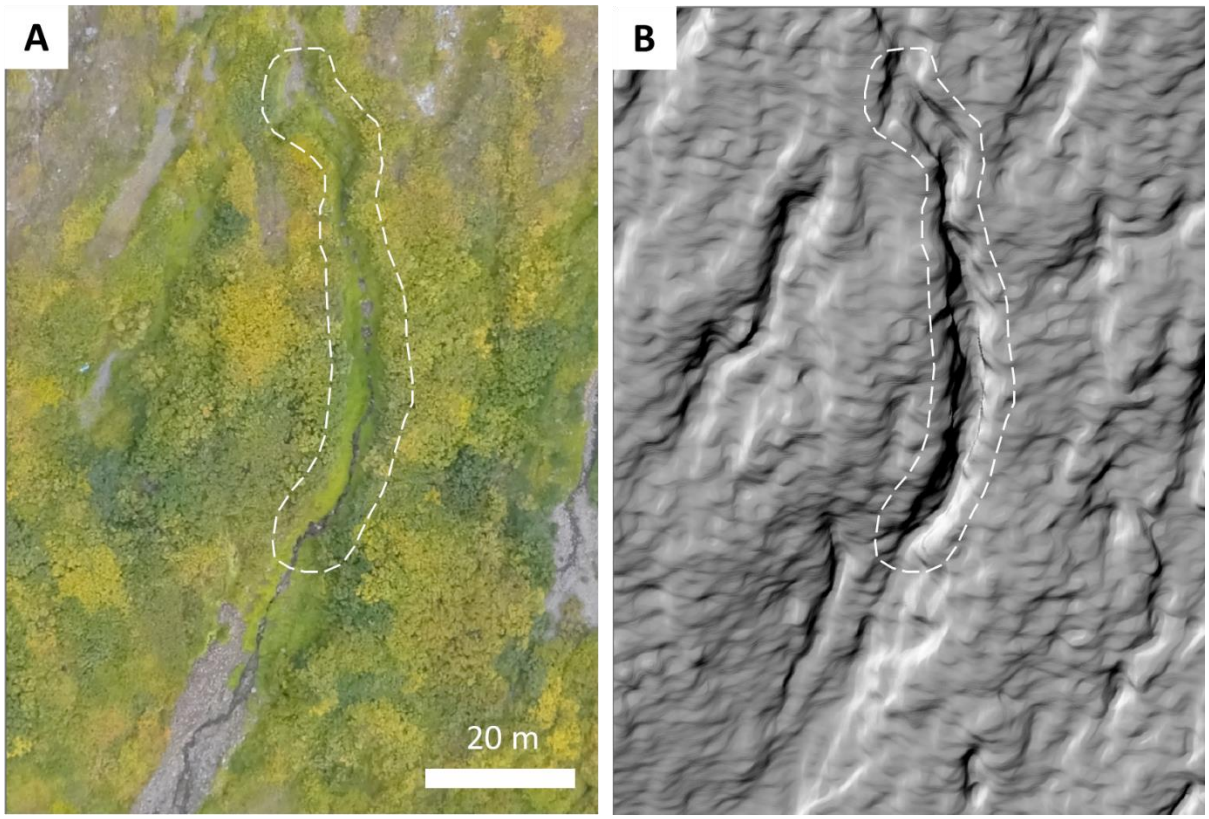

Figure 13: Drone orthophoto (A) and shaded drone DEM (B) show the same part of the DF8_2 flow path. The white line indicates the allegedly channel which is caused by the high vegetation (adapted from Vieli, 2019).

4.1.2 Orthophoto

Two drone flights had to be done to generate the presented drone data. Therefore, the lighting can be different in the orthophoto. Due to wind during the drone flights some of the pictures are not perfectly in focus. Hence, in the orthophoto some areas are sharper than others.

4.2 ArcticDEM

The ArcticDEM is a high resolution, high quality, and opensource DSM covering all land area located north of 60°N. It is constructed from optical satellite images (0.5 m resolution) from different sources (Porter et al., 2018). The arcticDEM can be accessed over the ArcticDEM explorer or directly on the server on https://www.pgc.umn.edu/data/arcticdem/.

The ArcticDEM covers the whole research area and is therefore a very important data source for this thesis. There are ArcticDEMs available from different time periods. Although the resolution is always the same, the quality of the ArcticDEM differ highly. In the best available ArcticDEM from the study area there are still some artefacts of different sizes visible, which change the topography locally.

ArcticDEMs from different periods sometimes correlate very badly. Hence, they were corrected in their absolute height. This was conducted at the weather station near the Arctic Station, where the flat ground is considered to be at constant height. According to the metadata table of the weather station data the weather station is located at 69°15'12.558" N, 53°30'50.863" W and is situated 25 m a.s.l (GEM, 2018). The difference of an ArcticDEM to the weather station was subtracted from the respective ArcticDEM. After the correction the ArcticDEMs mutually still differ up to 2 m at the same location due to their noisy surface.

4.2.1 Elevation-difference

Due to the availability of an ArcticDEM before and after the debris flow events, an ArcticDEM-difference-raster was produced. The subtraction was done with the raster calculator in ArcMap. A snippet of it can be viewed in Figure 11D. Values between -0.5 m and 0.5 m are not shown in this dataset due to the fact that the source datasets are quite noisy.

4.3 Google Earth

Because the satellite imagery from Google Earth only could be used as screenshots they needed to be georeferenced manually. But this was very difficult and couldn’t been done satisfactorily. This is probably caused by the combination of a blurred image and the steep headwall of Lingmarksfjeld.

4.4 Field Photos

From field trips in 2014, 2018, and 2019 several field photos have been provided by Andreas Vieli. These are overview photos like Figure 4 or more detailed pictures of debris flow related features like Figure 23.

5 Methods

In this section the different methods, which were used for this thesis are described. All the debris flow channels from the event in 2014 have been mapped, but only four debris flows were analysed in greater detail. These four were chosen because of their different run out lengths and event volumes (cf. Table 5), but another criterion was a continuous flow path without being cut off by another channel.

5.1 High Resolution Mapping

Although as pointed out in chapter 2.2, geomorphological mapping shouldn't be done only digitally. However, it was not possible to conduct field work for this thesis. The reason were the regulations regarding COVID-19 in summer 2020 due to which the planned field trip to Disko Island was cancelled.

A first broad overview of the study area was carried out with two Google Earth pictures from 2013 and 2015 which are described in section 4.3. From comparing these two pictures the active debris flows in 2014 were defined. This then was verified and clarified with the available field photographs, which are described in section 4.4.

5.1.1 Legend Structure

The mapping of the debris flow features and vegetation classes is carried out in the GIS software ArcMap developed by Esri. A geodatabase containing a line and a polygon feature class is constructed. Feature class representations are created inside the feature classes. The representations stores the symbology rules inside the geodatabase together with the elements geometry. Symbology rules are easily editable, complex representations can be created and the appearance of features is improved (ESRI, 2019).

The legend was structured according to the geometry of the mapped elements. Thus, areal features like *vegetation*, *initiation*, and *deposition zones* are mapped as polygons. Linear elements like the flow paths and the levees are traced as line features. All the mapped features can be seen in Figure 24.

For erosive processes (channel erosion, side erosion) red colours are used. For *transport zones* yellow is applied and for deposition features (lobes, levees) blue elements are used.
For intact vegetation dark green, for partly damaged vegetation light green, and for fully damaged vegetation brown colours are used.

Normally, the elements are drawn with solid colours. If uncertainties about the correct feature/ zone arose or the exact location was not detectible dashed lines or hatched polygon fills are used.

5.1.2 Debris Flow Features

The mapping of debris flow features started with the respective channels, where the lowest point inside the channel defined the location of the flow path line. In the upper debris flow channel parts, where no drone data was available (cf. Figure 21) the mapping of the channel was done with the help of the other available data, presented in chapter 4. Hence, the detail and quality of geomorphological mapping is reduced. The *initiation zones* shown in Figure 21, are mapped only for the sake of completeness. Thus, they are not further investigated, described, or discussed. They shall only give an idea for possible initiation locations detected in the field photos and on satellite imagery, which were transferred onto the maps.

The levees were mapped at their highest points along the channel, which are visible on the drone data (section 4.1). The depositions are mapped as areas and were distinguished according to the orthophoto and the drone DEM. Examples of the different debris flow features on the orthophoto and the drone DEM are visible in Figure 11 A, B.

5.1.3 Debris Flow Zones

The debris flow paths were classified into four different zones. The defined zones differ partly from the relatively general introduced zones in the literature (cf. chapter 2.1). The different zones, their definitions and classification criteria can be seen in Table 4. Due to low data quality the initiation area could not be defined (cf. chapter 5.1.2). The other major zones were determined as follows: The *erosion zones* are defined for areas where material was entrained along the flow path. The *transport zones* on the other hand are defined where none to very little erosion is visible and the debris is just transported through. Where the channel bed material is bedrock and no erosion is possible, *bedrock zones* are defined. *Deposition zones* were defined in areas at the end of the flow path, where all the debris deposits.

The channel shape was one of the major parameters to determine the zone of a certain channel part. Other important parameters were the surface colour, the presence of vegetation inside the channel, the presence of side erosion, and the channel material as listed in Table 4. The data basis for the mapping of the zones were the drone data described in chapter 4.1. The decision whether *erosion zones*

and *transport zones* relied on the drone data and is exemplary shown in Figure 14. Additionally, cross profiles gave valuable insights into the channel geometry, if the zone definition was difficult.

When no drone data was available the zone classification relied on the remaining data and therefore are not of the same quality.

Table 4: Overview over the most important decision parameters for the mapping of different debris flow zones.

		Erosion zone	**Transport zone**	**Bedrock zone**	**Deposition zone**
Decision parameter	**Channel and contour line shape**	Concave	+/- Straight	-	Convex
	Surface colour	Reddish or greyish	Greyish	Greyish	Greyish
	Presence of vegetation inside the channel	No	Possible	No	Very rarely
	Side erosion	Possible	No	No	No
	Channel material	Debris	Debris	Bedrock	Debris
	Height difference of centre line and outside the channel perimeter	Inside lower	Inside and outside +/- the same	Inside lower	Inside higher

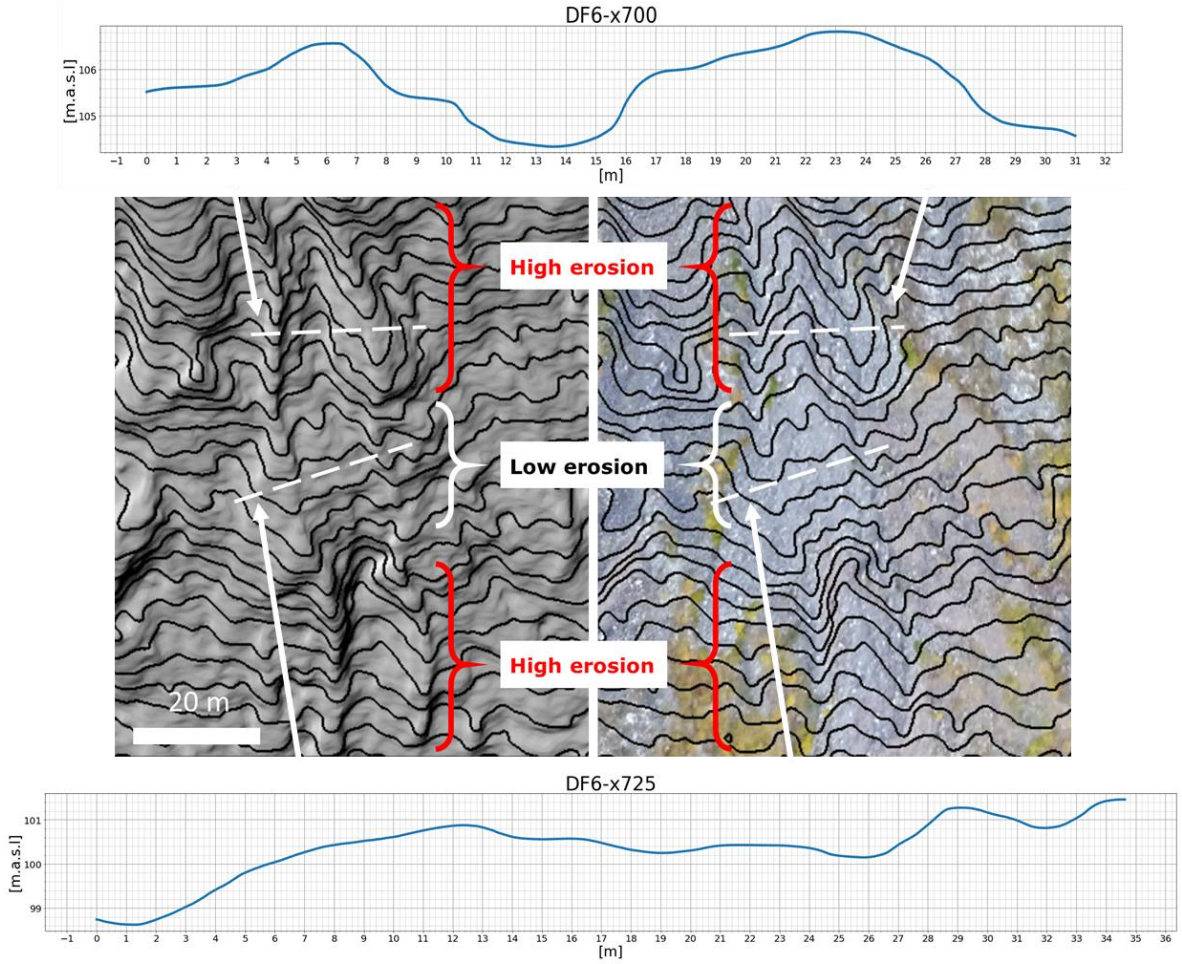

Figure 14: Change of high and low erosion at 725 m travel distance of DF6. The hillshade and the contour lines with an equidistance of 1 m show clear differences between high and low erosion parts (adapted from Vieli, 2019). Two cross profiles, indicated with the white lines, visualize the channel geometry.

5.1.4 Vegetation

The mapping of different vegetation classes was conducted on the basis of the drone orthophoto. Thus, it represents the distribution of the vegetation in summer 2019. Additionally, the field photos gave another good indication on the vegetation distribution, especially because some of them were taken directly after the debris flow events in August 2014. The areas, for which there were no photos available for comparison, are mapped reluctantly as e.g. *possibly damaged vegetation*.

The vegetation was classified into the three classes *intact vegetation*, *partly damaged vegetation,* and *fully damaged vegetation*. The polygons were assigned manually and this was only done for the debris flows, which were investigated in detail. The classifications of *partly damaged* and *fully damaged* areas are only related to erosive processes and therefore are not mapped in deposition areas. *Fully damaged vegetation* areas are mapped upon the assumption, that if a dense vegetation

cover is visible besides the channel, some vegetated areas must have existed in the channel.

5.2 Channel Parameter Measurements and Calculations

The measurements and illustrations of different parameter were only done for four debris flow paths. Producing more long profiles would have exceeded the scale of this thesis. To have a more consistent database for all the four flow paths, different parameter were only determined in areas where the high resolution drone data was available (cf. Figure 21). Hence it is possible that parts of the constructed long profiles don't show any data.

The different data used to create the long profiles are shown in Figure 15. More explicit descriptions about the production of the data are explained subsequent. The long profiles were generated with Python using Jupyter Notebook. The scripts written for this purpose are attached in Appendix 12.2.

It is important to mention, that the height and depth measurements described in chapter 5.2.1 and the calculations in chapter 5.2.2 are conducted vertically and not perpendicular to the surface. These measurements are not corrected afterwards according to the local slope. Thus, the heights, depths, and wetted areas are overestimated in very steep parts (e.g. 50°) up to 35 % and in flatter parts (e.g. 10°) as low as 2 %. With this correction only the single values would have changed, but the overall behaviour would remain as presented in the results.

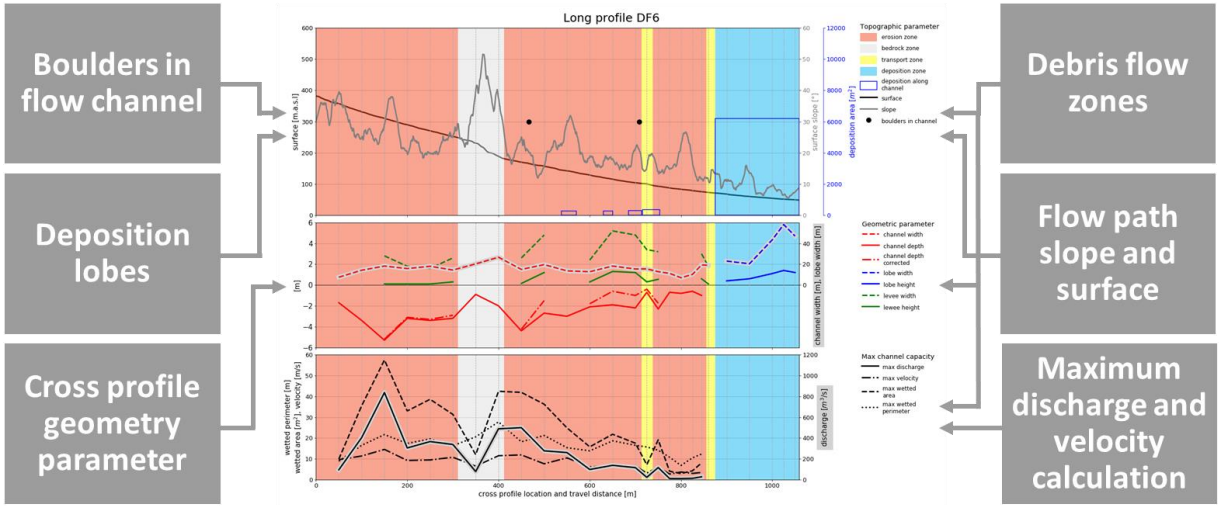

Figure 15: All input data used in the different sections, to create the long profiles as they are presented in the results.

5.2.1 Geometric Channel Cross Profile Parameter

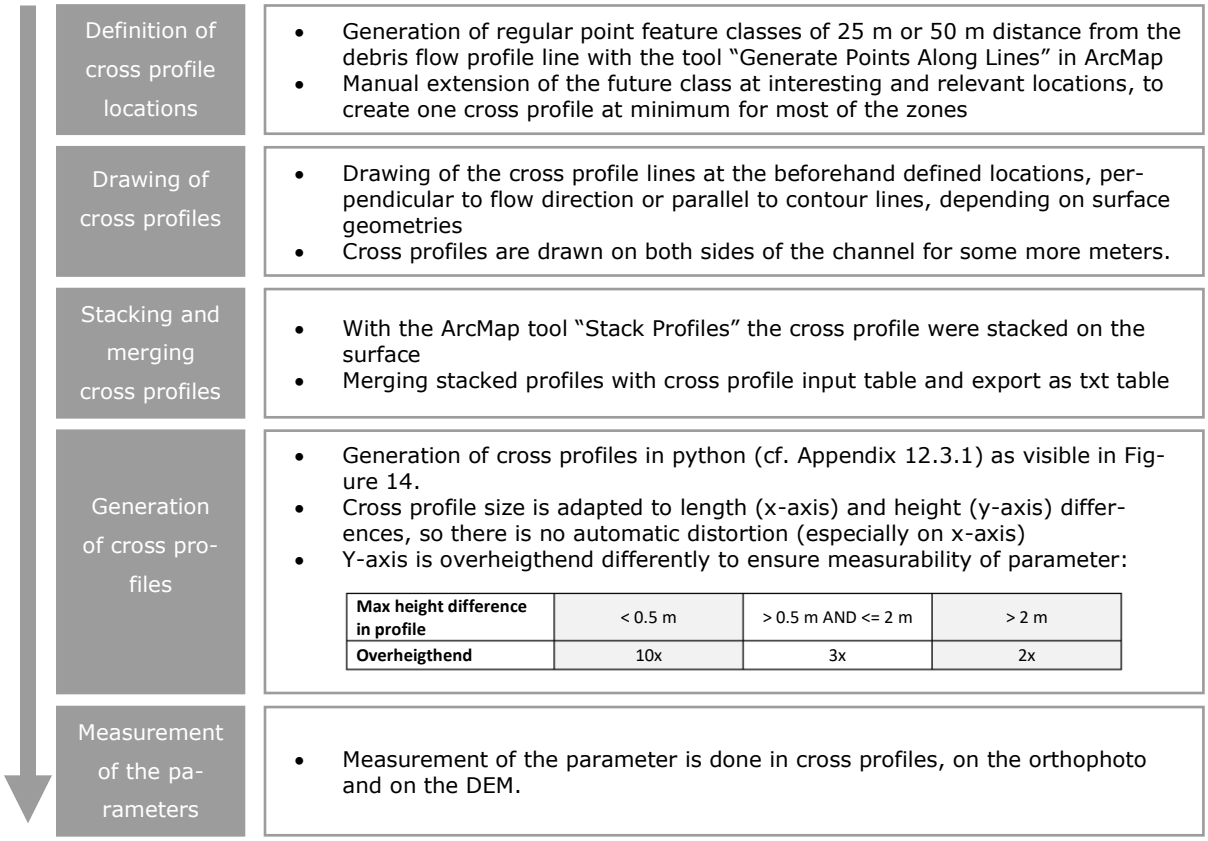

Figure 16: Most important steps in the workflow used to generate the channel geometry parameter dataset.

Several different geometric channel parameters were chosen to describe the channel appropriately. How these different parameter were measured is described below. Examples of different parameter measurements are shown in Figure 17.

Channel width: Was often derived from orthophoto and compared with the cross profile. Were measured between the levee peaks (Figure 17). If no levees were present, the channel edge defined the border.

Channel depth: If possible, a bankfull scenario was assumed, like shown on Figure 17. The channel depth was always measured from the lowest point in the channel and therefore can also be expressed as maximum channel depth. If e.g. a channel depth of 1 m was measured, this describes the difference between bankfull scenario line and the lowest point in the channel. Hence it is displayed in the long profile as -1 m. If the measurement was done in a deep eroded channel, it was measured up to the line of the channel width measurement.

Levee width: Was derived from the orthophoto, the drone DEM, and the cross profiles as show in Figure 17. If only one levee was present, this defined the levee

width. If levees on both sides were present, the mean of the eastern and western levee width was calculated and is used to define the levee width.

Levee height: Was measured out of the cross profiles like shown in Figure 17. If only one levee was present, the maximum distance defined the levee height. If levees on both sides were present, the mean of the eastern and western heights was calculated and is used to define the levee height.

Deposition width: The deposition width mostly was determined from the drone orthophoto along the cross profile.

Deposition height: Measured in the cross profiles with the knowledge of the starting and ending point in the profile. The maximum difference between interpolated starting and ending points and the event surface of the deposition geometry defined the deposition height.

True channel depth: The channel depth includes the levee height. Thus, the true channel depth was calculated as the difference of channel depth and levee height (Figure 17).

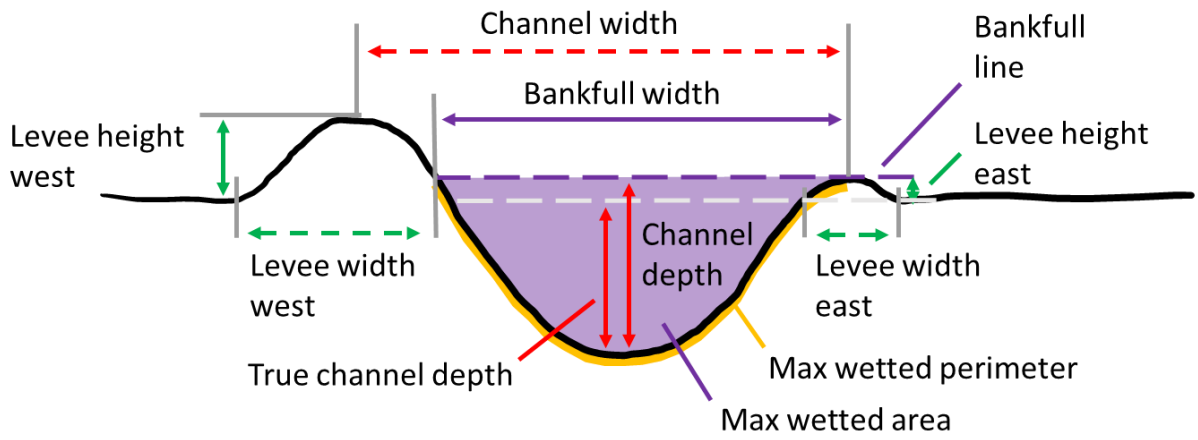

Figure 17: Schematic figure of how the different channel parameter were measured for the geometry and discharge analysis in the real cross profiles as shown in Figure 14. The figure is drawn up slope a virtual debris flow channel.

5.2.2 Maximum Discharge and Velocity Calculation

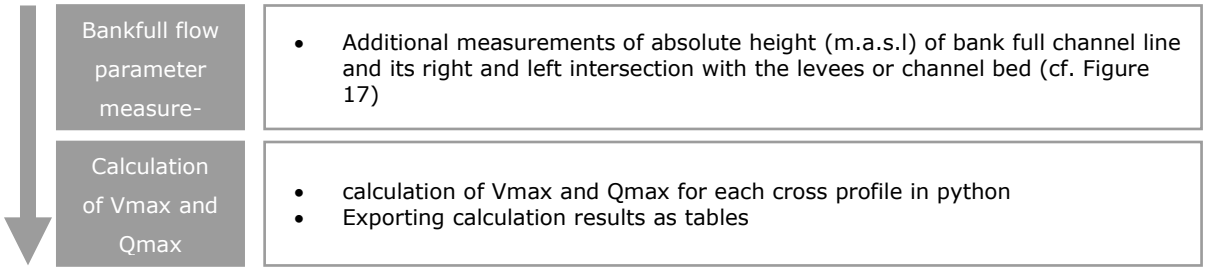

Figure 18: Most important steps in the Vmax and Qmax calculation workflow.

The formula described in section 2.1.5 is used to calculate the bank full discharge at the cross profile locations along the flow paths. This means the maximum possible velocity and discharge describe values before the moment at which the debris would flow out and is therefore comparable to the understanding of a bankfull river in the hydrological research field. To get the *maximum velocity* (Vmax) and *maximum discharge* (Qmax) the variables *maximum wetted perimeter* (Pmax) and the *maximum wetted area* (Amax) are needed. Therefore, additionally the absolute height (m.a.s.l) of the bankfull line (Figure 17) and its right and left intersection with the levees or channel bed need to be determined in the cross profiles. Especially the widths are not necessarily the same values as measured before and described in section 5.2.1. The calculations were done in python and the used script is attached in Appendix 12.3.2. The wetted area is calculated as the difference of the integrated bankfull line and the integrated channel surface. With Pythagoras the distances of neighbouring channel surface points are calculated and summed up. This therefore provides the wetted perimeter.

5.2.3 Flow Path Slope and Surface

From the drone DEM a slope layer was calculated in ArcMap. The slope long profile data then was generated along the debris flow path with the ArcMap tool "Stack Profiles". Due to the high resolution of the drone DEM the slope long profile is very noisy and hardly readable (cf. Figure 19). Hence before the data was plotted, a filter was applied in the python script to smoothen out the slope long profile as it is presented in Figure 19. The so called "savgol_filter" from the "scipy" library in python applies a Savitzky-Golay filter. For this, the length of the filter window size and the order of the polynomial used to fit the sample, needs to be defined (The SciPy community, 2021). These values were defined visually, until the balance between too much and too few accuracy was found. For all four long profiles the

same savgol_filter, with a window size of 299 and the polynomial order of 1, were used.

The surface data table is derived from the ArcMap tool "Stack Profiles" and included without any changes in the long profile.

The slope and surface information in high resolution are only available in the drone DEM parameter (df. Figure 21) and thus, only displayed for the specific long profile sections.

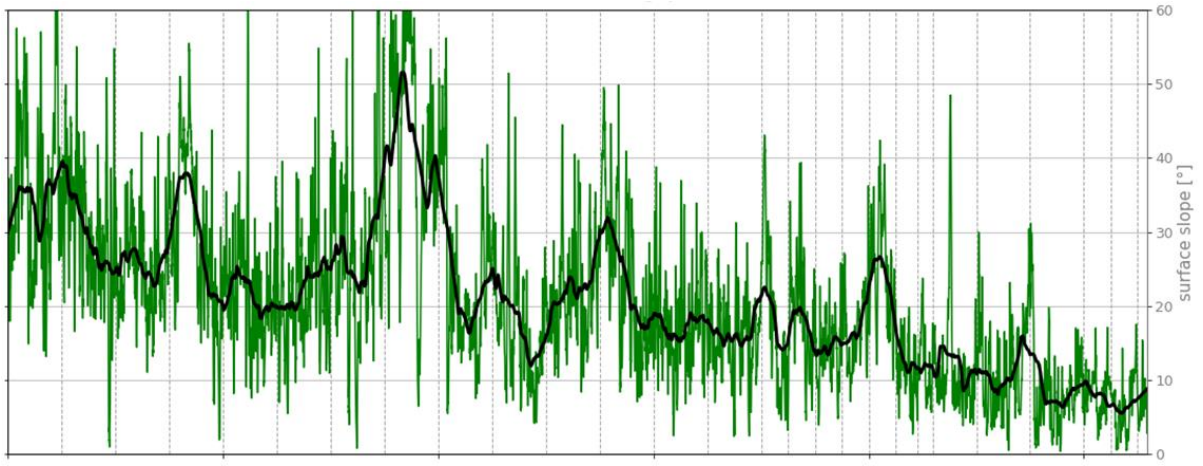

Figure 19: Original slope (green) in the debris flow channel and smoothed slope values (black) of DF6.

5.2.4 Debris Flow Zones

The mapped debris flow zones (cf. section 5.1.3) were exported from ArcMap and manually sorted. The start and endpoint for each zone was calculated according to the shape length of the zones.

5.2.5 Deposition Lobes

The start- and endpoint of all the deposition lobes in, besides, and at the end of the flow path were measured. The deposition lobes besides the channel were measured perpendicular to the flow path line. The deposition lobe area was copied from the debris flow feature mapping.

5.2.6 Boulders in Flow Channels

Along the flow path all big boulders or boulder accumulations inside the debris flow channel are mapped and included in the long profile

5.3 Numerical Modelling

For the debris flow modelling, the latest release of RAMMS::DEBRIS FLOW version 1.7.32 was used. Only the four debris flows under closer investigation (cf. chapter

6.2) were simulated with RAMMS. Otherwise this would exceed the scope of this thesis. Due to lack of information about the initiation areas and the fact of no high resolution data from the upper parts, the debris flows in the model were initiated after some meters on the flow path (cf. Table 6 for exact locations). Hence, the input hydrograph method of RAMMS was used (cf. chapter 2.3.1). The input hydrograph was placed in the channel at the highest possible location with available accurate surface data.

The simulations were conducted on the drone DEM and not on the arcticDEM due to two reasons. First, the drone DEM has a more than 20 times higher resolution and second, there are no local artefacts visible on the drone DEM. According to Wehrli (2019) the DEM resolution should be at least ten times smaller than the debris flow channel to ensure its correct representation in the simulation. This can only be achieved with the drone DEM. The simulation resolutions used are listed in Table 6.

5.3.1 General Calibration

The calibration of debris flow models is often done with the run out length (McArdell B., personal communication, 2020) and therefore this value is used to calibrate the debris flows in this thesis. For calibration of the friction values of each debris flow, different parameter needed to be estimated and defined. The necessary pre-simulation parameter and their derivation is listed below and the used values are shown in Table 6.

Volume: The lobe volume is summed up from all deposition polygon volumes per debris flow (cf. Table 5). The deposition polygon volumes were calculated by the mapped deposition areas and mean deposition heights, estimated from drone DEM. This are not the same deposition heights as described before in chapter 5.2.1.
The levee volumes for each debris flow were estimated from the mean levee height in the long profile (e.g. Figure 25) multiplied with the summed length of the mapped levees.
As total volume for modelling input, only the lobe volumes are used.

Table 5: Estimated lobe and levee volumes and measured run out lengths for each debris flow.

	DF1	DF2_3	DF6	DF8_2
Estimated lobe volume [m^3]	1100	30	5600	450
Estimated levee volume [m^3]	150	80	460	200
Measured runout length [m]	493	365	1059	1171

Maximum discharge: The automatic calculation in RAMMS was generally used (cf. chapter 2.3.1) and crosschecked at the location of the input hydrograph with the Qmax values presented in chapter 6.2.

Velocity: Assumptions are based on the Vmax calculations at the input hydrograph location (cf. chapter 6.2). In a second step they were adjusted regarding to the automatic levelling out in the first hundred meters of the flow path.

Stopping criteria: Are generally left at the default value of 5 % flow momentum. It only was adjusted, if otherwise the simulation of a debris flow was not adequately possible.

Flow path and deposition areas: The already mapped flow path and deposition areas are used here.

Runout length: Is measured along the flow path including the terminus deposition area. The model outputs were compared to the run out length and the friction parameter were calibrated to fit the run out length. Thereby, flow and deposition heights lower than 0.1 m are generally not taken into account. Because such thin flows are questionable and single boulders can easily be deposited (McArdell B., personal communication, 2021). Also, below 0.1 m flow height RAMMS does not calculate velocities and shear stress.

The calibration of the parameter is done for every debris flow separately and for this followed the descriptions in the RAMMS::DEBRIS FLOW User Manual (cf. Bartelt et al., 2017). First, 16 simulation runs with ξ = 100, 200, 300, 400 [m/s^2] and μ = 0.1, 0.2, 0.3, 0.4 [-] were done with each value of ξ combined with each value of μ. The best fitting values were selected. Figure 20 gives an idea of the influence of ξ and μ on the deposition behaviour of the results from these first model runs.

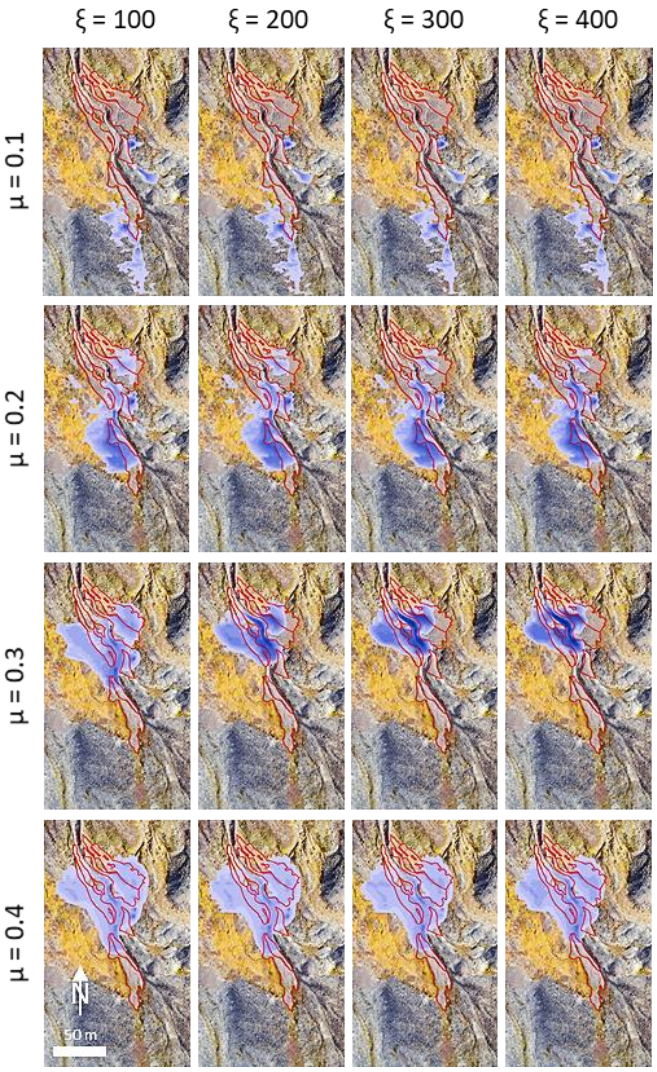

Figure 20: Influences of different μ [-] and ξ [m/s²] values on the debris depositions and the total run out length in RAMMS, at the example of DF6. These values were used for the first calibration attempts without using the RAMMS erosion module.

In a second step, around the current best fit parameter set, again different μ and ξ were combined. But this time smaller step changes of μ are used, until the most plausible parameter combination, who matches the run out length best, was found. Due to vague velocity estimation the calibration of ξ was much more difficult and therefore was only conducted in steps of 100. The most plausible parameter combination then was the base for the inclusion of the erosion module.

5.3.2 Erosion Module Calibration

When using the erosion module of RAMMS the debris flow entrains sediment along the flow path, and thus the initial volume must be reduced. How much this volume needed to be reduced is different for every debris flow and it was determined through several model runs. The initial and final flow volumes of the most plausible simulations used in this thesis are listed in Table 6 in the Result chapter. Besides

conducting calibration only on the run out distance again, it was also the goal to properly simulate the estimated total volumes (cf. Table 6).

For all the channel sections where erosion or transportation was mapped, erosion polygons were defined, from the input hydrograph, down to the beginning of the final *deposition zone*. The *bedrock zones* were not included due to the unerodable channel beds.
For the defined erosion polygons generally the default erosion parameter were used (cf. Table 6, DF6). Thus, the amount of possible most plausible simulations could be reduced. These default erosion parameter values are defined from field measurements (cf. chapter 2.3.3) and are therefore assumed to be reliable. The erosion parameter were only changed if it could be assumed from the available data (e.g. low bedrock cover for parts of DF8_2) or if the simulation of a debris flow was not satisfactory (cf. chapter 6.3.4).

As a first guess the ξ and μ values were inherited from the calibration already conducted (cf. chapter 5.3.1). Hence, mostly just a little fine tuning on the values had to be done to find a most plausible simulation.

6 Results

In this section, the results of this study are presented. First the mapping of different debris flow features and zones is shown for the entire research area and briefly described. Afterwards, the mapping results of the four debris flows, which were investigated and modelled in greater detail, are shown and described more in-depth. Then the channel analysis results are presented and finally the simulations outputs are described.

6.1 Spatial Distribution Analysis

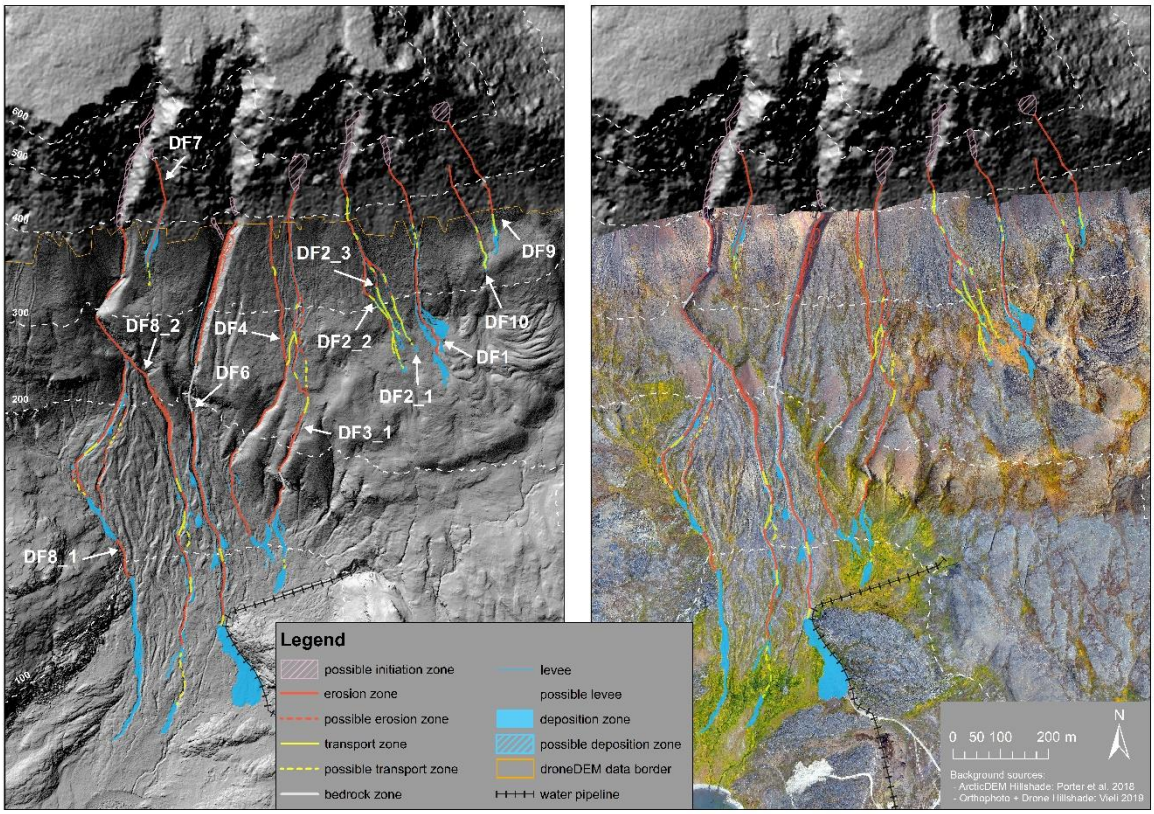

Figure 21: Overview over the mapped debris flows in the study area. On the left the drone DEM and on the right the drone orthophoto is displayed in the background. The upper parts of the study area are displayed by the ArcticDEM from 2012. The original sized map is provided in Appendix 12.1.

Figure 21 shows the mapping results of all the debris flows triggered by the event in 2014 within the study area. They originate from nine individual *possible initiation zones* in the steep headwall of Lingmarksfjeld. Three debris flows (DF2_x, DF3_x, DF4_x) flow for the first hundreds of meters in the same channel and then divide in to separate debris flow paths. DF3_2 even joins into the channel where DF4 is mapped after approximately one third of the flow path. It can further be seen that there is great variation of flow length. The debris flows to the west, flowing out in

to the complicated debris flow fan, have clearly bigger run out lengths, than the debris flows in the east of the study area.
DF9 and DF10 are partly flowing over rock glacier and even deposit debris on them. DF1 deposits material on top and just besides the rock glacier.

All investigated debris flows are mapped as *erosion zones* for at least 50 meters after initiation. Afterwards the developments of the debris flows are very different. Some change from *erosion zone* to *transport zone* and end with the *deposition zone* (e.g. DF9 and DF10). Others don't have a *transport zone* before the deposition and therefore directly change from erosion to deposition. Five debris flows flow over steep bedrock parts and therefore are mapped as *bedrock zones*. Patterns of erosion-transportation-erosion can be detected in eight debris flow paths. In four of them this sequence can even be detected several times. These patterns are also very nicely visible in the long profiles shown in section 6.2. At DF3_1 and DF8_1 *assumed debris flow paths* are mapped. These indicate possible flow paths, for which it can't be determined conclusively on the basis of the available data, if they originated in 2014 or not.

6.1.1 DF1

DF1 shows an *erosion zone* for the first 125 meter, visible in Figure 22 and Figure 25, which is followed by a 50 m long *possible transport zone*. After 125 m travel distance, the first levees can be recognized on both sides, which limit the channel almost continuously until the first deposition areas and even beyond. Shortly after 175 m channel length, again a long *erosion zone* is mapped until the last depositions. Between 250 m and 300 m the debris flow fully damaged the vegetation. Afterwards a second area of *fully damaged vegetation* is assumed. Some very small patches of *partly damaged vegetation* can be found along and within the channel. The debris flow depositions divide into several parts and lobes, and the lower deposited material eroded a channel through the upper depositions. Overall, the depositions cover an area of approximately 2900 m^2.

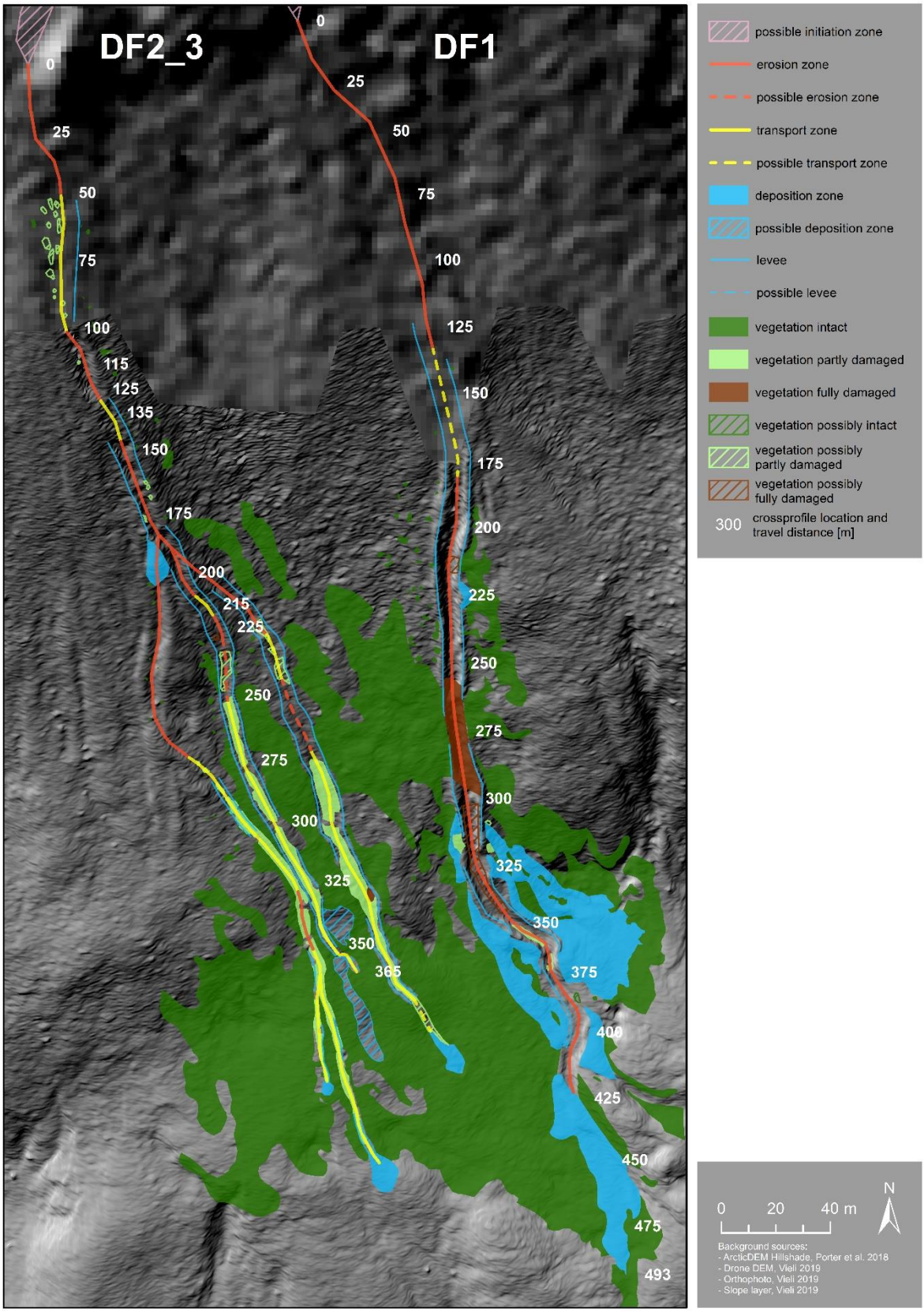

Figure 22: Detailed mapping results of DF 1 and DF2_3 (middle debris flow channel). The white numbers indicate the cross profile locations and the travel distances.

6.1.2 DF2_3

DF2_3 starts with a short *erosion zone* of 50 m, which is followed by a sequence of changes to *transport zone* and back (Figure 22 and Figure 26). Shortly after 175 m distance, the channel divides into three separate debris flow channels. DF2_1 was the first debris flow and its channel is closed by a levee. DF2_2 occurred afterwards and is closed by approximately 30 m^3 of deposition material. DF2_3 continuous with an *erosion zone* until 250 m and changes then to *transport zone* down to the end of the debris flow channel. At the end of this debris flow channel, no *deposition zone* is mapped. Although, two areas are indicated near the end of the channel, which could be depositions from the event in 2014.

In the upper part several levee pieces align along the channel on both sides. From the dividing point of the debris flow channels, the levees can be recognized almost continuously until the end of the channel.

Already in the first *transport zone* multiple patches of *partly damaged vegetation* are assumed. Most of the last 130 m of DF2_3 has *partly damaged vegetation* in the channel and sometimes also on the levees. Next to the channel, there are big areas of intact vegetation. In Figure 23 for DF2_1, DF2_2 and DF2_3 the situation from a few days after the debris flows event is portrayed. Here the *partly damaged vegetation* can be recognized in the channel as well as this is visible in Figure 7D.

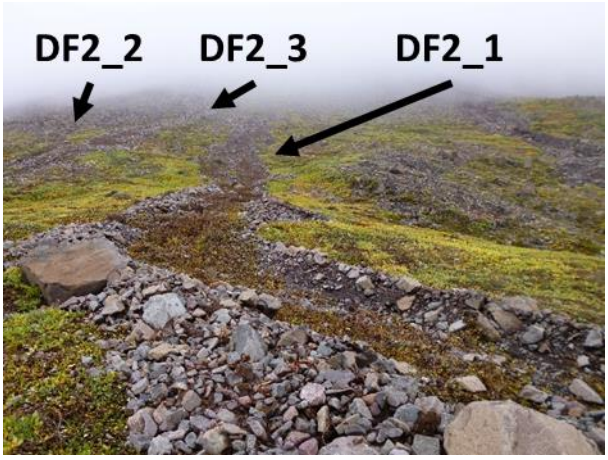

Figure 23: Upslope picture of the channel and the levees of DF2_1. In the back also DF2_2 and DF2_3 are visible. In all of the three channels partly damaged vegetation, like inside the channel of DF2_1, is present. (Photo: Andreas Vieli, August 2014)

6.1.3 DF6

DF6 flows for the first 300 m in a deep gully, which eroded into the scree slope. On the eastern gully slope, side erosion can be detected while on the other gully side a levee is present. Then, a short passage of a steep bedrock cliff with no

possible erosion, follows and afterwards the next *erosion zone* begins (Figure 24 and Figure 27). Around the 725 m mark, a short *transport zone* is followed by another erosive part. A couple meters before the deposition area starts, another *transport zone* can be seen. The debris flow terminates with a quite big debris lobe of about 6200 m^2, just at the foot of a rocky crest. Over this deposition, the water pipeline and gravel road were rebuilt. The first deposition area at the side of the channel starts at 550 m travel distance and is followed by three other small deposition lobes which range between 280 – 360 m^2 area. Three of the deposition areas are located at the outside bend of small curves of the debris flow path (cf. Figure 24).

Levees can be detected almost continuously after 450 m and they end shortly before the last deposition area. Some of the levees, especially in the last part of the channel, are vegetated. With some very small exceptions, there is no vegetation found inside the channel and the *intact vegetation* is situated alongside the channel. Generally, the vegetation increases in the lower parts of the flow path, with its maximum around the terminal deposition area.

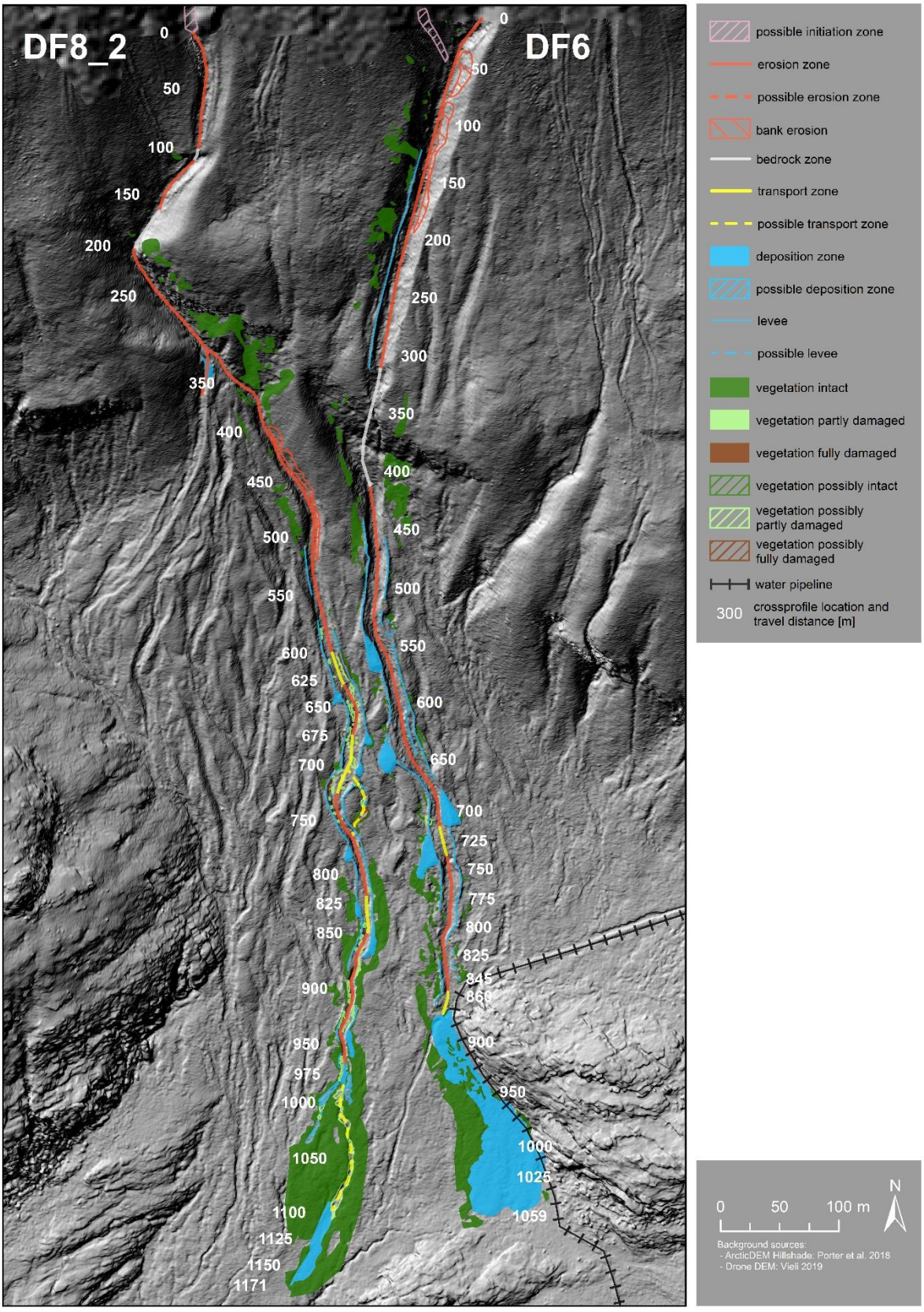

Figure 24: Detailed mapping results of DF6 and DF8_2. The white numbers indicate the cross profile locations and the travel distances.

6.1.4 DF8_2

As visible in Figure 24 and Figure 28, DF8_2 starts with a sequence of alternating channel *erosion* and *bedrock zones* in a deep eroded gully. After the division of DF8_1 and DF8_2, the flow path is erosional for 300 m. Side erosion occurred in this zone on the orographic left side. Between 600 m – 630 m, 675 m – 725 m and 820 m – 850 m three short *transport zones* alternate with erosional parts. Onward, the channel is characterized as *erosion zone* again. Around 970 m travel distance, a 130 m long *possible transport zone* leads to the terminal deposition area which covers 170 m^2. At the beginning of this last *possible transport zone,* three *possible deposition zones* are visible. Further up at the channel sides, multiple small deposition lobes can be found ranging from 29 m^2 to 72 m^2. At 700 m travel distance, the beginning of a possible small side channel can be seen, which already joins the main channel after 60 m. The first levees can be found around 570 m and are almost continuously present to the end of the last *erosion zone*.

From 600 – 750 m travel distance multiple small patches of *possibly partially damaged vegetation* can be found. Along the channel in this section, there is just few vegetation. Also, from 830 m ongoing a big amount of *possibly partially damaged vegetation* is mapped. But here, there is remarkably more vegetation along the channel. Especially from the beginning of the *possible transport zone* until the end of the final *deposition zone* there are loads of quite high vegetation.

6.2 Channel Analysis

6.2.1 DF1

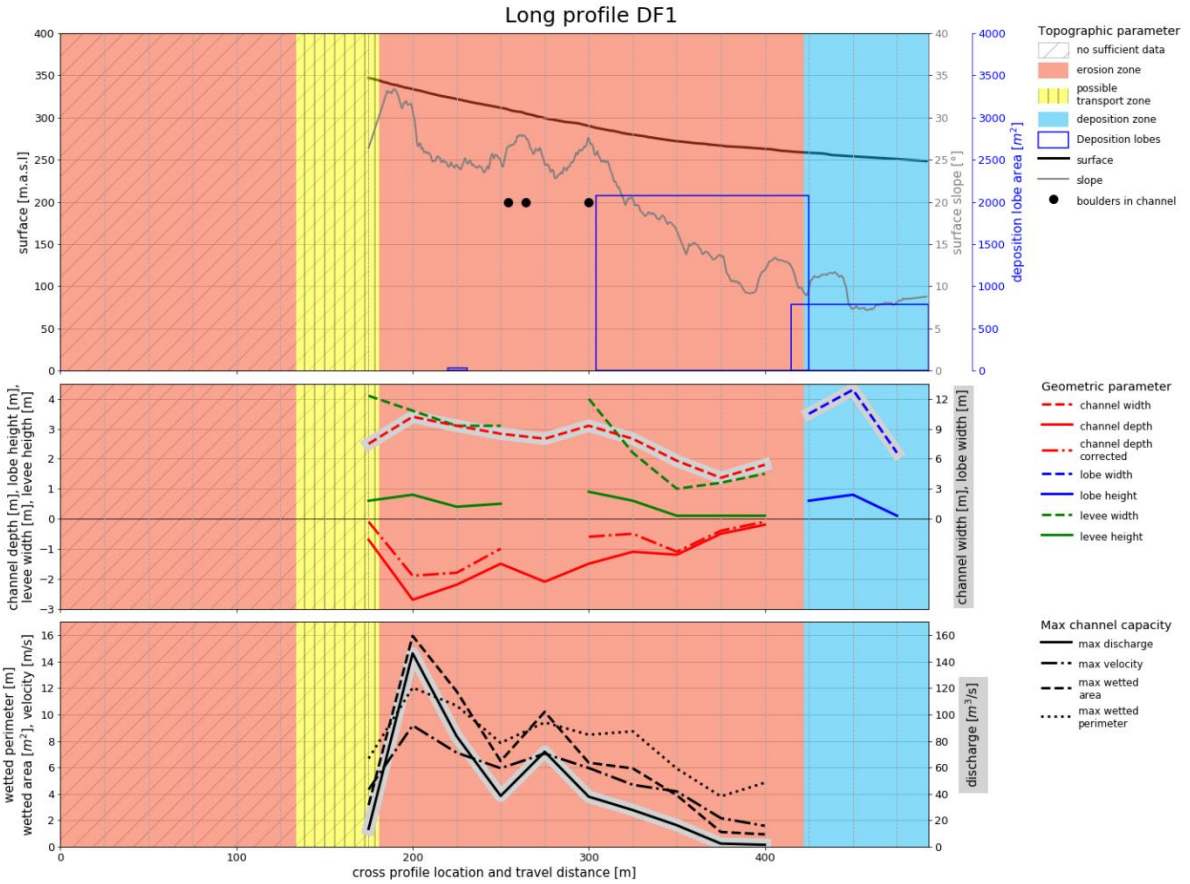

Figure 25: Long profile of DF1 presenting the topographic parameter (upper part), the geometric parameter (middle part), and the max channel capacity (lower part). In the background of all parts, the mapped debris flow zones are displayed. The grey oblique hatched area on the left side of the figure indicates the absence of accurate data. The original sized figure is provided in Appendix 12.2.1.

DF 1 has a total travel distance of 493 m (Figure 25), whereof for the first 175 m the absence of accurate data doesn't allow measurements. The first measured height is at ~350 m.a.s.l, while the debris flow path ends at 250 m.a.s.l. The slope decreases almost continuously from 27° and stabilizes just below 10° for the last 100 m. A small deposition area along the channel is present at 250 m travel distance and from 300 m ongoing big debris depositions occurred. Three big boulders can be detected between 250 m and 300 m path flow length. The mapped debris flow zones are shown in the background like they are described in section 6.1.1. The transition from erosion to deposition is approximately at a slope of 10°.

Channel width and channel depth decrease with ongoing flow length from 10.2 m to 4.1 m and from 2.7 m to 0.2 m respectively. Also the levee width and depth show a generally decreasing behaviour. Due the absence of levees no

measurements could be done at 275 m. The effect of *channel depth* and *levee height* on the *corrected channel depth* is clearly visible. Its values tend to zero at 175 m and 400 m. *Deposition width* and *deposition height* show the highest values in the first third along the flow path, before decreasing towards the end.

While *Pmax* and *Vmax* develop very similarly along the flow path, so do *Amax* and the *Qmax*. From the first to the second measurement all values increase greatly to e.g. over 140 m^3/s of *Qmax*. Afterwards, they decrease almost continuously to e.g. 1.5 m^3/s for *Qmax*. *Vmax* drops from 9 m/s and reaches 1.6 m/s after 400 m travel distance.

6.2.2 DF2_3

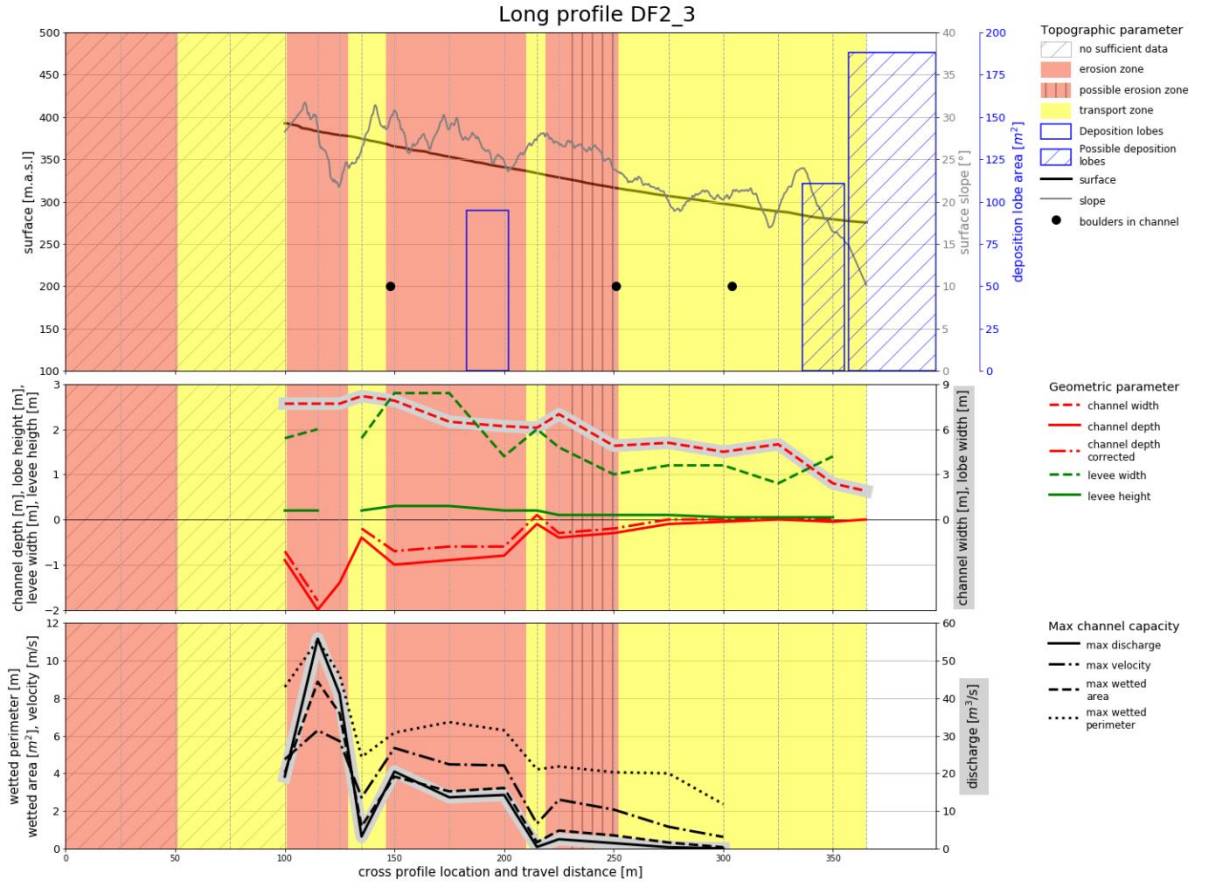

Figure 26: Long profile of DF2_3 presenting the topographic parameter (upper part), the geometric parameter (middle part), and the max channel capacity (lower part). In the background of all parts, the mapped debris flow zones are displayed. The grey oblique hatched area on the left side of the figure indicates the absence of accurate data. The original sized figure is provided in Appendix 12.2.1.

The run out distance of DF2_3 is 365 m. For the first 100 m the absence of accurate data doesn't allow measurements (Figure 26). In the measured part, the debris flow path declines from 390 m.a.s.l to 275 m.a.s.l. The slope thereby decreases relatively steadily from over 30° to 12° at the end of the flow path. In between

the slope partly rises gently, especially in *transport zones*. The erosion in DF2_3 ends at a slope value of 23°. Big boulders or boulder accumulations are existent at three locations (~145 m, ~250 m, ~305 m). Around 200 m flow distance a deposition besides the channel contains approximately 28 m^3 and covers almost 100 m^2 (cf. chapter 6.1.2). At the end of the flow path two areas, which are *possible deposition zones* cover a total area of 300 m^2.

The channel width decreases constantly to a minimum of 2 m. Two steep increases interrupt the generally steady decrease of channel depth at 135 m and 215 m travel distance. Thereby the corrected channel depth almost goes to zero at 135 m and even gets positive at 215 m. The levee heights are generally very low along the whole flow path and are not measurable at the debris flow end.

All the measurements and the calculations for Vmax and Qmax display the same pattern as the channel depth. Thus, the maximum values are at 115 m travel distance and two local low points at 135 m and 215 m. The calculated maximum discharge reaches almost zero at 300 m flow distance. Afterwards no measurements of the wetted area and perimeter are possible due to the low levee height and channel depth values.

6.2.3 DF6

The slope of DF6 is 30° at the beginning and 9° at the end of the flow path after the total travel distance of 1059 m. But the steepest part with over 50° is located around the 370 m mark in the *bedrock zone*. This slope peak is also clearly depicted in the surface presented in Figure 27. The slope, where the first *transport zone* is mapped, is approximately at 18°, while erosion ends at ~12°. Deposition starts at 14° and ends at 7.5°. The flow path starts at an elevation of 390 m.a.s.l and terminates at an elevation of 50 m.a.s.l. Two boulders are present in the channel at 470 m and 710 m flow distance. There are four small debris depositions besides the channel, covering 280 – 360 m^2 area.

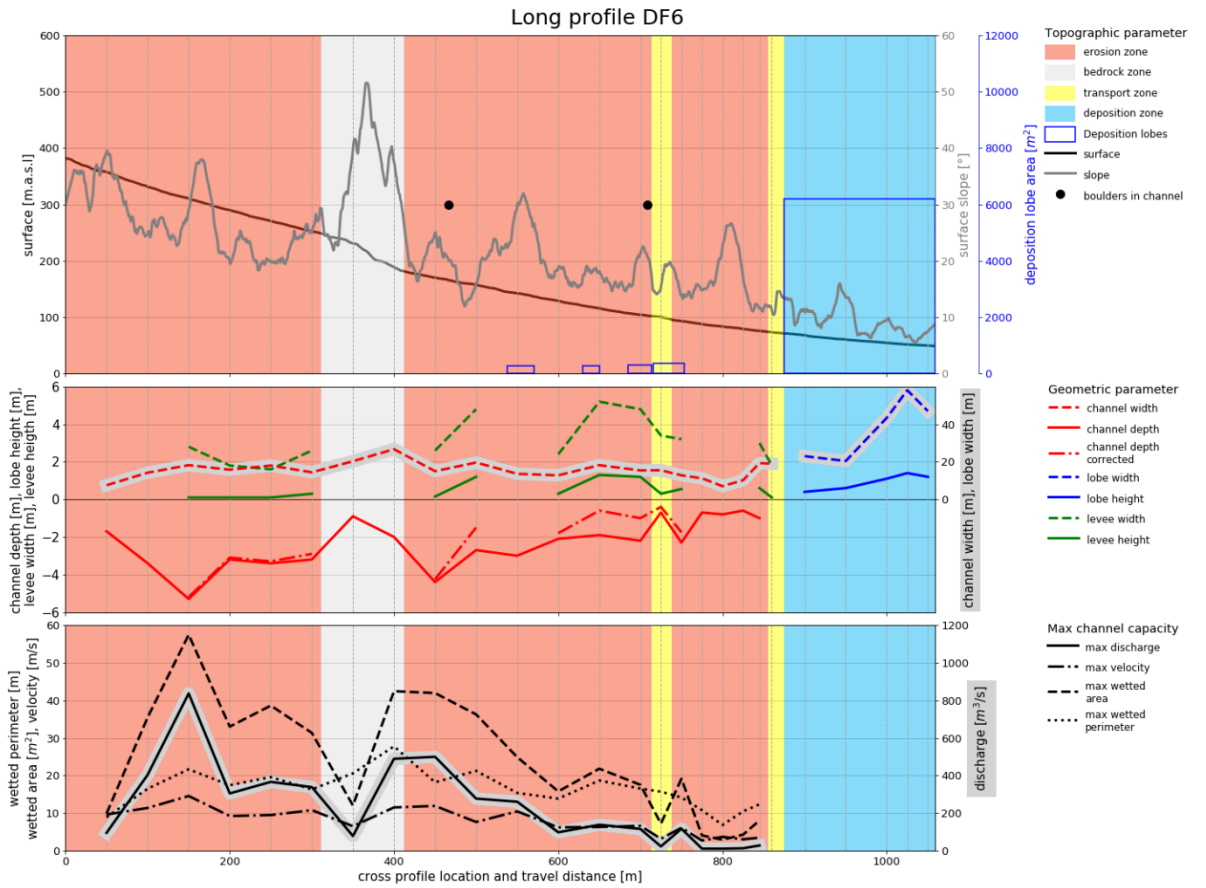

Figure 27: Long profile of DF6 presenting the topographic parameter (upper part), the geometric parameter (middle part), and the max channel capacity (lower part). In the background of all parts, the mapped debris flow zones are displayed. The original sized figure is provided in Appendix 12.2.1.

The channel width ranges between 10 m and 20 m for most of the debris flow path, with slightly higher values at the foot of the steep bedrock cliff. Although the channel depth is clearly lower in this *bedrock zone*, it generally decreases along the debris flow path. Two peaks of channel depth show values over 4 m and 5 m respectively. The levees can only be measured partly along the channel and have their maximum in height and width around 650 m to 700 m travel distance. Therefore, they influence the corrected channel depth greatly in this area and lower them more than half. The deposition width and height show their maximum at the second last cross profile due to the geometric form of the deposition (cf. Figure 24).

Qmax and *Amax* decease greatly between the first hundreds of meters and the last few datapoints before the final deposition area starts. *Qmax* and *Amax* is 840 m^3/s and 57 m^2 respectively after 150 m travel distance. These two parameter show almost the same behaviour along the flow path and are very similar to the

behaviour of the channel depth. The velocity is around 10 m/s for the first 550 m and then drops under 4 m/s at the last measurements.

6.2.4 DF8_2

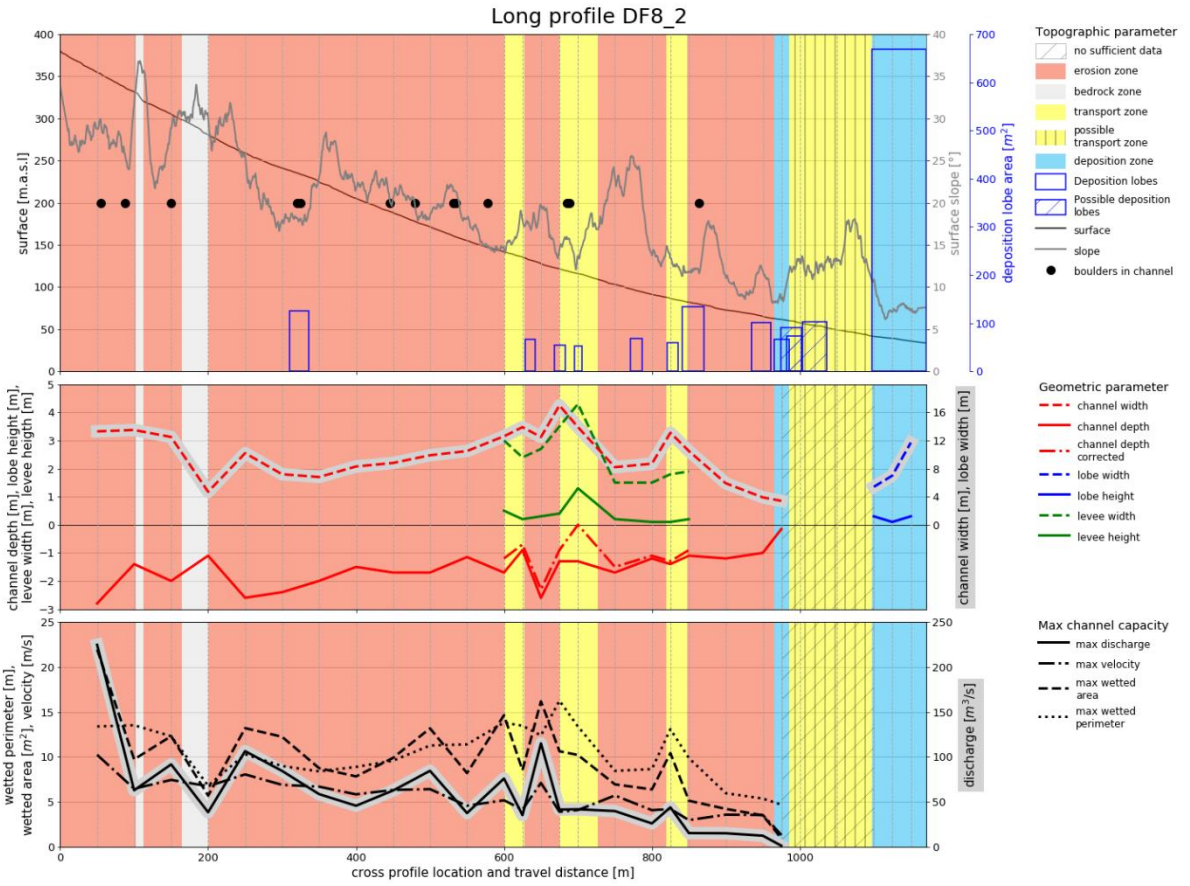

Figure 28: Long profile of DF1 presenting the topographic parameter (upper part), the geometric parameter (middle part), and the max channel capacity (lower part). In the background of all parts, the mapped debris flow zones are displayed. The grey oblique hatched area on the right side of the two lower figure parts indicates the uselessness of the drone data due to vegetation influence. The original sized figure is provided in Appendix 12.2.1.

The debris flow channel 8_2 starts at 380 m.a.s.l and terminates at 33 m.a.s.l with a total flow length of 1171 m. The first 200 m contains two *bedrock zones*. These steps are visible in the surface plot and the slope shows two peaks. Otherwise, the upper half of the flow path is dominated by erosion. The channel bed slope starts in the upper part at over 30° and is in the final depositional area approximately 8°. Within three of the four *transport zones* the slope rises. The slope where the first *transport zone* starts is at approximately 18°. The slope where the erosion ends, and the first deposition occurs is at 8°. There are 10 very small (~50 m^2 - ~130 m^2) debris depositions on both sides and also in the channel (975 m) (cf. Figure 28). Further, the two *possible depositions* described in chapter 6.1.4 are displayed with a hatched pattern at 1000 m travel distance. In the channel, 13

boulders are present and a major part of them are situated in the first half of the flow path. Some of them lay very close to each other.

The channel width increases to the maximum of 17 m at 675 m flow distance and afterwards decreases to under 4 m at the end of the measurements. The three channel width peaks from 600 m and ongoing are all measured in *transport zones*. The channel depth gradually decreases from approximately 2.9 m to 0.2 m. After 700 m travel distance, the *corrected channel depth* reaches 0 m. This cross profile is situated in one of the *transport zones*. Here the levee width and height reach their maximum. Generally, only 250 m of levees could be measured. Measured deposition heights are 0.3 m or lower at the terminal deposition area. The deposition width ranges between 5 m and 12 m.

The values for maximum discharge differ from 225 m^3/s at the first cross profile location to 1.2 m^3/s after 975 m flow distance. The wetted area shows the same pattern along the flow path. While the wetted area and therefore the maximum discharge show similarities to the channel dept, the wetted perimeter seems to match more with the behaviour of the channel width. Vmax decreases almost constantly from 10 m/s down to 1.3 m/s.

6.3 Numerical Modelling

For all four debris flows under closer examination a most plausible input parameter set was found with and without using the RAMMS erosion module. In the following chapter, only the most plausible model runs with the erosion module are presented and described. The used input parameters for each debris flow are listed in detail in Table 6. The parameters used for model runs without erosion are shown in Appendix 12.4.2.

Table 6: Input parameter and output volumes of the most plausible simulations for each debris flow using the RAMMS erosion module.

		DF1	DF2_3	DF6	DF8_2
Input parameter	DEM used	drone DEM	drone DEM	drone DEM	drone DEM
	Initiation distance on long profile [m]	200	100	60	50
	Data resolution [m]	0.07	0.07	0.07	0.07
	Simulation resolution [m]	0.5	0.2	0.5	0.5
	Stopping criteria [%]	5	5	5	10.7
	Simulation length [s]	325	75	355	755
	Dump stem [s]	5	5	5	5
	Density [kg/m^3]	2000	2000	2000	2000
	ξ [m/s^2]	100	500	300	200
	μ [-]	0.17	0.10	0.11	0.13
	Obstacle/Dam used	No	No	Yes	No
Release parameter	Volume released [m^3]	500	50	1600	50
	Qmax [m^3/s]	20.6	2.6	47	3
	t1 [s]	3	1	3	2
	v [m/s]	6	5	10	6
	t2 [s]	56.5	38.5	68.1	38.5
Erosion parameter polygon 1	Erosion density [kg/m^3]	2000	2000	2000	2000
	Erosion rate [m/s]	0.025	0.025	0.025	0.013
	Pot. erosion depth [per kPa]	0.1	0.1	0.1	0.1
	Critical shear stress [kPa]	1	1	1	1
	Max erosion depth [m]	0	0	0	0
Erosion parameter polygon 2	Erosion density [kg/m^3]	2000		2000	2000
	Erosion rate [m/s]	0.013		0.025	0.013
	Pot. erosion depth [per kPa]	0.1		0.1	0.1
	Critical shear stress [kPa]	1		1	1.5
	Max erosion depth [m]	0.5		0	0.1
Erosion parameter polygon 3	Erosion density [kg/m^3]				2000
	Erosion rate [m/s]				0.013
	Pot. erosion depth [per kPa]				0.1
	Critical shear stress [kPa]				1
	Max erosion depth [m]				0
Output parameter	Eroded volume [m^3]	603	25	3932	563
	Flow volume [m^3]	1102	45	5520	590
	Calculation domain outflow volume [m^3]	0	30	12	23
	Volume in mapped deposition area [m^3]	340	-	3588	256
	Runout length [m]	503	368	1062	1173

6.3.1 DF1

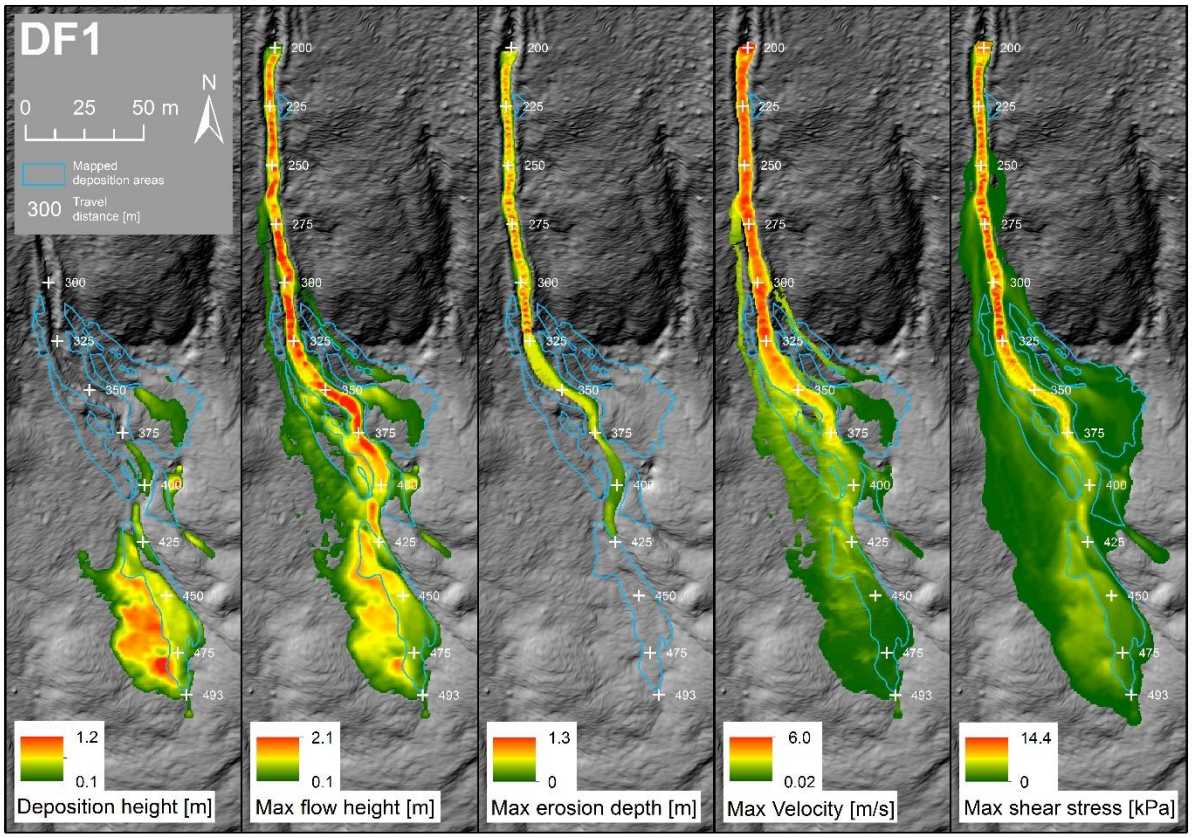

Figure 29: Deposition height, max flow height, max erosion depth, max velocity, and max shear stress of the most plausible simulation including erosion of DF1. The mapped deposition areas are indicated in blue. The white numbers indicate the travel distances. In the background are the hill-shade of the drone DEM displayed. The original sized map is provided in Appendix 12.2.2.

To simulate DF1, a start volume of 500 m^3, a μ of 0.17, and a ξ of 100 m/s^2 were used as input parameters. The simulation was stopped as the default stopping criteria threshold of 5% was reached. This most plausible simulation contains two *erosion zones*. Whereof the first one is defined until the flow channel reaches the first deposits at 325 m travel distance and it is defined with the default erosion value. The second erosion polygon is mostly placed on debris flow depositions and ends at 425 m. Its erosion rate is lowered to 0.013 m/s and the maximum erosion depth is 0.5 m (cf. Table 6). This change of the maximum erosion depth is based on the true channel depths described in chapter 6.2.1.

The run out length of the simulated debris flow is 503 m and from a total of 1102 m^3 flow volume, 602 m^3 were eroded. In the upper channel part, the highest erosion depths are calculated, while in the lower part less erosion is displayed due to the definitions described above. Otherwise, material is eroded very continually, except at around 400 m flow distance where a local minimum is calculated. Most

of the debris flow material is deposited in the lower flow path next to the mapped *deposition zone* and with deposition heights up to 1.2 m. In some of the upper mapped *deposition zones* even no material is accumulated. The flow heights are higher in the channel centre and after 400 m travel distance the values drops for some meters. Velocities up to 6 m/s are calculated before the first deposition areas, but then decrease continuously until the flow terminates.

6.3.2 DF2_3

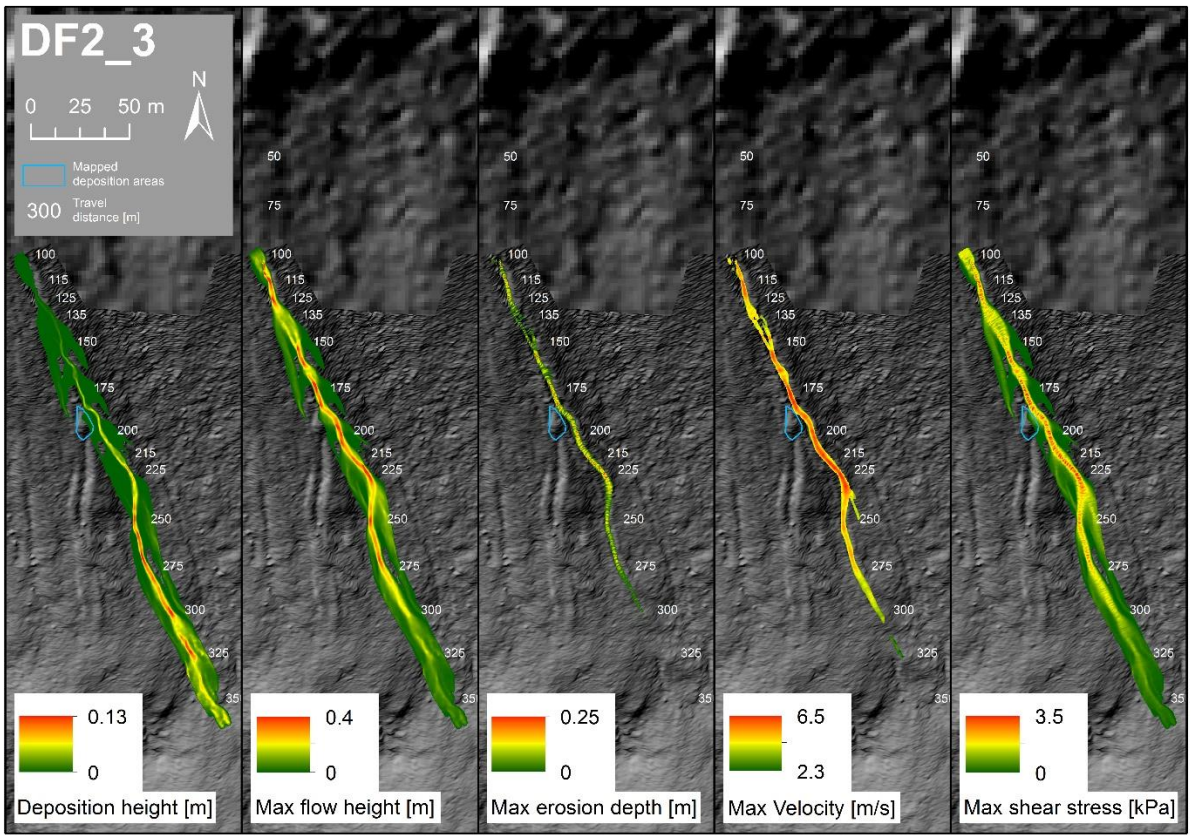

Figure 30: Deposition height, max flow height, max erosion depth, max velocity, and max shear stress of the most plausible simulation including erosion of DF2_3. The mapped deposition areas are indicated in blue. The white numbers indicate the travel distances. In the background are the hillshades of the drone DEM and the ArcticDEM displayed. The original sized map is provided in Appendix 12.2.2.

The most plausible model run was initiated with 50 m^3 volume at 100 m travel distance. Friction values ξ and μ are defined with 500 m/s^2 and 0.10, respectively. The erosion polygon reaches from the release hydrograph until the terminus of the debris flow, because there are only *possible deposition zones* mapped near the end of the flow path. The default erosion values and stopping criteria were used for this model run (Table 6).

In total 75 m^3 mass was moved in this most plausible simulation. Thereof 45 m^3 stay inside the project domain, while 30 m^3 are flowing out of it. In total 25 m^3 material is eroded with maximum erosion depths of 0.24 m. Between 135 m and 150 m travel distance the erosion greatly decreases. The most erosion takes place afterwards and erosion ends at around 300 m travel distance. There are generally very small maximum flow and deposition heights calculated. If applying the lower threshold of 0.1 m for minimum deposition and flow height, almost all depositions disappear, and flow heights would be displayed only until 325 m travel distance. A clear difference of values between 135 m and 150 m travel distance is visible for flow height and velocity. Otherwise, the velocity stays around 5 m/s until the 240 m mark and then start to decrease. Due to flow heights below 0.1 m, for the last 40 m, no velocities are calculated.

6.3.3 DF6

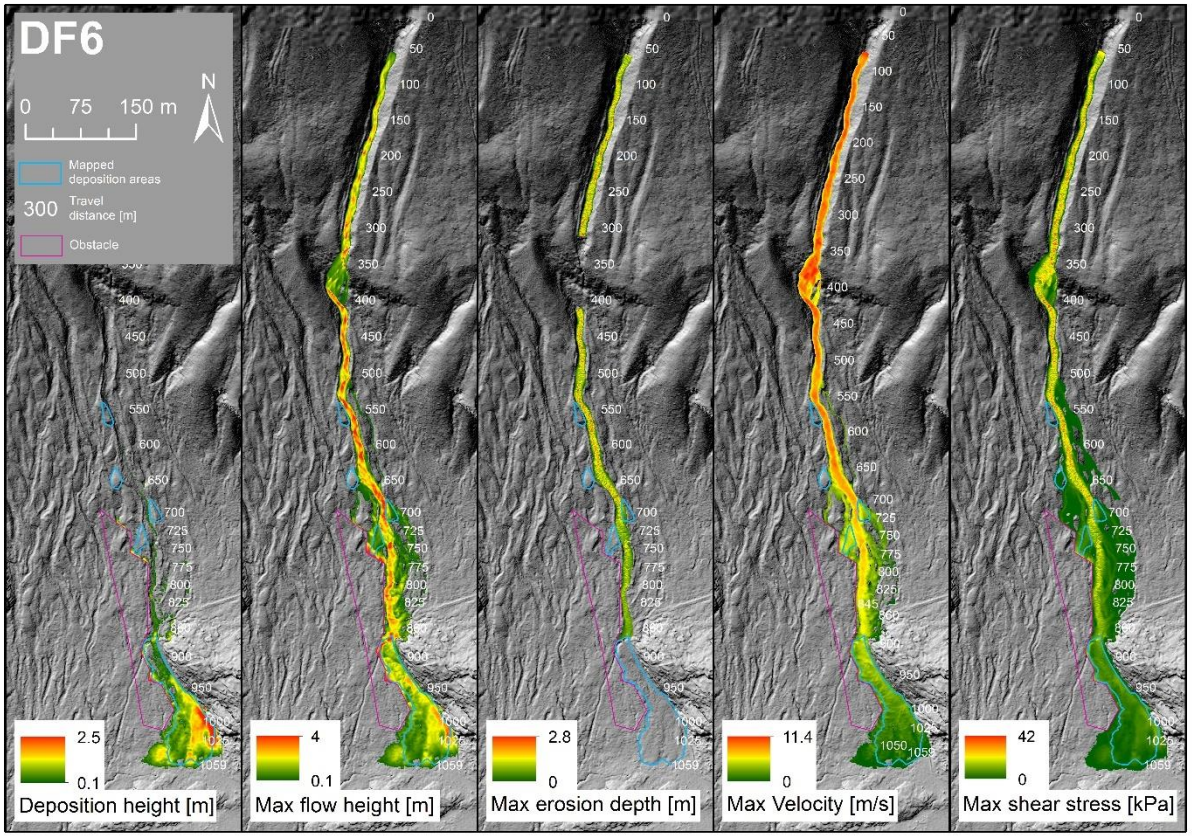

Figure 31: Deposition height, max flow height, max erosion depth, max velocity, and max shear stress of the most plausible simulation including erosion of DF6. The mapped deposition areas are indicated in blue. The white numbers indicate the travel distances. The pink polygon shows the obstacle polygon used. In the background are the hillshades of the drone DEM and the ArcticDEM displayed. The original sized map is provided in Appendix 12.2.2.

In Figure 31, different modelling outputs of the most plausible flow conditions of DF6 are shown. The debris flow is initiated at 60 m flow path length and an

initiation volume of 1600 m^3 is used (Table 6). For friction values μ = 0.11 and ξ = 300 m/s^2 were used. The default values were utilized as erosion parameter and stopping criteria. More input and output values are listed in Table 6. An obstacle polygon was defined besides the flow path in the lower part (cf. Figure 31), to keep the debris flow on track and let it reach the terminal deposition area.

The total simulated run out length for DF6 is 1062 m. 3932 m^3 of the total 5520 m^3 flow volume is eroded channel material. The maximum deposition height is 2.5 m and is measured in the eastern part of the modelled depositions. Most of the modelled deposition area lies within the mapped deposition area. There are maximum flow heights of over 4 m calculated. These are only very small patches or some pixels with such high values calculated. In most channel parts values under 2.3 m are calculated. The high values lay in the steep bedrock cliff and above. Velocities are calculated up to 11.4 m/s. The erosion and velocity decrease towards the flow terminus and they are generally higher in the middle of the channel. The majority of erosion values are under 1.5 m. Around 500 m, 650 m, and 725 m travel distance, the maximum flow height and the erosion values are locally lower, compared to the values before and afterwards. Whereas for the velocity this behaviour is only clearly recognisable at 500 m and 725 m.

6.3.4 DF8_2

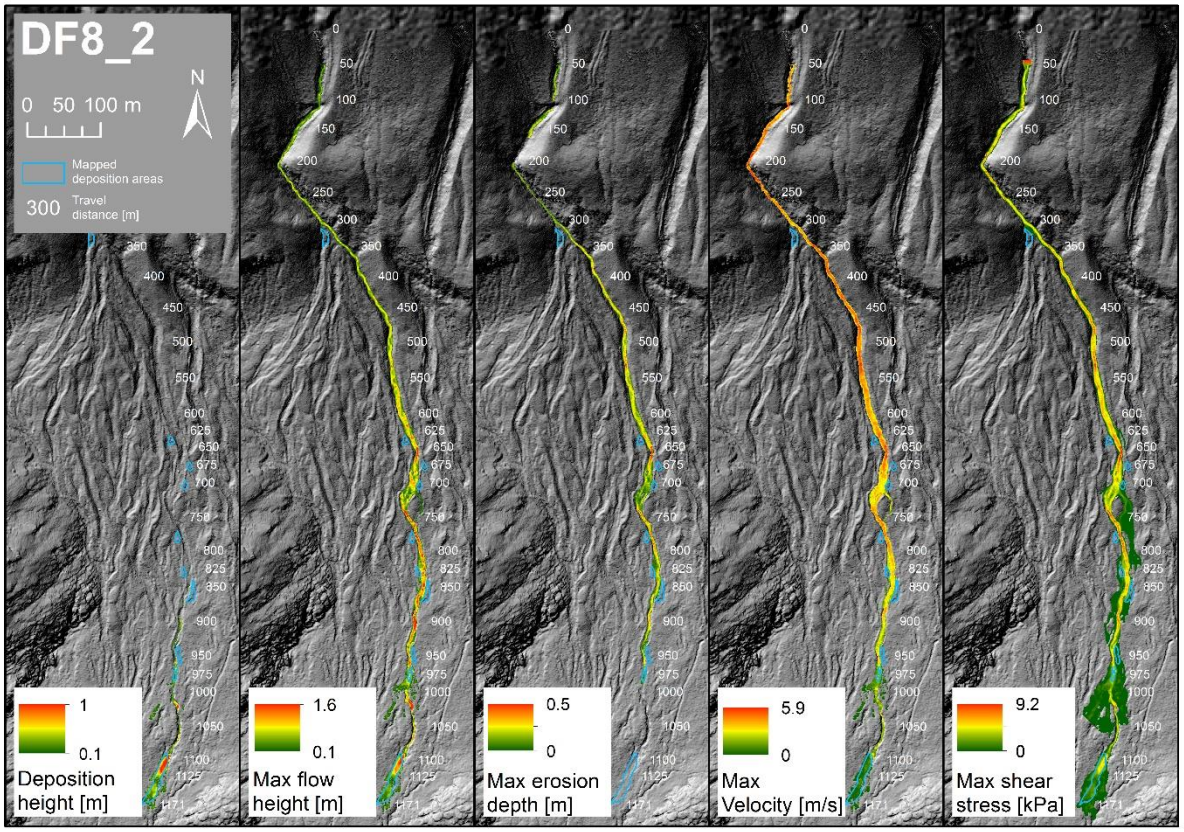

Figure 32: Deposition height, max flow height, max erosion depth, max velocity, and max shear stress of the most plausible simulation including erosion of DF8_2. The mapped deposition areas are indicated in blue. The white numbers indicate the travel distances. In the background are the hillshades of the drone DEM and the ArcticDEM displayed. The original sized map is provided in Appendix 12.2.2.

An initiation volume of 50 m^3 was used to simulate the most plausible debris flow presented in Figure 32. For this simulation, the friction parameters $\mu = 0.13$ and $\xi = 200$ m/s^2 were used. The channel was split up into three *erosion zones*. Zone 1 ranges from 50 m to 165 m, zone 2 from 200 m to 300 m and zone 3 from 300 m to 990 m. For all zones lowered erosion rates of 0.013 m/s were applied, but otherwise zone 1 and zone 3 are defined with the default erosion parameter. The reasons to use lower erosion values are described and discussed in chapter 7.3.2. Erosion zone 2 has a higher critical shear stress value and a maximum erosion depth of 0.1 m. This is based on the observation of very low bed rock coverage in this part of the flow path in the drone orthophoto. The debris flow simulation was stopped already at a flow momentum of 10.7 %. This was the only option, to actually reach the terminal *deposition zone* but prevent the material from diffluence. It also must be remarked that the changes of each dump step within the last 200 seconds of simulation are minimal.

The simulated erosion pattern displays the initial *erosion zones* definition, with a rise of erosion depth after entering the third *erosion zone*. Also otherwise, several changes of erosion depths can be recognized. The highest values are calculated in quite narrow channel parts (e.g. 535 m, 660 m), while wide channel parts show lower erosion rates (e.g. 675 m -740 m). A similar pattern can be observed for the flow height and the velocity. But for the latter, very high values are simulated at the two steep bedrock cliffs in the first 200 m. Very low velocity values are present, where the material gets deposited and between 970 m and 990 m travel distance.

In total 590 m^3 flow volume was calculated, whereof 563 m^3 is gained through erosion processes and 23 m^3 flowed out of the calculation domain. Within the mapped terminal deposition area the simulated depositions are at maximum 1 m thick. The mapped and simulated terminal deposition areas, match spatially very well. 256 m^3 material is deposited in the simulation inside this last mapped *deposition area*. Some simulated depositions are located besides the main flow channel on *possible deposition areas* (cf. chapter 6.1.4).

7 Discussion

In this chapter different noticeable points from the results are discussed regarding the research questions. They are structured according to the three research subtopics. At the end of each research subtopic, problems, difficulties, and limitations are discussed.

7.1 Spatial Distribution Analysis

7.1.1 Debris Flow Features

The different debris flow features are not present everywhere along the debris flow paths. Levees are mostly visible in the lower part of the flow path, few also align in the upper part. This observed distribution matches well with the descriptions of Hungr (2005). Also, the small debris depositions besides the flow channels exist generally in the lower half of flow path. Sometimes they are debris plugs closing older debris flow path. Remarkably often, they are deposited in the outside bend of the channel curves. This, sometimes repetitive behaviour of outside depositions fits well with the descriptions and definitions of e.g. VanDine (1996) and Hungr (2005).

Except for DF2_3 all debris flows have the typical terminal debris depositions (cf. Hungr, 2005; VanDine, 1996). Either the absence of depositions at the end of DF2_3 could be caused by very small debris deposition, which were reworked and washed away by water directly after the deposition (Hungr, 2005). Or, the areas mapped as *possible debris deposition*, are really its terminus depositions. The levees of DF2_3 constantly decrease along the flow path to under 10 cm. This could also indicate, that the debris flow just ran out of coarse material when forming the levees, while the fine material got washed away. Also, additional retention of coarse material in the vegetation is imaginable. Another possibility could be the influence of continuous yearly snow and ice melt on top and in the active layer, as described in a study on Svalbard by De Haas et al. (2015 a), and thereby eroding the fine sediment.

The observed deposition lobe patterns of DF1 leads to the assumption of a multi surge event, which is not unnormal for debris flows (Hungr, 2005; Iverson, 1997). The lower debris deposition material flowed over the upper depositions, eroded its material and was probably additionally deflected by the present rock glacier margin. It can’t be determined certainly from the data available for this thesis if only

two surges occurred, because more surges would also match the deposition pattern. The temporal distance between the single surges cannot be derived. But they probably either occurred at one of the precipitation peaks on August 9th or August 16th or at minimum one surge was initiated at both peaks. This temoral multi-surge behaviour is also transferable for other debris flows in the study area (e.g. DF2_x, DF3_x, DF8_x).

7.1.2 Debris Flow Zones

For a majority of the debris flow paths, all the three zones *erosion*, *transport,* and *deposition* are mapped. In the upper parts of the debris flow tracks mostly erosion is dominant, which is sometimes interrupted by bedrock parts (cf. Figure 21). Such bedrock segments are not unusual (Hungr, 2005) and in the case of Disko Island possibly caused due to the presence of the stratified plateau basalt (cf. chapter 3.1). Levees or small deposition lobes are often present at the channel sides of *erosion zones* in the lower parts of the debris flow channels. This shows the simultaneous occurrence of erosion and deposition as described by e.g. Fannin & Wise (2001); Schürch (2011).

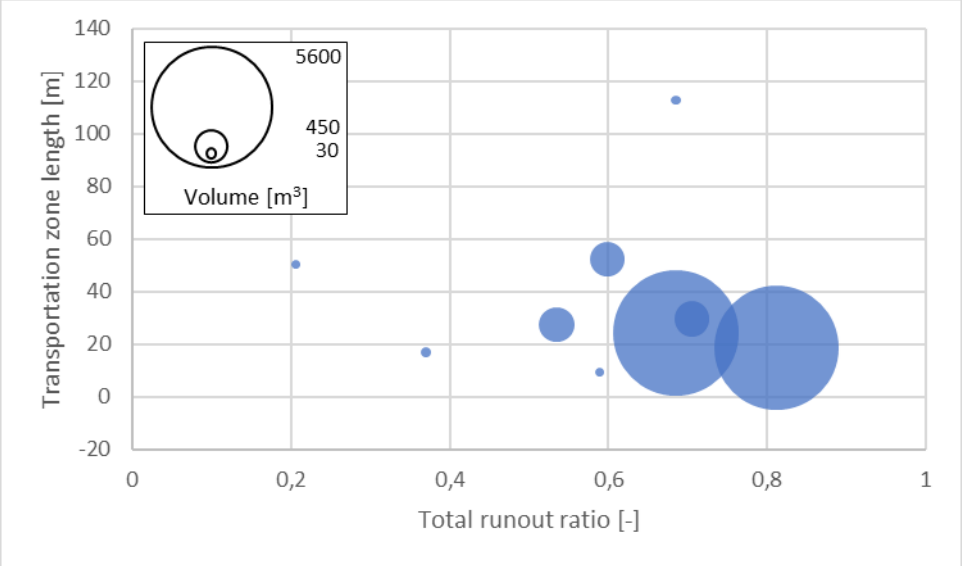

Figure 33: Transport zone length plotted against the total runout distance. The size of the circles indicates the estimated volumes of the debris flow of each transport zone.

A great number of the *transport zones* are mapped in the lower half of the debris flow path (cf. Figure 33). There seems to be a trend for debris flows with bigger volumes, that *transport zones* occur later along the debris flow path. The length of the *transport zones* ranges from 9 m to 112 m and without any pattern regarding the total runout ratio (position in long profile divided through the total run out

distance) or the volume. But most of them seem to be shorter than 50 m. The *transport zones* sometimes alternate with *erosion* zones (cf. Figure 26). Two examples of such alternating higher and lower erosive zones are shown on a field photo from August 2014 in Figure 34. Although not all of the indicated lower erosive zones are also mapped as *transport zones*. Such patterns of higher and lower erosion are visible in the data of Schürch et al. (2011) from the Illgraben catchment, where they relate erosion and deposition with flow depth and channel geometry. Iverson et al. (2011) suggest from their large scale experiments, a correlation of high saturated channel beds and erosion. Flow depth, channel geometry and channel bed saturation could be possible explanations for the observed behaviour. There is no concluding suggestion about the reason for this pattern due to the lack of field investigations and records of pre-event topography, which makes understanding such phenomena very difficult or almost impossible (Schürch, 2011).

For a majority of the mapped *transport zones*, there is at minimum a levee present on one side and sometimes even a small debris deposition. This means that although no or almost no erosion occurred, debris was deposited at the sides.

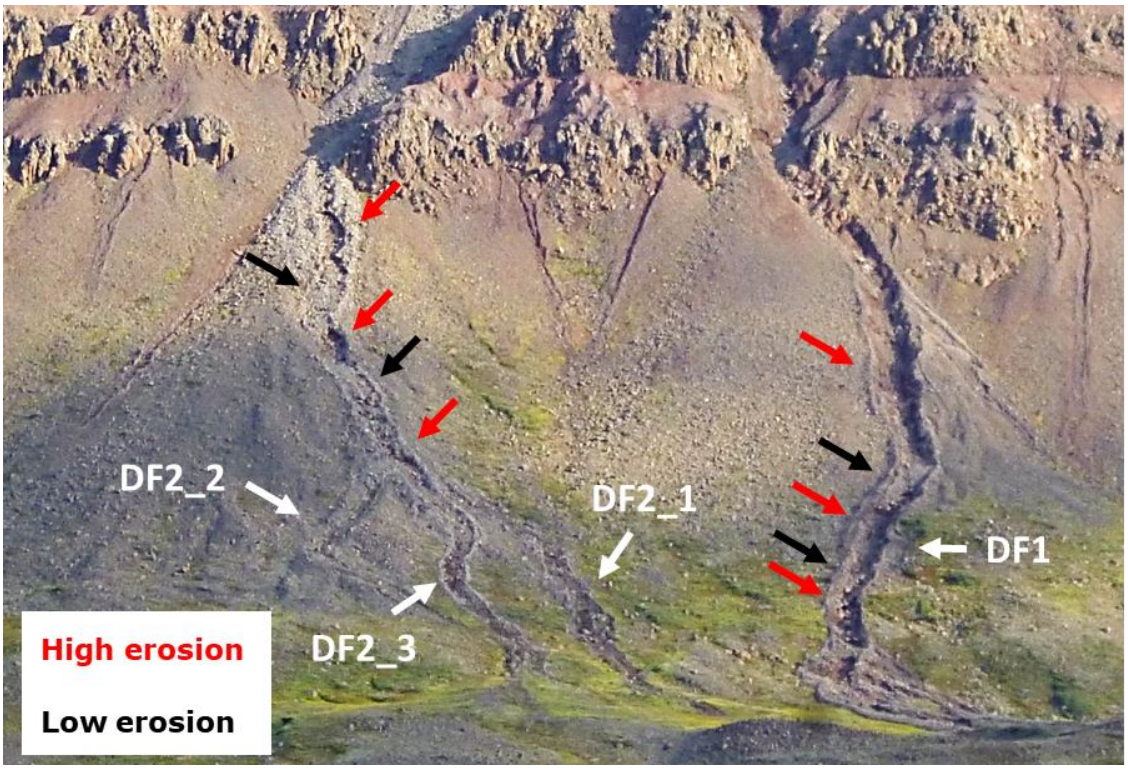

Figure 34: High and low erosion zones in the channels of DF1 and DF2_x. This areas of high and low erosion alternate in both debris flow channels. (Photo: Andreas Vieli, August 2014)

Half of the debris flows with a terminal debris deposition, change directly from erosion to deposition. The other half has a *transport zone* in between. Therefore, no trend for the sequence of *transport zones* before a final deposition can be suggested and their occurrence seems rather random. To verify this observation further investigations would be necessary.

7.1.3 Vegetation

Generally, in lower hillslope parts more vegetation is present while in most of the channels no vegetation is observed. It was either never there or was ripped off by the debris flows (e.g. Jakob & Hungr, 2005; Regmi et al., 2015). But in some channels, it was possible to map patches of vegetation. These are typically small and present in the lower half of the flow channel. They must have resisted the debris flow forces and regrown afterwards, or they colonized at these patches in the five years between the debris flow event and the drone flight. In the debris flow channels of DF2_1, DF2_2 and DF2_3 there is a lot of vegetation present (cf. Figure 23). This photo was taken just a few days after the debris flow and shows still quite intact and only partly damaged vegetation. This resistance of the vegetation leads to the assumption, that the shear forces of the debris flow must have been quite low.

This could refer to quite small debris flow volume (as already discussed in chapter 7.1.1) or it could also be assumed, that the debris flow was very dilute and maybe something similar to a hyperconcentrated flow (cf. Pierson, 2005). Hence, it could flow easily around the vegetation. These are only suggestions and further research (especially out in the field) could give a deeper understanding.

7.1.4 Uncertainties, Challenges, and Limitations

Although mapping shouldn’t be done only digitally as described in chapter 2.2, it was the only possibility for this thesis. As it was not possible to verify the mapping results in the field this could possibly lead to higher uncertainties and more misinterpretation.

It was very challenging to define the exact location where e.g. an *erosion zone* changes to a *transport zone*. Hence, an error of some meters must probably be taken into account and in reality, the changes are more likely smooth transitions. Also, the decision whether a potential section is a *transport zone* or only a debris plug (cf. Hungr, 2005; VanDine, 1996) was very difficult and here field observations could have helped to clarify this. Two examples for this are DF1 at 150 m

and DF2_3 at 135 m. In both cases, the decision for *transport zones* was based on the observation that the same surface texture was present inside and just next to the channel.

Also unsharp parts of the orthophoto, probably caused by wind during the drone flight (Vieli A., personal communication, 2021), the included vegetation in the DEM (cf. chapter 4.1.1 and 7.3.4), and the construction works at the pipeline, which may have dislocated material of the channel, enhanced the difficulties and uncertainties. Additionally, the lack of fully coverage of the study area with high resolution data, leads to different separation of some debris flow paths in upper, low resolution and lower, high resolution parts (cf. Figure 21). Thus, comparability of different zones is not always guaranteed along the flow path.

7.2 Channel analysis

7.2.1 Topographic Parameters

Table 7: Slope values of different zone changes for each debris flow. These values are mainly determined from the smoothed slopes used in the long profiles (cf. chapter 6.2).

	DF2_3	DF8_2	DF1	DF6
First transport zone	30*	15	27	18
Erosion end	23*	8	9,5	12
Deposition start	N/A	8	9,5	14
Deposition end	N/A	7	8	7,5

* this value is derived from the ArcticDEM due to unavailability of drone data at this location

In Table 7 the different slope values for the first zone occurrence, zone termination, or zone beginning are summarized. The same values are illustrated in Figure 35 according to their estimated total volume. For all debris flows, the first *transport zones* are mapped at clearly steeper parts, than the other three zones present. The end of the erosion slopes matches quite well with the proposed value of 10° by Hungr et al. (2005), above which erosion can occur. Only the value for DF2_3 is much higher, probably because of the very small, estimated event volume of ~30 m^3 (cf. Table 5). Due to the fact, that smaller debris flows can deposit on steeper slopes (cf. Corominas, 1996; Hungr et al., 2005), it is assumed that also erosion can end on steeper slopes. The slopes where deposition starts matches very well with the values mentioned and referred to in chapter 2.1.3. But these values seem to increase with rising volume. A possible explanation for this is the

damming of material back up the flow path by the debris in the front. When bigger volumes are involved, the material gets dammed even further up. The slopes at the deposition end on the other hand don't seem to be dependent on the volume and all range between 7° and 8°.

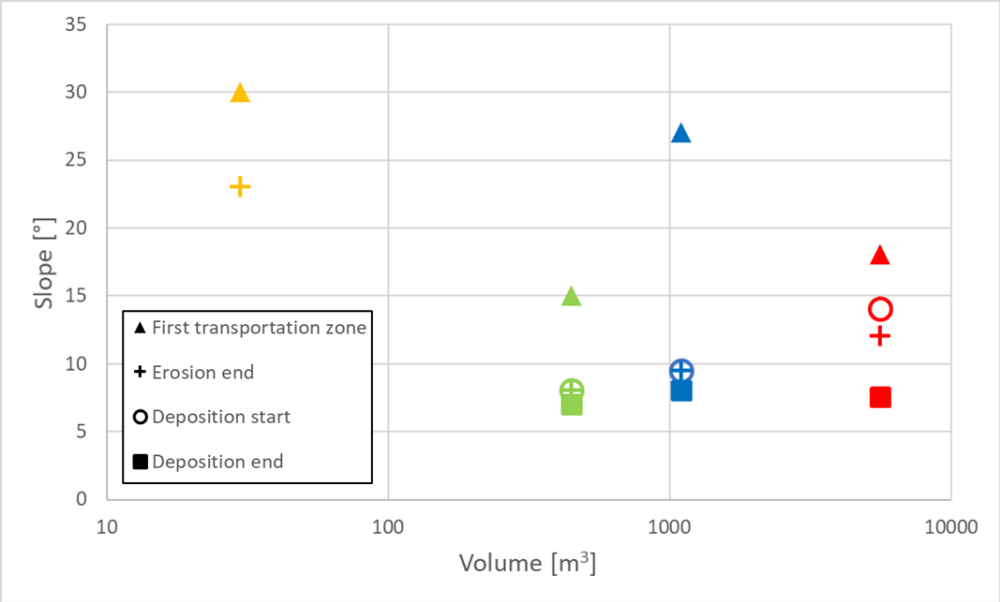

Figure 35: The slope values shown in Table 7 are plotted against the estimated debris flow. The colours indicate the different debris flows.

When comparing the slopes in the different debris flow zones (cf. Figure 25 – Figure 28), the pattern in the *transport zones* stands out. In most of the *transport zones* a rise of the slope values towards the end of the zone can be detected. For better comparison, the peaking slope in the first meters and the peaking slope in the last meters of the *transport zones* are summarized in Table 8. The values are derived from the already smoothed slope values (cf. chapter 5.2.3) as they are displayed in the long profiles. If the original slope data would be used, the differences would be even bigger. Due to the uncertainties regarding the channel zone classifications (cf. chapter 7.1.4), only the smoothed values are used. The data is visualized according to the runout ratio and the estimated debris flow volume in Figure 36.

Table 8: Slope values of different mapped transport zones. The debris flow, the location along the flow path, and the volume are shown for each transport zone. The slope peak around the beginning and the slope peak around the end, and their difference are listed for every transport zone.

	Location in long profile [m]	Peak slope at start [°]	Peak slope at end [°]	Difference [°]	Volume [m^3]
DF6	725	15	20	5	5600
DF6	845	11	15	4	5600
DF8_2	600	15	19	4	450
DF8_2	675	12.5	19	6.5	450
DF8_2	825	15	12	-3	450
DF8_2	975	8	18	10	450
DF2_3	135	25	29.5	4.5	30
DF2_3	215	26	27.5	1.5	30

The rise of the slope ranges between 1.5 ° and 10 ° with a mean value of 5° within the positive values. Only one *transport zone* shows the opposite behaviour of slope reduction. A possible explanation of this rise of the slope is that first a certain threshold of channel slope must be reached to gain enough energy to again erode material. This occurrence of an *erosion zone* after a *transport zone* is the case for most of the *transport zones* (cf. chapter 7.1.2). Although Hungr et al. (2005) describe very low correlation between erosion depth and slope from data of the Queen Charlotte Island database, it seems to be connected in this presented case. Between the difference values neither a correlation with the debris flow volume nor a correlation with the total run out length seems to be detectable.

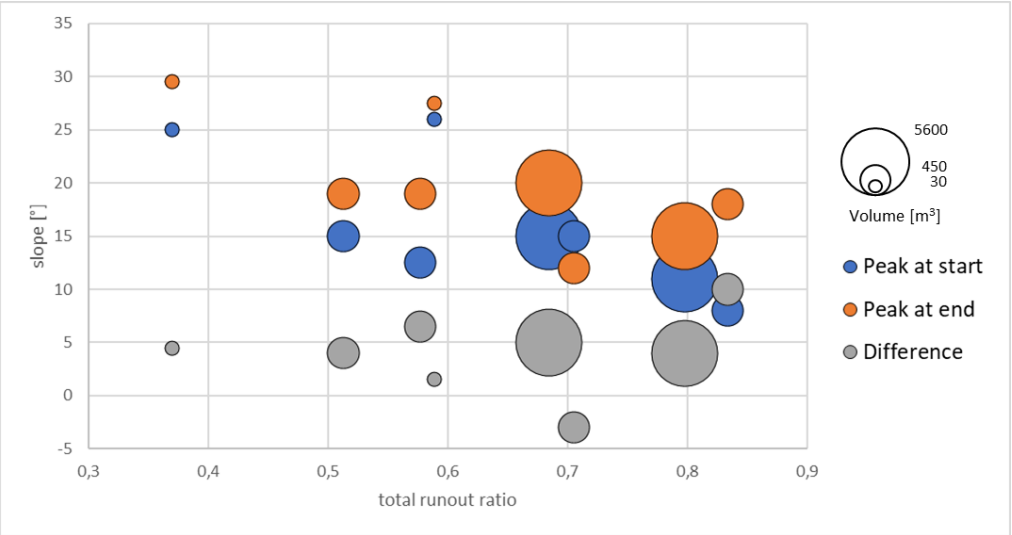

Figure 36: Relationship of transport slopes against total runout ratio. The circle size indicates the estimated volume of the respective debris flow. The difference of slope (grey) of the peak around the beginning (blue) and the end (orange) of transport zones. The exact values are shown in Table 8.

7.2.2 Geometric Parameters

When comparing the debris flow zones with the geometric measurements, it becomes clear, that the deepest and widest channel sections occur in the *erosion zones*. This makes purely sense, regarding the definition of *erosion zone* (cf. chapter 5.1.3) and due to its nature of entraining loose material from the bed and the sidewalls (cf. Hungr, 2005).

In the *transport zones* other relations to the geometry values are detected. The channel depth often shows local minimums where a *transport zone* is mapped. This is very nicely visible in e.g. DF2_3 at the 135 m and 215 m mark or DF6 at 725 m travel distance (cf. Figure 26 and Figure 27). The values tend to zero without reaching it. When regarding the *real channel depth*, which is the *levee height* subtracted from the *channel depth,* this tendency of very low channel depth is even much higher, as visible in the examples mentioned before. Even positive channel depths are presented, which is caused by the measuring methods used (cf. chapter 5.2.1). This observation of low channel depths in *transport zones* supports the assumption of very low erosion in *transport zones*

Peaks in channel width can be observed only for three of the *transport zones*. Such a behaviour of widened channel is mentioned in Hungr (2005) and Schürch (2011). In these studies it is related to a possible build-up of temporary levees, boulder pockets, and in-channel depositions. In the present thesis it seems as if the channel width is not the only factor influencing the occurrence of *transport zones*.

Generally, the height and width values in the terminal *deposition zones* display the different forms of the deposition lobes pretty well. They mostly show higher values in the middle part or towards the end of the depositions. These observations and measurements match very well with the results and examples provided in Haas et al. (2015 c). In a study carried out by Bernhardt et al. (2017) on Svalbard, recurring periods of debris flows were investigated and the temporal evolution of colluvial fans was looked at. They measured about 0.4 m deposition height in an excavated hole, of an approximately 440 m^3 deposition lobe. This measurement is described to be comparable to other major deposition lobes in the investigated area, where they also measured levee heights of 0.4 m. This deposition and levee heights match very well with the measured values on Disko Island, regarding the debris flow volume.

7.2.3 Maximum Channel Capacity

In all the long profiles a clear similarity of maximum discharge and wetted area can be seen. This makes purely sense, when looking at the formula used to calculate Qmax (cf. chapter 2.1.5). However, the wetted area seems to be dependent on the channel depth, as they show almost the same behaviour along the flow paths. This would mean, that the Qmax values are highly dependent on the channel depth. With this coherence, the low values of Qmax in *transport zones* can be explained with the small channel depths present. At the same time, it seems, that channel widening doesn't necessarily have a big influence on the Qmax rise. This stands a bit in contrast to the proposition of Wehrli (2019), who stipulates the channel width as a big influencing factor on the discharge.

The velocity seems to be more dependent on the wetted perimeter as e.g. DF1 shows extremely nice. Furthermore, the wetted perimeter displays the behaviour of the channel width along the flow path.

In general, the maximum discharge decreases along the flow path, due to its dependence on the channel cross section, which decreases with longer travel distance.

7.2.4 Uncertainties, Challenges, and Limitations

Analysing the cross profiles and determining the correct start and endpoint for the parameters measures was a main challenge in this part of the thesis and is probably prone to errors. This applies also to the whole process of long profile generation, where a lot of measurements in different programs and on different datasets

have been done. Further, a lot of different calculations, methods, and processes (cf. chapter 5.2) are applied and joined in the construction of the long profiles.

The method used to calculate the maximum discharge and velocity after Henderson (1966) shows this high dependency on the wetted area and on the channel depth. Therefore, the availability of very accurate data (cf. Wehrli, 2019), determinations or calculations of these values is crucial for this method. Hence it is clear, that small changes or errors when e.g. defining the bank full height, have very high influence on Qmax. Also, the usage of a bankfull height does not represent reality correctly. Due to superelevation (visible schematic in Figure 17) especially in curves, flow heights might differ (e.g. Hungr, 2005; cf. cross profiles in Schürch et al., 2011). As the bankfull scenario only takes the lower levee into account, this leads to an partial underestimation of Amax and Qmax. This is probably partly compensated in steep parts, by the overestimations described in chapter 5.2.

7.3 Numerical Modelling

7.3.1 Parameter Settings

For the model runs without using the entrainment module there was found one most plausible parameter set for each debris flow (cf. Appendix 12.4.2). This is not always true when including the entrainment model. During the calibration and exploration process for DF6 and DF2_3, two parameter sets were found, which produce very similar results regarding the run out length and total volume.
Due to the inclusion of the erosion model more parameters gained in importance and in sensitivity. The initiation volume and maximum discharge are two examples for this. Their changes had lower influence on the results without the entrainment model. But they became very sensitive using the erosion module and therefore complicated the calibration process. The example of DF6 shows that a reduction of the initiation volume can be compensated with higher Qmax values and vice versa, without changing the erosion volume mainly. This works, because with a higher Qmax value more erosion takes place and thus the debris flow grows much quicker. However, this other parameter setup does not consider the relationship between total volume and maximum discharge described by Rickenmann (1999) anymore. Therefore it is not used as a main result in this thesis and not further described. This different values of initiation volume and Qmax can be compared in Table 6 and in Appendix 12.4.1.

As mentioned and visible in the results, an obstacle polygon was necessary to reproduce DF6 adequately. At this obstacle, the debris flow is deflected and therefore, the relatively high max flow height at its margins is produced. Without this unpassable zone for the debris flow, the debris material would have flowed to the west, and partly out of the calculation domain. This is visible in a simulation run without the obstacle, illustrated in Appendix 12.4.1. For this simulation, the same input parameters were used as for the most plausible parameter set of DF6.
A very similar behavior is detected in the simulated depositions of DF1, where a great part of the simulated deposits next to the mapped depositions (cf. Figure 30). The simulated debris tends to flow off the real depositions, which makes purely sense. So it can be assumed, that the need of the obstacle for DF6 is caused by modelling on a post-event terrain. The issue that the modelling needs to be done on post-event DEM is a common problem, because detailed data is often only measured after a debris flow event (McArdell B., personal communication, 2020).

7.3.2 Modelling Outputs

For DF1 great parts of the simulated debris is deposited in the lower part of the mapped depositions, while on the upper mapped deposition areas almost no debris depositions are simulated. This behavior supports the assumption of a multi-surge event, as discussed in chapter 7.1.1. Hence, different volumes and friction parameter would be needed for the modelling for every surge. In RAMMS it would actually be possible to model surging debris flows, where the terrain could be changed according to the erosion and depositions after every surge, as described in Bartelt et al. (2017) and used in the study of Frank et al. (2015). Such complicated modelling scenarios would have exceeded the scope of this thesis and are therefore not undertaken. However, when comparing the max flow height with the mapped deposition areas of DF6, the channel break out locations of the upper, western depositions are still modelled very well and also its run out length matches pretty good (cf. Figure 29).

To simulate DF8_2 fairly well, the erosion parameter needed to be changed. Otherwise too much erosion occurred, and the total debris flow volume would have been too big. Also, with the current most plausible parameter set the modelled volume is 590 m^3. The estimated volume from mapping is 456 m^3 and with this volume it was possible to find a reliable most plausible parameter set, when the entrainment model is not used (cf. Appendix 12.4.2). However, these low erosion

parameters are not impossible, but still there had to be done lot of changes on them. If the two areas around 1000 m travel distance would definitely be depositions from the event in 2014, the estimated total volume would have been higher. With an assumed deposition height of 0.3 m, which is slightly higher than the other depositions surrounding, they would contribute around 80 m^3 of debris material. This is not too much, but the estimated and simulated total volumes would match a bit better. However, another possibility could be, to lower the initiation volume in the input hydrograph even more and therefore the erosion rates would also decrease (cf. Frank et al., 2017). A second option may have been to rise the critical shear stress value for all erosion polygons due to the small modelling volumes as described in Frank et al. (2015).

7.3.3 Erosion and Deposition Pattern

When looking at the erosion pattern of the simulated debris flows the effect of higher erosion rates in narrow channel parts (e.g. DF8_2: 535 m and 660 m) and lower erosion rates at wider channel parts (e.g. DF8_2: 700 m) becomes obvious. This behavior fits the statements of Frank et al. (2017), that locally higher shear stress causes more erosion in narrow channel parts. Similar patterns of erosion and deposition related to channel width are shown and described in Schürch et al. (2011).

For most of the mapped *transport zones* a local decrease of erosion is detectable. This is true for DF2_3: 135 m, DF6: 725 m and DF8_2: 615 m, 700 m, 825 m. Locally the erosion gets at minimum lowered about 50%, compared to the erosion rates before and afterwards. For half of all the *transport zones* also a clear decrease of flow height, velocity, and shear stress is calculated. This behavior of value drops can only partly be related to the wider channel sections and correspond to the suggestion of Frank et al. (2017), that channel widening is not the only influencing factor. However, for the *transport zone* in DF2_3: 215 m and DF6: 860 m no decrease is assessed, while for DF6 at two locations (~500 m, ~650 m) such decrease is simulated but no *transport zone* is mapped.

DF2_3 has a very long *transport zone* until the end, which is not followed by an *erosion zone* again. Around the change from *erosion zone* to the *transport zone* at 250 m, a clear drop of simulated erosion and velocity values are detected, while the flow height doesn't change. Just after 250 m travel distance, the first polygon of partly damaged vegetation is drawn. The erosion depths here are mainly below 0.05 m and the shear stress below 1.5 kPa. It is therefore suggested that it is

possible for the vegetation to resist such low shear stress and erosion depths. This would match the observations and assumptions discussed in chapter 7.1.3. However, the erosion and the velocity are only calculated until approximately 300 m. Also, for the whole debris flow very low small volumes and flow heights are calculated. When applying the lower flow height threshold of 0.1 m also the maximum flow height terminates around 300 m travel distance. Therefore, it is suggested, that although the values changes distinctively at this *transport zone*, it seems like this debris flow case is at the edge of the modelling possibility of RAMMS.
It must be remarked for DF2_3 that the calibration was done without applying the minimum deposition height of 0.1 m.

7.3.4 Uncertainties, Challenges, and Limitations

The mentioned influence of the vegetation on the DEM in chapter 4.1.1 is also important for modelling. On the one hand, it can contain "channels" (cf.

Figure 13) or "levees", produced by vegetation. These would not confine the debris flow like e.g. levees do this (cf. Hungr, 2005). On the other hand, it can serve as much denser erosion material in the simulation, as vegetation would in reality be. Therefore, it can be summarized, that the vegetation influences not only the investigations and measurements for the distribution and channel analysis, but also is a major challenge for modelling. To cope with this issue, the orthophoto is an important data source to clarify things.

The estimation of the debris flow volumes from the available data only, was quite difficult, although the resolution of the drone DEM was very good and the estimated deposition heights match with the ones of Bernhardt et al. (2017) as discussed in chapter 7.2.2. Therefore, this must be treated as a source for errors, with a big influence on debris flow modelling. Here, field work could have provided important measurements and information for better volume estimations.

The calibration of the model was the main challenge in this part of the thesis. And especially the calibration of the friction parameter is crucial (Bartelt et al., 2017). While the influence of μ was mostly very dominant and obvious on the run out, this was not true for ξ. This behaviour can be comprehended in Figure 20 and explained with the high influence of ξ when the debris flow is at high speed. This observation and interpretation is also made in the RAMMS sensitivity analysis of Frank et al. (2017).

To correctly and more precisely calibrate ξ, additional data like velocities or travel times would be needed (cf. Bartelt et al., 2017; Frank et al., 2015; Frank et al., 2017). The absence of such data is a common problem (McArdell B., personal communication, 2021) as also mentioned in e.g. in Frank et al. (2015).

One limitation in this thesis (as already discussed in chapter 7.1.4 and 7.2.4) is the lack of drone data coverage for the upper parts and *initiation zones* of the debris flows. If the initiation areas could have been identified, the block release method in RAMMS could have been used. This method is better suited for small debris flow volumes (Deubelbeiss & Graf, 2013) and in combination with the entrainment model, this probably could have produced very good or even better results for Disko Island debris flows. The block release method was adequately applied to similar debris flow volumes in Switzerland by Frank et al. (2017) and produced reliable results.

During comparison of the mapped debris flow zones with the modelling outputs it was noticeable, that the mapped channel centre lines and the simulated e.g. max flow heights sometimes don't match very well, with its meandering behaviour (cf. Figure 37). This probably shows the limits and subjectivity of the used mapping approach.

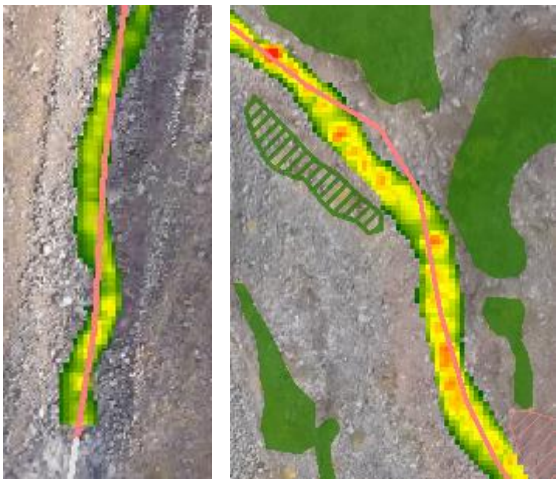

Figure 37: Mismatching of mapped centre line and modelled "meandering" max flow height at the example of DF8_2.

8 Conclusion

One of the main goals of this thesis was to investigate debris flow dynamics in relation to geometry in an arctic environment. Within this, the spatial patterns of erosion, transportation, and deposition were the main focus and were addressed with a range of different methods such as high resolution mapping, detailed geometric analysis, and numerical modelling. Combining these methods allowed detailed insights into the interaction between geometry and debris flow behavior as well as the current capabilities of debris flow models. The main findings of this thesis are summarized and concluded by answering the posed research questions the following.

Spatial Distribution Analysis

RQ 1: *What debris flow features, debris flow zones, and vegetation cover classes can be found in the study area? How are they spatially distributed and how do they relate to each other?*

For most of the investigated debris flow paths it was possible to map all the typical debris flow features such as eroded channels, levees, and terminus depositions and they could be categorized into zones of *erosion*, *transport*, and *deposition*. In the upper channel sections erosion was typically the dominant process. In the lower half of the flow paths, several relatively short *transport zones* (< 50 m) were found, sometimes alternating with *erosion zones*. Another possible trend shows that with increasing debris flow volumes the *transport zones* occur further downstream. The mapped and categorized vegetation was a useful indicator to determine the different debris flow zones as it was generally absent in *erosion zones* and sometimes present in *transport zones*.

Channel Analysis

RQ 2: *What is the mutual relationship between the spatial pattern of debris flow erosion, transport, and deposition zones and the maximum channel capacity and topographic and geometric channel parameter along the debris flow paths?*

The observed topographic and geometric patterns along the debris flow paths, are consistent with values from the literature. Principally these geometric channel parameters continuously decrease with travel distance and decreasing slope. In general, the biggest channel depths and widths were measured for the *erosion zones*.

Also, the steepest slopes are measured in *erosion zones* and they terminate at slopes between 8° and 23°. In *transport zones* often very low channel depths are observed with occasional vegetation cover within the channel, which indicates low to no erosion in these areas. In this *transport zones* the slopes are generally lower than in the *erosion zones*. From the beginning to the end for most of the *transport zones*, the slopes increase approximately 5°, until it typically changes to an *erosion zone* again. The terminal *deposition zones* end at slopes of around 7° - 8°, while the slopes at the deposition onset vary considerably and is possibly dependent on the event volume. Finally, the maximum channel discharge capacity calculated from channel geometry data shows a general decrease along the flow path. However, this estimate is strongly dependent on the cross-sectional area and thereby extremely sensitive to the channel depth. Thus, for such calculations, exact geometry measurements are crucial.

Numerical Modelling

RQ 3: *What parameter settings are needed, to model some of the debris flows and their spatial patterns of erosion and transportation adequately with the RAMMS debris flow and entrainment model?*

This study shows that it is possible to simulate the investigated debris flows and related flow zones on Disko Island with RAMMS adequately. Using the entrainment module, useful results can be produced and the patterns of erosion and transportation are in general well simulated with the model. To simulate the debris flows accurately, for one debris flow an obstacle polygon was necessary to keep it on track and for another debris flow very low erosion parameter values were necessary. For some of the debris flows, two most plausible parameter sets could be found that matched the observations well and possibly there are further parameter sets which would produce similar results.

The modelling also showed that at the mapped *transport zones* the values of max flow height, velocity, erosion, and shear stress are typically lowered. Although erosion is modelled in this zones it shows a noteworthy local reduction of at least 50%. So, if the mapped *transport zones* are correct, the model is able to calculate these patterns very well.

If there would be more information and data available (e.g. from field measurements), more detailed model calibrations could be undertaken and model

parameter be better constrained, which would benefit also the performance of the simulations.
Overall, it seems like the modelled erosion patterns and depths agree well with the measured channel parameter and support the models ability to simulate erosion.

Disko Island Debris Flow Zones

MRQ: *How can the erosion, transportation, and deposition patterns of Disko Island debris flows be characterized, described, and differentiated, according to their spatial distribution, channel geometry, and modelling outputs?*

Summarizing the three subtopics from above, the investigated debris flow zones and the findings of their characteristics can be described and differentiated over all as following:

Transport Zone:

- Are often located in the lower half of the flow path and with increasing debris flow volumes they occur further downstream.
- Often low channel depths and sometimes channel width peaks are measured.
- Most of the time, within *transport zones* a slope rise (mean value of 5°) is detected and they are generally shorter than 50 m.
- Model outputs often show locally lower max flow heights, velocities, erosion depths, and shear stress values.
- Sometimes alternating behavior with *erosion zones* can be detected.
- Sometimes only *partly destroyed vegetation* can be observed.
- Often a levee is present at least on one side.

Erosion Zone:

- Regularly contains steepest, deepest, and widest channel sections.
- Is dominant in the upper half of the flow path.
- Erosion depth generally decreases along the flow path.
- Terminate at slopes between 8° and 23°
- In narrower sections, the erosivity is higher.
- In lower channel parts levees are mostly present besides the channel.

Deposition Zone:

- Typically located as the last zone.
- Ends at slopes around 7° - 8°.
- Often contains typical debris lobe forms, with greatest widths and heights in the last half of the lobe.
- Match more or less with the modelled depositions.

Over all, it could be shown that the results of the different methods used within the three subtopics show a good mutual correlation. They generally indicate a similar spatial pattern of erosion, transportation, and deposition along the debris flow paths. Hence, they can be applied in further research areas alone or in combination with each other for the investigation of debris flow channels.

Especially zones of high and low erosion can change within short distances and even several time. With changing erosivity the volume gain of a debris flow along the flow path is influenced. The debris flow volume is one of the major parameters influencing the run out length and is therefore crucial whether a debris flow can reach inhabited areas or infrastructure (Corominas, 1996; Fannin & Wise, 2001; Hungr, 2005). Hence, understanding the patterns of this changes and their reasons, can be valuable information regarding numerical modelling and hazard assessment.

Additionally, the values extracted for the end of erosion and the beginning of deposition match with the values indicated in the literature, although the big uncertainties described remain. Nevertheless, the number of debris flows which were investigated according to these values could be increased with this thesis, and this especially for rather small debris flows in the arctic region. In general, this thesis contributes with its descriptions and results to the few studies in arctic region, especially also including numerical modelling of debris flows. Moreover, it was possible to apply the RAMMS erosion module successfully on rather small debris flows. The results increase the trust in the models ability to properly model erosion processes of debris flows. Although, when simulating very small volumes and its low flow heights, the limits of RAMMS, modelling the debris flows adequately, are probably reached.

9 Outlook

The characteristics and descriptions of the investigated zones are not final and not fully understood. Some reasons for the appearances and behaviours of several parameters are suggested in this thesis, based on the observations on Disko Island. Further investigation should be done on erosion and non-erosion patterns for other debris flow channels with different (particularly larger) event magnitudes. Especially the rise of the slope within the *transport zones* thereby should be studied in more detail, to find out if this observation is more generally valid.
For future investigations high resolution drone data can serve as a very important data source, especially if they cover the whole flow paths. Such further surveys should also be combined with field investigations to generate more reliable results.

Another topic to concentrate on in future studies could be the patterns of total or partly destroyed vegetation by debris flows. Cases where vegetation only gets partly destroyed, could give insights into the behaviour of debris flows, as this is probably just at the edge before erosion would occur. Making simple strength test of the vegetation and looking at their rooting depth could probably deliver important data to improve debris flow models like RAMMS, especially for its entrainment module.

Investigating recurrence periods and triggering reasons for Disko Island debris flow events and looking at possible changes of ground and variable disposition by climatic changes, would be another interesting topic to focus on.

10 Acknowledgement

I would like to thank everyone who was part of this master thesis journey:

First, Prof. Dr. Andreas Vieli and Dr. Brian McArdell for answering all my questions and supporting me with many good discussions and hints. Further, Alessandro Cicoira and Philipp Rastner for giving me new ideas and answering my questions. The WSL, SLF and the whole RAMMS team for the possibility to use the software and quick support, if something went wrong. A special thanks to Anna, for reading through, correcting, commenting, and polishing up my thesis. Also, thanks to Hans for revising and commenting my maps and graphs and thanks to Resli for commenting my python scripts. And finally, thanks to my family, friends, flatmates, and especially Kim, for support and distraction, when motivation was low.

11 References

Bartelt, P., Bieler, C., Bühler, Y., Christen, M., Deunelbeiss, Y., Graf, C., McArdell, B., Salz, M., & Schneider, M. (2017). RAMMS Debrisflow User Manual. In *WSL-SLF*.

Berger, C., McArdell, B. W., & Schlunegger, F. (2011). Direct measurement of channel erosion by debris flows, Illgraben, Switzerland. *Journal of Geophysical Research: Earth Surface*, *116*(1). https://doi.org/10.1029/2010JF001722

Bernhardt, H., Reiss, D., Hiesinger, H., Hauber, E., & Johnsson, A. (2017). Debris flow recurrence periods and multi-temporal observations of colluvial fan evolution in central Spitsbergen (Svalbard). *Geomorphology*, *296*, 132–141. https://doi.org/10.1016/j.geomorph.2017.08.049

Bierman, P. R., & Montgomery, D. R. (2014). *Key concepts in geomorphology*.

Brown, J., Ferrians Jr., O. J., Heginbottom, J. A., & Melnikov, E. S. (1997). *Circum-Arctic map of permafrost and ground-ice conditions*. https://doi.org/10.3133/cp45

Chevalier, G. G., Medina, V., Hürlimann, M., & Bateman, A. (2013). Debris-flow susceptibility analysis using fluvio-morphological parameters and data mining: Application to the Central-Eastern Pyrenees. *Natural Hazards*, *67*(2), 213–238. https://doi.org/10.1007/s11069-013-0568-3

Christen, M., Bühler, Y., Bartelt, P., Leine, R., Glover, J., Schweizer, A., Graf, C., Mcardell, B. W., Gerber, W., Deubelbeiss, Y., & Feistl, T. (2012). Integral Hazard Management Using a Unified Software Environment Numerical Simulation Tool "RAMMS." *Congress Interpraevent*, 77–86.

Christen, M., Kowalski, J., & Bartelt, P. (2010). RAMMS: Numerical simulation of dense snow avalanches in three-dimensional terrain. *Cold Regions Science and Technology*, *63*(1–2), 1–14. https://doi.org/10.1016/j.coldregions.2010.04.005

Cooke, R. U., & Doornkamp, J. C. (1990). *Geomorphology in environmental management, A New Introduction*. Clarendon Press.

Corominas, J. (1996). The angle of reach as a mobility index for small and large landslides. *Canadian Geotechnical Journal*, *33*(2), 260–271. https://doi.org/10.1139/t96-005

Costard, F., Forget, F., Jomelli, V., Mangold, N., & Peulvast, J.-P. (2009). Debris flows in Greenland and on Mars. *The Geology of Mars*, *January*, 265–278. https://doi.org/10.1017/cbo9780511536014.011

Costard, F., Mercier, D., & Peulvast, J. (2001). *Debris Flows on Mars : Comparison with Terrestrial Analogs*. *February 2014*, 1–3.

De Haas, T., Kleinhans, M. G., Carbonneau, P. E., Rubensdotter, L., & Hauber, E. (2015 a). Surface morphology of fans in the high-Arctic periglacial environment of Svalbard: Controls and processes. *Earth-Science Reviews*, *146*, 163–182. https://doi.org/10.1016/j.earscirev.2015.04.004

De Haas, T., Hauber, E., Conway, S. J., van Steijn, H., Johnsson, A., & Kleinhans, M. G. (2015 b). Earth-like aqueous debris-flow activity on Mars at high orbital obliquity in the last million years. *Nature Communications*, *6*(May), 1–6. https://doi.org/10.1038/ncomms8543

De Haas, T., Braat, L., Leuven, J. R. F. W., Lokhorst, I. R., & Kleinhans, M. G. (2015 c). Effects of debris flow composition on runout, depositional mechanisms, and deposit morphology in laboratory experiments. *Journal of Geophysical Research F: Earth Surface*, *120*(9), 1949–1972. https://doi.org/10.1002/2015JF003525

De Haas, T., McArdell, B. W., Conway, S. J., McElwaine, J. N., Kleinhans, M. G., Salese, F., & Grindrod, P. M. (2019). Initiation and Flow Conditions of Contemporary Flows in Martian Gullies. *Journal of Geophysical Research: Planets*, *124*(8), 2246–2271. https://doi.org/10.1029/2018JE005899

Deubelbeiss, Y., & Graf, C. (2013). Two different starting conditions in numerical debris flow models–Case study at Dorfbach, Randa (Valais, Switzerland). *GRAF, C.(Red.) Mattertal–Ein Tal in Bewegung*, 125–138. http://www.wsl.ch/wsl/dienstleistungen/publikationen/pdf/12488.pdf

Dramis, F., Guida, D., & Cestari, A. (2011). Nature and aims of geomorphological mapping. In *Developments in Earth Surface Processes* (Vol. 15). Elsevier B.V. https://doi.org/10.1016/B978-0-444-53446-0.00003-3

ESRI. (2019). *Understanding representation rules*. https://desktop.arcgis.com/en/arcmap/10.6/map/working-with-layers/understanding-representation-rules.htm

Fannin, R. J., & Wise, M. P. (2001). An empirical-statistical model for debris flow travel distance. *Canadian Geotechnical Journal*, *38*(5), 982–994. https://doi.org/10.1139/cgj-38-5-982

FOEN. (2016). Protection against Mass Movement Hazards. Guideline for the integrated hazard management of landslides, rockfall and hillslope debris flows. Federal Office for the Environment, Bern. *The Environment in Practice*, *1608*, 97.

Frank, F., McArdell, B. W., Huggel, C., & Vieli, A. (2015). The importance of entrainment and bulking on debris flow runout modeling: Examples from the Swiss Alps. *Natural Hazards and Earth System Sciences*, *15*(11), 2569–2583. https://doi.org/10.5194/nhess-15-2569-2015

Frank, F., McArdell, B. W., Oggier, N., Baer, P., Christen, M., & Vieli, A. (2017). Debris-flow modeling at Meretschibach and Bondasca catchments, Switzerland: Sensitivity testing of field-data-based entrainment model. *Natural Hazards and Earth System Sciences*, *17*(5), 801–815. https://doi.org/10.5194/nhess-17-801-2017

Frederiksen, J. D., Hass, A. E., Hoffmann, A. H., Karkauskaite, P., Larsen, B. G., Mariager, T., Nissen, E. L., & Ramos, M. M. (2014). *Active Layer Modelling and Flocculation Processes in the Disko Area, West Greenland*.

French, H. M. (1988). The periglacial phenomena: ancient and modern. *Journal of Quaternary Science*, *3*(1), 110 pp.

GEM. (2018). *DiskoBasis Meteorology*. Greenland Ecosistem Monitoring (GEM). https://data.g-e-m.dk/

GEUS. (2021). *Geological Maps 1:500 000*. Geological Survey of Denmark and Greenland. http://maps.greenmin.gl/geusmap/?mapname=greenland_portal&lang=en#baslay=baseMapEsriImagery&optlay=&extent=-95397.39258228126,7741492.077729935,-47450.08435408891,7764391.911920171&layers=northpole_graticule,grl_geus_500k_geology_map

Google Earth. (2013). *Qeqertarsuaq, Greenland*. 69°15’52.03"N, 53°32’32.62"W. Maxar Technologies. Accessed: 09.05.2020.

Google Earth. (2015). *Qeqertarsuaq, Greenland*. 69°15’52.03"N, 53°32’32.62"W. Maxar Technologies. Accessed: 09.05.2020.

Hansen, M. A. (2011). *Methane dynamics in a permafrost landscape at Disko Island, West Greenland*.

Henderson, F.M. (1966). *Open channel flow* (pp. 522). Macmillan Publishing Co., INC.

Hubbard, B., & Glasser, N. (2005). *Field Techniques in Glaciology and Glacial Geomorphology*. J. Wiley & Son.

Hungr, O. (2005). Classification and terminology. In M. Jakob & O. Hungr (Eds.), *Debris-flow Hazards and Related Phenomena* (pp. 9–24). Springer Berlin Heidelberg. https://doi.org/10.1007/b138657

Hungr, O., McDougall, S., & Bovis, M. (2005). Entrainment of material by debris flows. In M. Jakob & O. Hungr (Eds.), *Debris-flow Hazards and Related Phenomena* (pp. 135–158). Springer Berlin Heidelberg. https://doi.org/10.1007/b138657

Iverson, R. M. (1997). The physics of debris flows. *Review of Geophysics*, *35*(97), 245–296.

Iverson, R. M., Reid, M. E., Logan, M., LaHusen, R. G., Godt, J. W., & Griswold, J. P. (2011). Positive feedback and momentum growth during debris-flow entrainment of wet bed sediment. *Nature Geoscience*, *4*(2), 116–121. https://doi.org/10.1038/ngeo1040

Jakob, M., & Hungr, O. (2005). Introduction. In Matthias Jakob & O. Hungr (Eds.), *Debris-flow Hazards and Related Phenomena* (pp. 1–7). Springer Berlin Heidelberg. https://doi.org/10.1007/b138657

Kienholz, H. (1995). Gefahrenheurteilung und -bewertung - auf dem Weg zu einem Gesamtkonzept. *Schweiz. Z. Forstw.*, *146*(9), 701–725.

Knight, J., Mitchell, W. A., & Rose, J. (2011). Geomorphological Field Mapping. In *Developments in Earth Surface Processes* (Vol. 15). Elsevier B.V. https://doi.org/10.1016/B978-0-444-53446-0.00006-9

Kroon, A., & Sigsgaard, C. (2014). *Arctic Station Annual Report 2014*. Board of the Arctic Station, University of Copenhagen, Denmark.

Kroon, A., & Sigsgaard, C. (2017). *Arctic Station Annual Report 2017*. Board of the Arctic Station, University of Copenhagen, Denmark.

Larsson, S. (1982). Geomorphological Effects on the Slopes of Longyear Valley , Spitsbergen , after a Heavy Rainstorm in July 1972. *Geografiska Annaler*, *64*(3), 105–125.

Morino, C., Conway, S. J., Balme, M. R., Hillier, J., Jordan, C., Sæmundsson, Þ., & Argles, T. (2019). Debris-flow release processes investigated through the analysis of multi-temporal LiDAR datasets in north-western Iceland. *Earth Surface Processes and Landforms*, *44*(1), 144–159. https://doi.org/10.1002/esp.4488

Pierson, T. C. (2005). Hyperconcentrated flow - transitional process between water flow and debris flow. In M. Jakob & O. Hungr (Eds.), *Debris-flow Hazards and Related Phenomena* (pp. 159–202). Springer Berlin Heidelberg. https://doi.org/https://doi.org/10.1007/b138657

Porter, C., Morin, P., Howat, I., Noh, M.-J., Bates, B., Peterman, K., Keesey, S., Schlenk, M., Gardiner, J., Tomko, K., Willis, M., Kelleher, C., Cloutier, M., Husby, E., Foga, S., Nakamura, H., Platson, M., Wethington Jr., M., Williamson, C., … Bojesen, M. (2018). *ArcticDEM* (V1 ed.). Harvard Dataverse. https://doi.org/doi/10.7910/DVN/OHHUKH

Regmi, N. R., Giardino, J. R., Mcdonald, E. v, & Vitek, J. D. (2015). A Review of Mass Movement Processes and Risk in the Critical Zone of Earth. In *Principles and Dynamics of the Critical Zone* (Vol. 19). Elsevier B.V. https://doi.org/10.1016/B978-0-444-63369-9.00011-2

Rickenmann, D. (1999). Empirical Relationships for Debris Flows. In *Natural Hazards* (Vol. 19).

Rickenmann, D. (2005). Runout prediction methods. In M. Jakob & O. Hungr (Eds.), *Debris-flow Hazards and Related Phenomena* (pp. 305–324). Springer Berlin Heidelberg. https://doi.org/10.1007/b138657

Schraml, K., Thomschitz, B., Mcardell, B. W., Graf, C., & Kaitna, R. (2015). Modeling debris-flow runout patterns on two alpine fans with different dynamic simulation models. *Natural Hazards and Earth System Sciences*, *15*(7), 1483–1492. https://doi.org/10.5194/nhess-15-1483-2015

Schürch, P. (2011). *Debris-flow erosion and deposition dynamics*. Durham Uiversity

Schürch, P., Densmore, A. L., Rosser, N. J., & McArdell, B. W. (2011). Dynamic controls on erosion and deposition on debris-flow fans. *Geology*, *39*(9), 827–830. https://doi.org/10.1130/G32103.1

Sidle, R. C., & Ochiai, H. (2006). *Landslides: Processes, Prediction, and Land Use* (Vol. 18). American Geophysical Union. https://doi.org/10.1029/WM018

Smith, M. J. (2011). Digital Mapping. Visualisation, Interpretation and Quantification of Landforms. In *Developments in Earth Surface Processes* (Vol. 15). Elsevier B.V. https://doi.org/10.1016/B978-0-444-53446-0.00008-2

Svennevig, K. (2019). Preliminary landslide mapping in Greenland. *Geological Survey of Denmark and Greenland Bulletin*, *43*(June), 1–5. https://doi.org/10.34194/GEUSB-201943-02-07

The SciPy community. (2021). *scipy.signal.savgol_filter*. Accessed: 20.01.2021. https://docs.scipy.org/doc/scipy/reference/generated/scipy.signal.savgol_filter.html

Turnbull, B., Bowman, E. T., & McElwaine, J. N. (2015). Debris flows: Experiments and modelling. *Comptes Rendus Physique*, *16*(1), 86–96. https://doi.org/10.1016/j.crhy.2014.11.006

University of Copenhagen. (2021). *About Arctic Station*. https://arktiskstation.ku.dk/english/about/

VanDine, D. F. (1996). Debris Flow Control Structures for Forest Engineering. In *British Columbia*.

Vieli, A. (2019). *Drone Data from Disko Island*.

Walker, D. A., Reynolds, M. K., Daniëls, F. J. A., Einarsson, E., Elvebakk, A., Gould, W. A., Katenin, A. E., Kholod, S. S., Markon, C. J., Melnikov, E. S., Moskalenko, N. G., Talbot, S. S., Yurtsev, B. A., Bliss, L. C., Edlund, S. A., Zoltai, S. C., Wilhelm, M., Bay, C., Gudjónsson, G., … Vairin, B. A. (2005). The Circumpolar Arctic vegetation map. *Journal of Vegetation Science*, *16*(3), 267–282. https://doi.org/10.1111/j.1654-1103.2005.tb02365.x

Weber, D. (2004). *Untersuchungen zum Fliess- und Erosionsverhalten granularer Murgänge* (pp 336). Birmensdorf, Eidgenössische Forschungsanstalt WSL.

Wehrli, S. (2019). *The influence of digital elevation model data on debris flow runout modelling*. Uniersity of Zurich

Wilken, M., & Mienert, J. (2006). Submarine glacigenic debris flows, deep-sea channels and past ice-stream behaviour of the East Greenland continental margin. *Quaternary Science Reviews*, *25*(7–8), 784–810. https://doi.org/10.1016/j.quascirev.2005.06.004

Zimmermann, M., Mani, P., & Romang, H. (1997). Magnitude-frequency aspects of alpine debris flows. *Eclogae Geologicae Helvetiae*, *90*(3), 415–420. https://doi.org/10.5169/seals-168173

12 Appendix

12.1 Overview Map of the Study Area with the Mapped Debris Flows

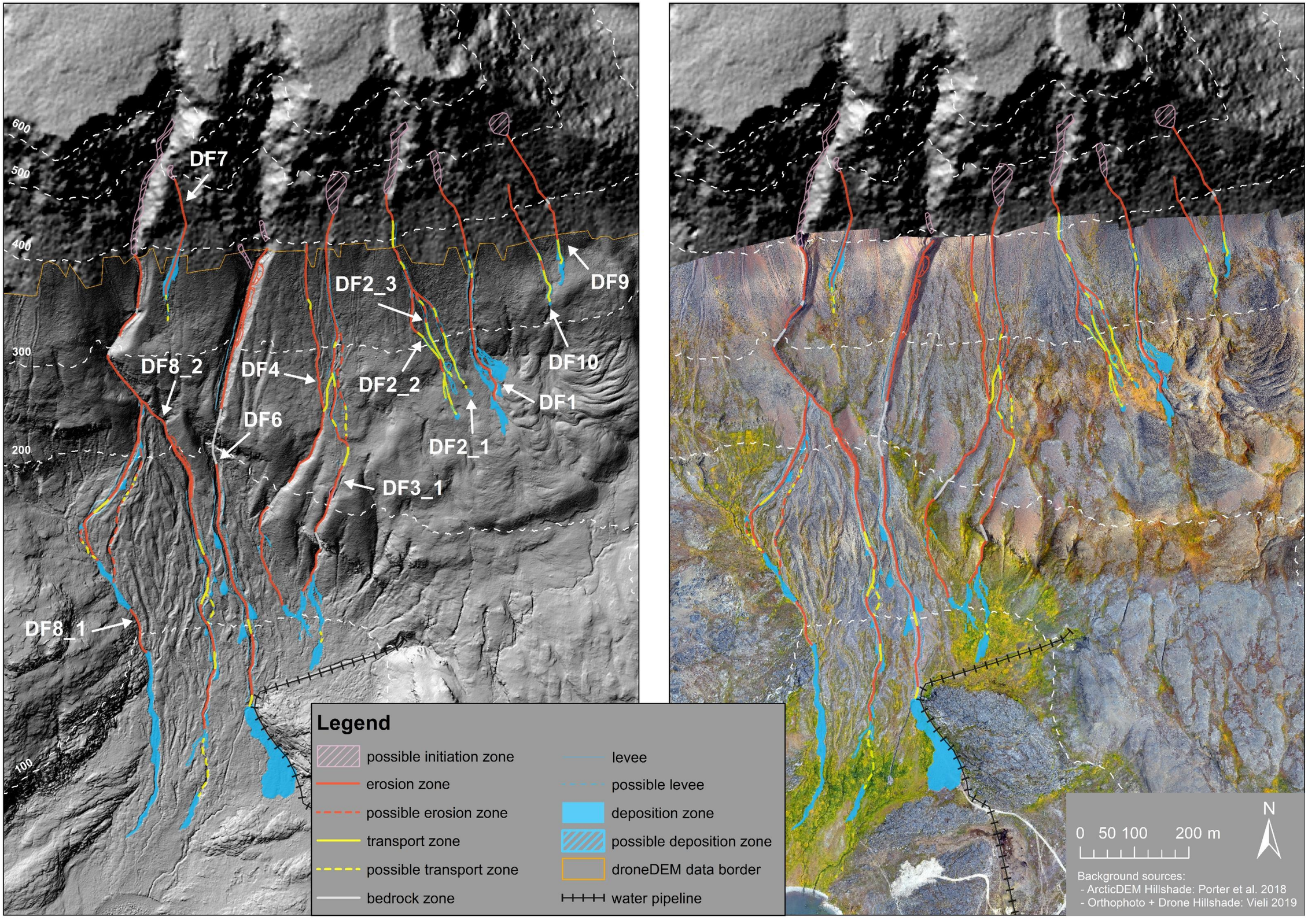

12.2 Original Size Maps and Figures

12.2.1 Long Profiles

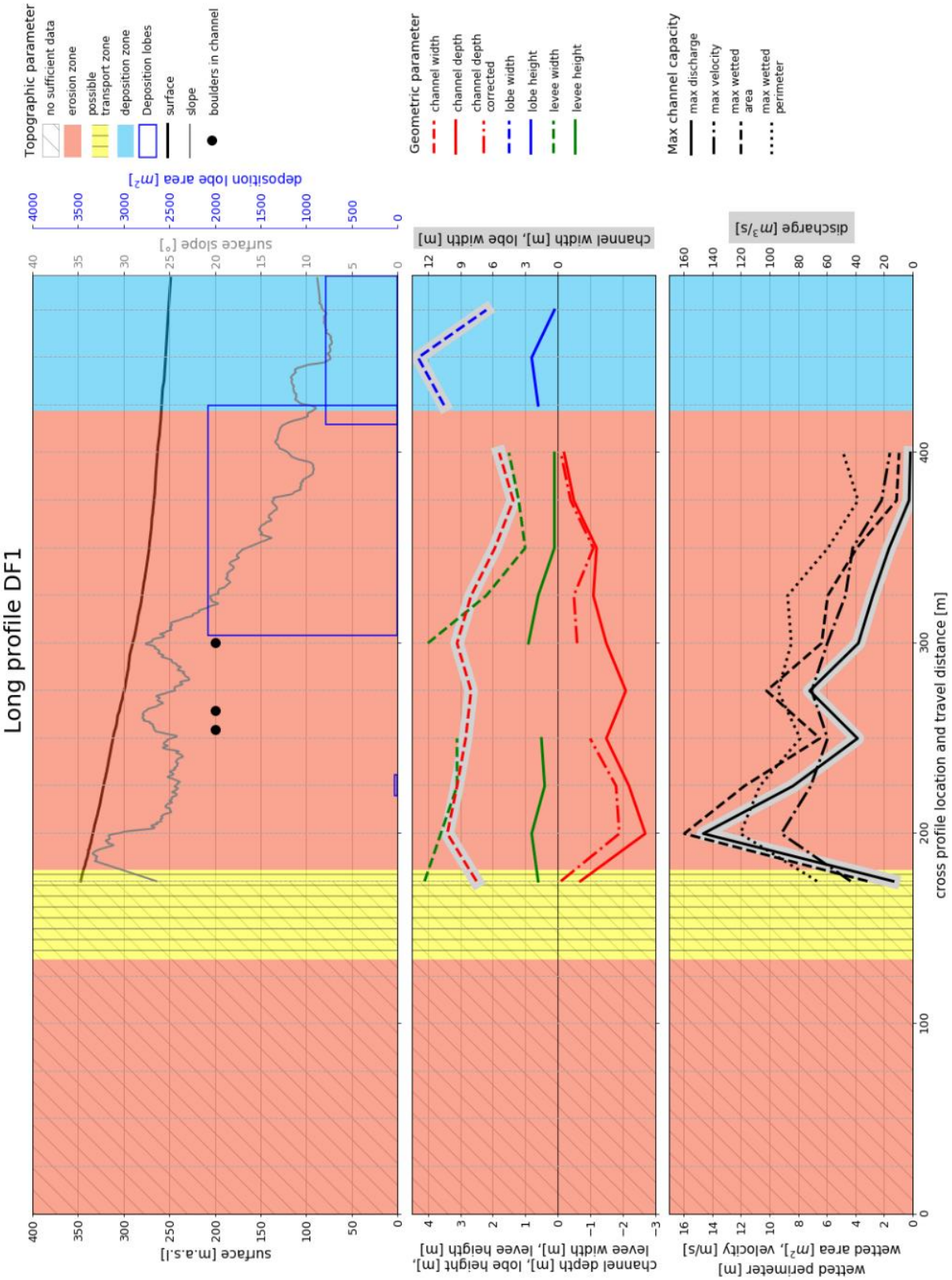

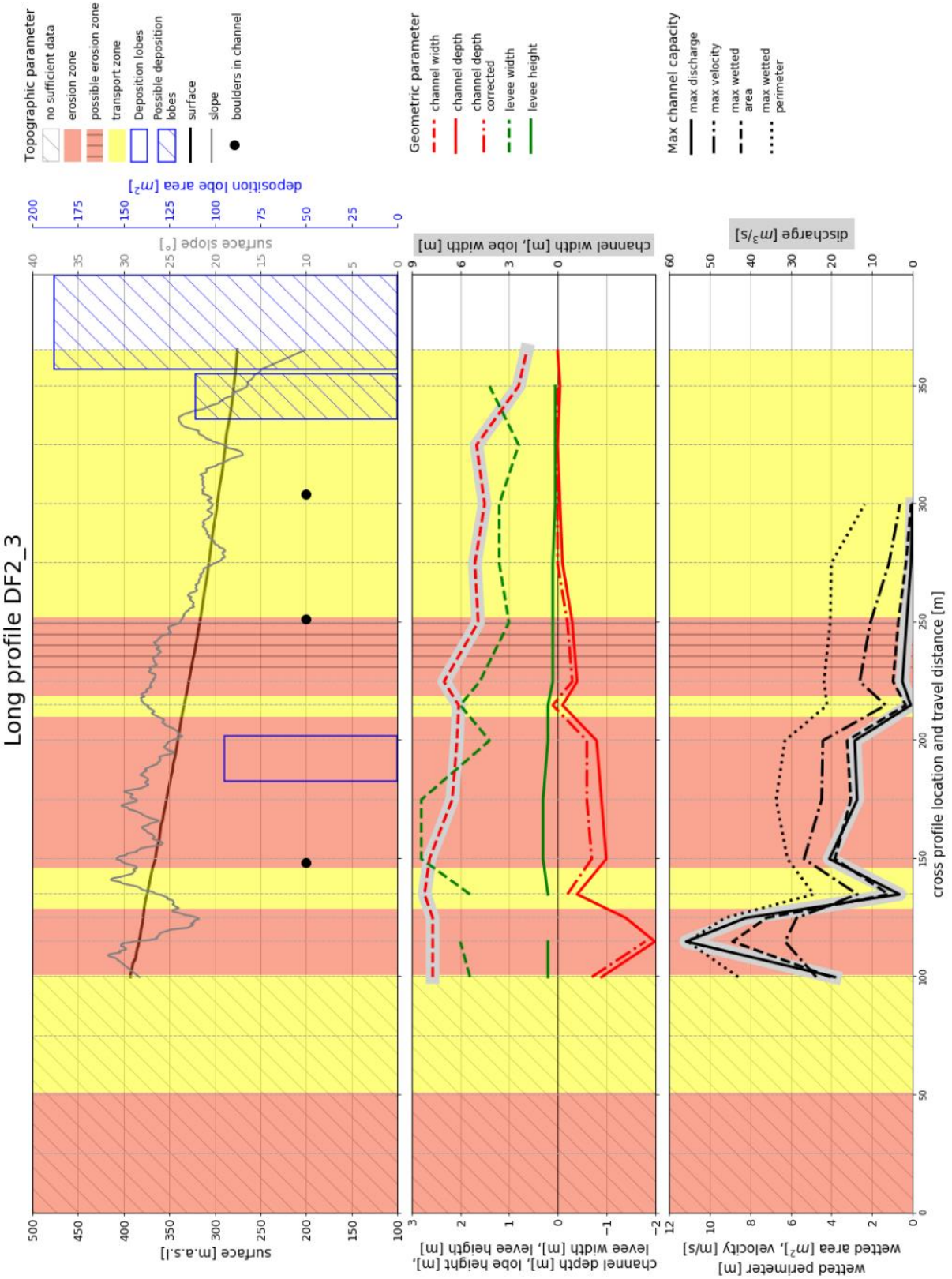
Long profile DF2_3
Topographic parameter
no sufficient data
erosion zone
possible erosion zone
transport zone
Deposition lobes
Possible deposition lobes
surface
slope
boulders in channel
Geometric parameter
channel width
channel depth
channel depth corrected
levee width
levee height
Max channel capacity
max discharge
max velocity
max wetted area
max wetted perimeter
deposition lobe area [m²]
surface slope [°]
surface [m.a.s.l]
channel width [m], lobe width [m]
channel depth [m], lobe height [m], levee width [m], levee height [m]
discharge [m³/s]
wetted perimeter [m]
wetted area [m²], velocity [m/s]
cross profile location and travel distance [m]

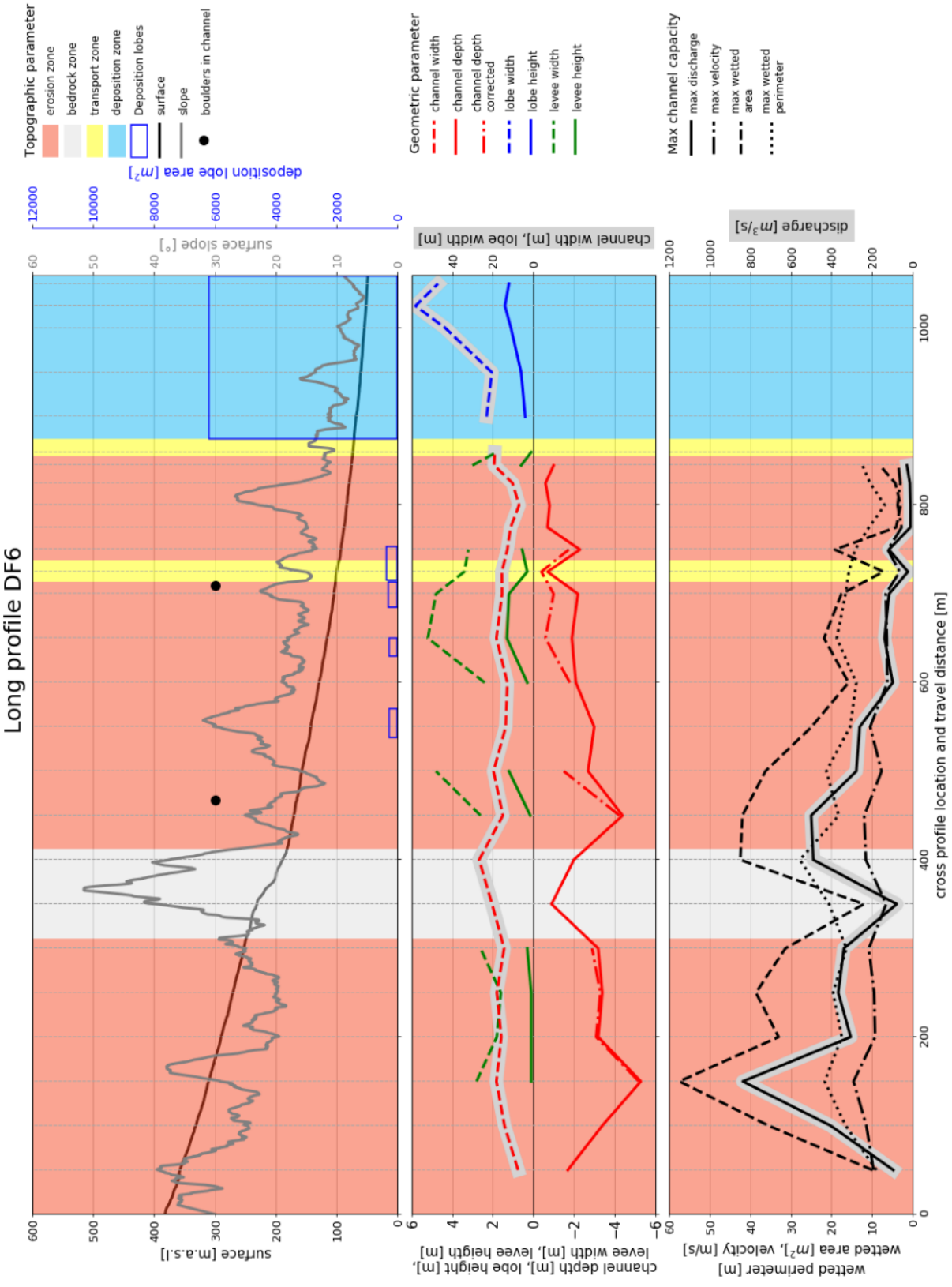
Long profile DF6
Topographic parameter
erosion zone
bedrock zone
transport zone
deposition zone
Deposition lobes
surface
slope
boulders in channel
Geometric parameter
channel width
channel depth
channel depth corrected
lobe width
lobe height
levee width
levee height
Max channel capacity
max discharge
max velocity
max wetted area
max wetted perimeter
deposition lobe area [m²]
surface slope [°]
surface [m.a.s.l]
channel width [m], lobe width [m]
channel depth [m], lobe height [m], levee width [m], levee height [m]
discharge [m³/s]
wetted perimeter [m]
wetted area [m²], velocity [m/s]
cross profile location and travel distance [m]

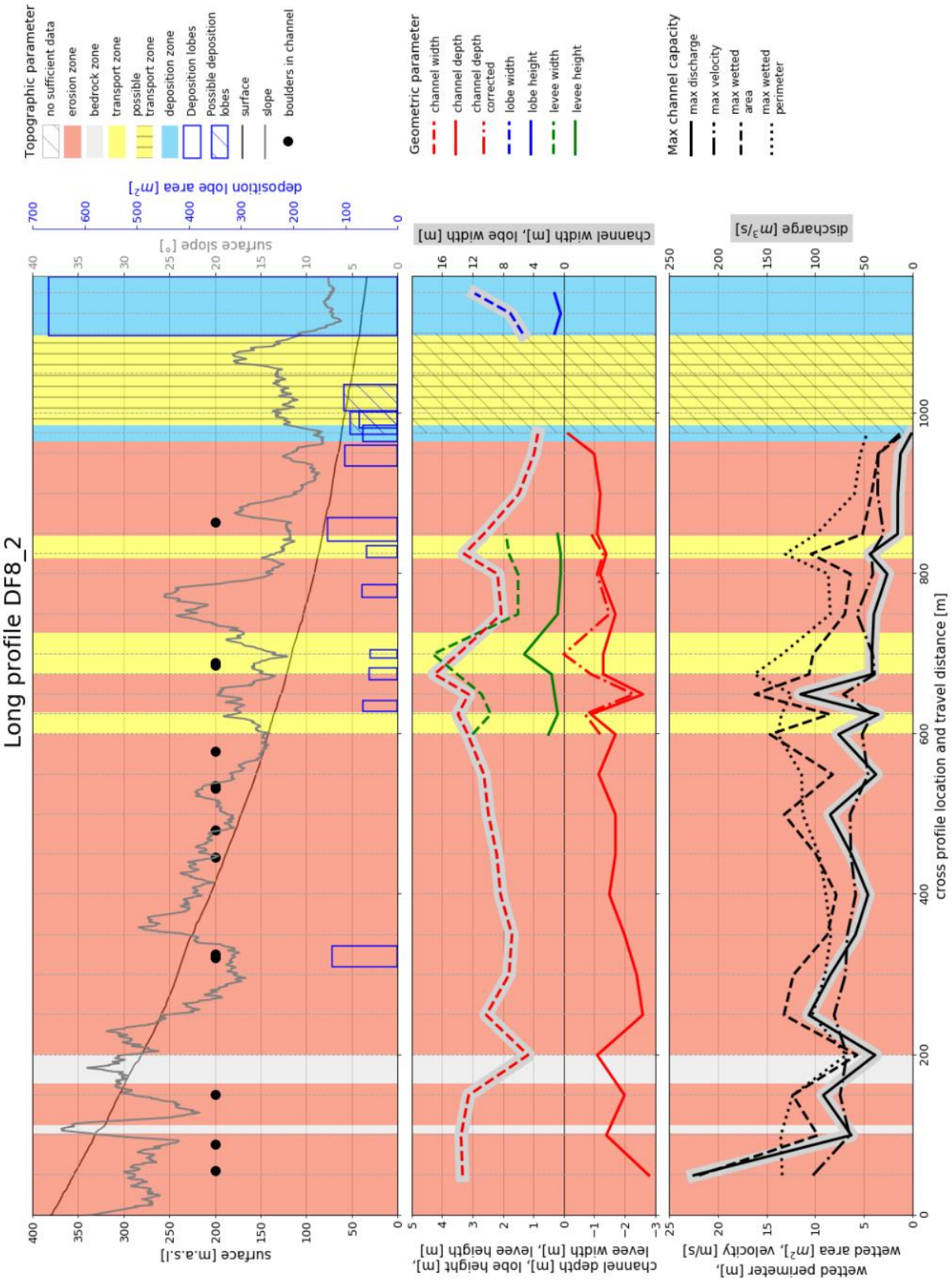
Long profile DF8_2
Topographic parameter
no sufficient data
erosion zone
bedrock zone
transport zone
possible transport zone
deposition zone
Deposition lobes
Possible deposition lobes
surface
slope
boulders in channel
Geometric parameter
channel width
channel depth
channel depth corrected
lobe width
lobe height
levee width
levee height
Max channel capacity
max discharge
max velocity
max wetted area
max wetted perimeter
deposition lobe area [m²]
surface slope [°]
surface [m.a.s.l]
channel width [m], lobe width [m]
channel depth [m], lobe height [m], levee width [m], levee height [m]
discharge [m³/s]
wetted perimeter [m], wetted area [m²], velocity [m/s]
cross profile location and travel distance [m]

12.2.2 RAMMS Output Maps

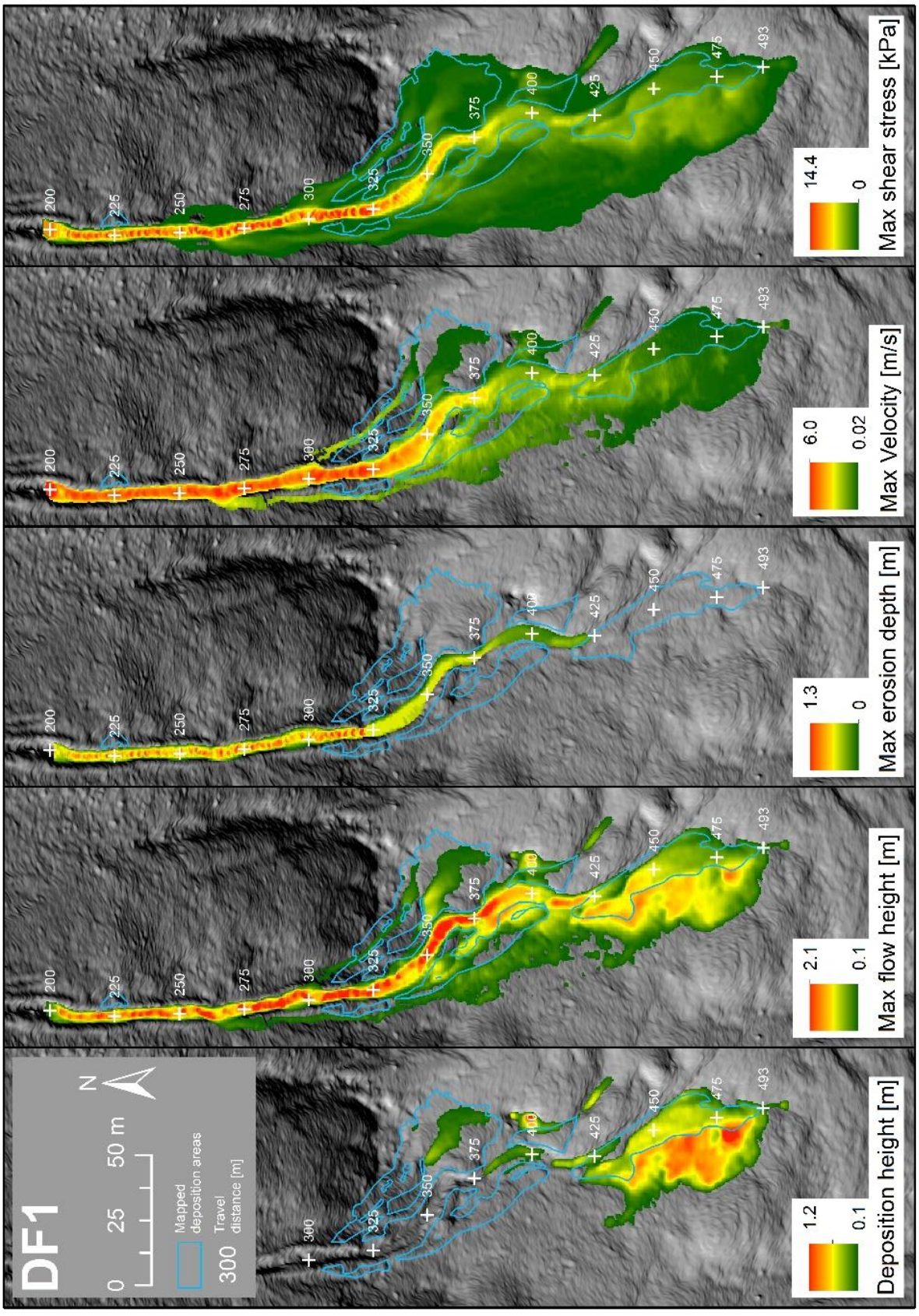

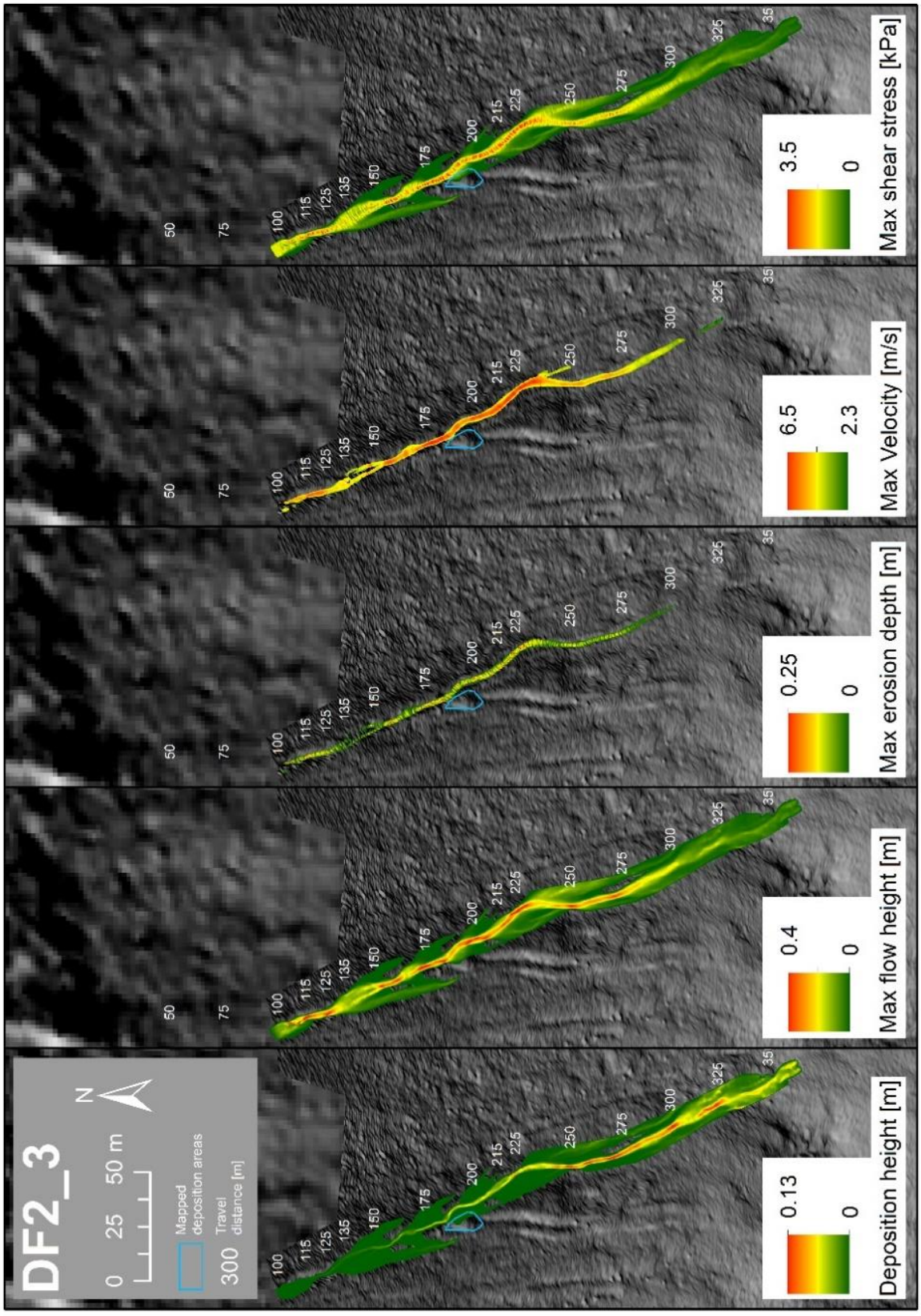
DF2_3
N
0 25 50 m
Mapped deposition areas
300 Travel distance [m]
Deposition height [m]
0.13
0
Max flow height [m]
0.4
0
Max erosion depth [m]
0.25
0
Max Velocity [m/s]
6.5
2.3
Max shear stress [kPa]
3.5
0

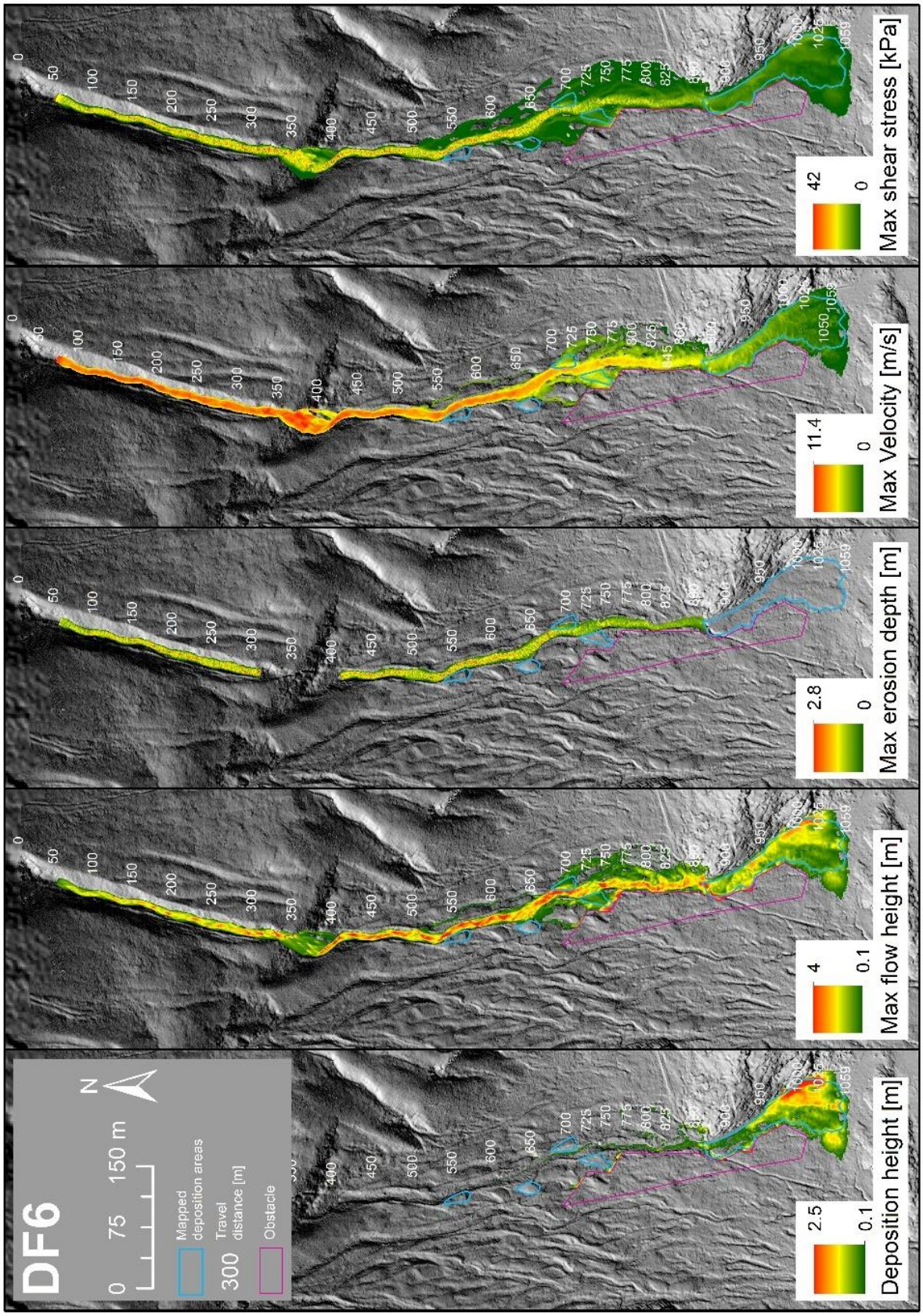
DF6
0 75 150 m
N
Mapped deposition areas
Travel distance [m]
300
Obstacle
Deposition height [m]
2.5
0.1
Max flow height [m]
4
0.1
Max erosion depth [m]
2.8
0
Max Velocity [m/s]
11.4
0
Max shear stress [kPa]
42
0

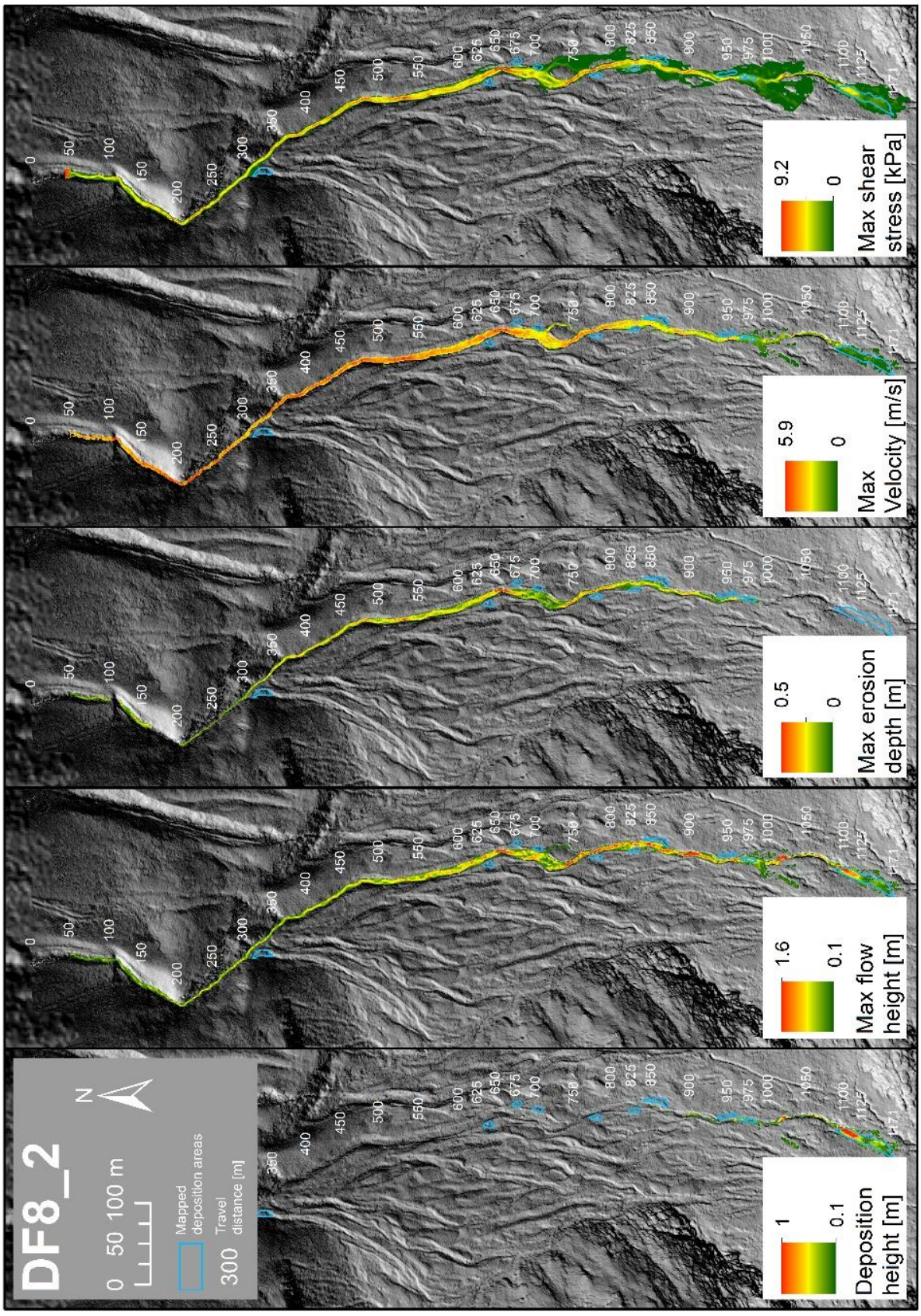
DF8_2
N
0 50 100 m
Mapped deposition areas
Travel distance [m]
300
Deposition height [m]
1
0.1
Max flow height [m]
1.6
0.1
Max erosion depth [m]
0.5
0
Max Velocity [m/s]
5.9
0
Max shear stress [kPa]
9.2
0

12.3 Python Codes

The presented python codes are an example of DF8_2.

12.3.1 Cross Profile Generation

```
# imports the needed librarys
import numpy as np
import pandas as pd
import matplotlib.pyplot as plt
from matplotlib.ticker import (AutoMinorLocator, MultipleLocator)
import math
from scipy.interpolate import InterpolatedUnivariateSpline as IUS

## creates the import function for the datasets to import .txt or .csv
files
def read_mes(filepath):
    table = pd.read_csv(filepath, sep = ',')
    return table

# defines the input and output paths of the files
debrisflo_nr = 'DF8_2'
datain = debrisflo_nr+'/crossprofiles_df8_2.txt'
dataout = debrisflo_nr+'/crossprofiles/'+debrisflo_nr+'_x{0}.png' # The 0
is a placeholder for the group name (distance on the longprofile)


# reads in the .txt file
raw_cross_data = read_mes(datain)
# making all the column names capitalized, so they are always be treated
the same
raw_cross_data.columns = map(str.upper, raw_cross_data.columns)


# groups the raw data by one column so every group (crossprofile) can be
treated individually
raw_cross_data = raw_cross_data.sort_val-
ues(by=['LONG_PROF_DIST','FIRST_DIST'])

gr_cross = raw_cross_data.groupby('LONG_PROF_DIST')


# Goes through all groups and plot each individually as crossprofile
for name, g in gr_cross:

    # the figuresize is depending on the real world extensions ratio.
    u = g.FIRST_DIST.iat[-1] # get the last value of the cross profile to
define the maximum width
    v = g['FIRST_Z'].max() - g['FIRST_Z'].min() # take the biggest and
smallest heigth value and subtract them to know the heigth difference in
the profile

    # makes sure that the heigth of the plot is big enough so that the pro-
files can be used for analysation.
    # According to the overall crossprofile vertical differences the 'over-
heigthing' is adjusted. The values are set according to observations.
    if v <= 2 and v > 0.5:
        o=3
    elif v<=0.5:
        o=10
    else:
```

```
        o=2

    v=v*o

    # this defines the figuresize for all the following figures if it is
not changed afterwards
    plt.rcParams['figure.figsize'] = [u, v] # u and v set the x- respec-
tively y-direction figuresize. v can be multiplied with a factor to get
overheigthed profiles

    # plot the grouped values
    fd = g['FIRST_DIST']
    fz = g['FIRST_Z']
    bh = g['BANKFULL_HEIGHT']

    plt.plot(fd, fz) # plot the surface
    plt.plot(fd, bh) # plot the bankfull mark line

    ax = plt.axes()
    # Change major ticks to show every 1 meter
    ax.xaxis.set_major_locator(MultipleLocator(1))
    ax.yaxis.set_major_locator(MultipleLocator(1))

    # Change minor ticks to show 5 between the major ticks
    ax.xaxis.set_minor_locator(AutoMinorLocator(5))
    ax.yaxis.set_minor_locator(AutoMinorLocator(5))

    # draw the grid with different style for major and minor grid lines
    plt.grid(b=True, which='major', linewidth=1.5)
    plt.grid(b=True, which='minor', linewidth=0.5)

    # label the x- and y-axis and create title according to the distance
from the headwallfoot on the longprofile of the debris flow
    plt.xlabel('[m]')
    plt.ylabel('[m.a.s.l], '+str(o)+'x')
    plt.title(debrisflo_nr + '-x' + str(name), fontsize=20)

    plt.tight_layout()

    #save the plots as single .png files in the corresponding folder ac-
cording to the group name (crossprofile name)
    plt.savefig(dataout.format(name))

    plt.show()
```

12.3.2 Maximum Discharge Calculation

```
# imports the needed librarys
import numpy as np
import pandas as pd
import matplotlib.pyplot as plt
import math
from scipy.interpolate import InterpolatedUnivariateSpline as IUS

## creates the import function for the datasets to import .txt or .csv
files
def read_mes(filepath):
    table = pd.read_csv(filepath, sep = ',')
    return table
```

```
# defines the input and output paths of the files
debrisflo_nr = 'DF8_2'
datain = debrisflo_nr+'/crossprofiles_df8_2.txt'
datain_para = debrisflo_nr+'/crossprofiles_parameter_df8_2.txt'

# reads in the .txt file
raw_cross_data = read_mes(datain)
# making all the column names capitalized, so they are always be treated
the same
raw_cross_data.columns = map(str.upper, raw_cross_data.columns)

# the parameter.txt file will be read in
raw_long_para_data = read_mes(datain_para)
raw_long_para_data.columns = map(str.upper, raw_long_para_data.columns)
raw_long_para_data = raw_long_para_data.rename(columns={'LONG_PROF_DIS-
TANCE': 'LONGPROF_DISTANCE'})
long_para=raw_long_para_data.sort_values(by=['LONGPROF_DISTANCE'])


# add the 2 columns for the calculation of the discharge Q and fill them
with no data
raw_cross_data["DX"] = np.nan
raw_cross_data["DY"] = np.nan

long_para["P"] = np.nan
long_para["A"] = np.nan
long_para["v"] = np.nan
long_para["Q"] = np.nan


# group the raw data by one column so every group can be treated individu-
ally
raw_cross_data = raw_cross_data.sort_val-
ues(by=['LONG_PROF_DIST','FIRST_DIST'])

gr_cross = raw_cross_data.groupby('LONG_PROF_DIST')

### calculation of different parameters
for name,g in gr_cross:
    if g.BANKFULL_HEIGHT.iat[1] > 0:

        # calculate P (wetted perimeter) in the crossprofile table
        # for every single datapoint and sum them up continously to get the
total wetted
        # perimeter
        g.DX.iat[0] = 0
        for i in range(1, len(g)):
                g.DX.iat[i] = g.FIRST_DIST.iat[i] - g.FIRST_DIST.iat[i-1]

        for i in range(len(g)):
            if g.BANKFULL_HEIGHT.iat[i]>g.FIRST_Z.iat[i]:
                g.DY.iat[i] = g.BANKFULL_HEIGHT.iat[i]-g.FIRST_Z.iat[i]
            else:
                g.DY.iat[i] = 0

        P = 0

        for i in range(1,len(g)):
            if g.BANKFULL_HEIGHT.iat[i]>g.FIRST_Z.iat[i] and
g.FIRST_DIST.iat[i] > g.X_START.iat[i] and g.FIRST_DIST.iat[i] <
g.X_END.iat[i]:
                dx = g.DX.iat[i]
```

```
                dy = g.DY.iat[i]-g.DY.iat[i-1]

                P = P + math.sqrt(dx**2 + dy**2)

        long_para.loc[long_para['LONGPROF_DISTANCE'] == name, 'P'] = P

        # calculate A through integration
        dist = g['FIRST_DIST']
        z = g['FIRST_Z']
        bank = g['BANKFULL_HEIGHT']

        z_interpol = IUS(dist,z,k=1)
        bank_interpol = IUS(dist,bank,k=1)

        A = bank_interpol.integral(g.X_START.iat[1],g.X_END.iat[1])-z_in-
terpol.integral(g.X_START.iat[1],g.X_END.iat[1])

        long_para.loc[long_para['LONGPROF_DISTANCE'] == name, 'A'] = A

        # get the slope in [°] from the parameter file and calculate it to
slope gradient [-]
        row = long_para.loc[long_para['LONGPROF_DISTANCE'] == name]
        slope = row['SLOPE']

        S = math.tan(slope * math.pi / 180)

        ## calculating the flow velocity
        # using the following Stricklercoefficient [m^(1/3)/s]
        ks = 10

        # using the hydraulic radius R [m]
        R = A/P

        v = ks * R**(2/3) * S**(1/2)

        #print(v)
        long_para.loc[long_para['LONGPROF_DISTANCE'] == name, 'v'] = v

        ## calculate the discharge of a bankfull event Q [m^3/s]
        Q = v * A

        #print(Q)
        long_para.loc[long_para['LONGPROF_DISTANCE'] == name, 'Q'] = Q

# export the parameter table as .csv file to the folder
long_para.to_csv('DF8_2/crossprofiles_parameter_df8_2_wQ.csv')
```

12.3.3 Long Profile Generation

```
## imports the needed librarys
import numpy as np
import pandas as pd
import matplotlib.pyplot as plt
import matplotlib.patches as mpatches
import matplotlib.lines as mlines
import matplotlib.markers as mmarkers
from matplotlib.ticker import (AutoMinorLocator, MultipleLocator)
from scipy.signal import savgol_filter
```

```
## creates the import function for the datasets to import .txt or .csv
files
def read_mes(filepath):
    table = pd.read_csv(filepath, sep = ',')
    return table

## Change these inputs for new debris flow path
debrisflo_nr = 'DF8_2'
datain_para = debrisflo_nr+'/crossprofiles_parameter_df8_2_wQ.csv'
datain_zones = debrisflo_nr+'/zones_df8_2.csv'
datain_sur = debrisflo_nr+'/longprofile_surface_slope_df8_2.txt'
datain_boulders = 'boulders_in_channel.txt'
datain_depositions = 'longprofile_deposition.txt'

# Define where the data gets stored
dataout = debrisflo_nr+'/longprofile_'+debrisflo_nr+'.png' # The 0 is a
placeholder for the group name (distance on the longprofile)

### import the data from the files
# read in the parameter table
raw_long_para_data = read_mes(datain_para)
raw_long_para_data.columns = map(str.upper, raw_long_para_data.columns) #
making all the column names capitalized, so they are always be treated the
same
raw_long_para_data = raw_long_para_data.rename(columns={'LONG_PROF_DIS-
TANCE': 'LONGPROF_DISTANCE'}) # corrects a wrong writen column name

# load in the .txt file for the background colour with the mapped debris
flow zones
raw_zones = pd.read_csv(datain_zones, sep = ';')
raw_zones.columns = map(str.upper, raw_zones.columns) # make all the column
names big caps
raw_zones['STARTPOINT'] = raw_zones.STARTPOINT.astype(int) # make sure the
data has integer format
raw_zones['ENDPOINT'] = raw_zones.ENDPOINT.astype(int) # make sure the data
has integer format

# load the .txt with slope and surface
raw_long_sur_slo = read_mes(datain_sur)
raw_long_sur_slo.columns = map(str.upper, raw_long_sur_slo.columns)

# load the .txt with boulders
raw_boulders = read_mes(datain_boulders)
raw_boulders.columns = map(str.upper, raw_boulders.columns)

# load the .txt with depositions
raw_depositions = read_mes(datain_depositions)
raw_depositions.columns = map(str.upper, raw_depositions.columns)

## manipulate different datasets
# sort all the files to be sure of the correct order
long_para=raw_long_para_data.sort_values(by=['LONGPROF_DISTANCE'])
zones=raw_zones.sort_values(by=['ORDER_NR'])

# group the .txt file with the surface and slope in it
long_sur_slo = raw_long_sur_slo.groupby('SRC_NAME')

#read out the length of the debris flow and safe it as variable
df_length = long_para.LONGPROF_DISTANCE.iat[-1]


### Define figure settings
```

```
# create the figure with two horizontal subplots ax1 and ax10
# set the figuresize, the width-height ratio, the space between the sub-
plots and define that the subplots share the x-axis
fig, (ax1, ax10, ax20) = plt.subplots(3, figsize=(20, 15), grid-
spec_kw={'height_ratios': [3, 2,2]}, sharex=True)

# label font size
lfs = 15

## Definition of ax1
colax1 = 'black'

ax1.set_ylim(0,400)
ax1.set_xlim(0,df_length)
ax1.set_ylabel('surface [m.a.s.l]', color=colax1, fontsize = lfs)
ax1.tick_params(axis='y', labelcolor=colax1, labelsize = 13)
ax1.grid(axis='y', zorder=1) # turn on only the y-axis grid lines


## Definition of ax2
colax2 = 'grey'

ax2 = ax1.twinx()  # instantiate a second axes that shares the same x-axis
as ax1
ax2.set_ylim(0,40)
ax2.set_ylabel('surface slope [°]', color=colax2, fontsize = lfs)
ax2.tick_params(axis='y', labelcolor=colax2, labelsize = 13)
ax2.spines['right'].set_position(('axes', 1.0)) # define position of y-axis
ax2.spines['right'].set_color(colax2)

## Definition of ax3
colax3 = 'blue'

ax3 = ax1.twinx()
ax3.set_ylim(0,700)
ax3.set_ylabel('deposition lobe area [$m^2$]', color=colax3, fontsize =
lfs)
ax3.tick_params(axis='y', labelcolor=colax3, labelsize = 13)
ax3.spines['right'].set_position(('axes', 1.05)) # define position of y-
axis
ax3.spines['right'].set_color(colax3)

## Definition of ax10
colax10 = 'black'

ax10.set_ylim(-3,5)
ax10.set_ylabel('channel depth [m], lobe height [m],\nlevee width [m],
levee heigth [m]', fontsize = lfs)
ax10.tick_params(axis='y', labelcolor=colax10, labelsize = 13)
ax10.grid(axis='y') # turn on only the y-axis grid lines
ax10.axhline(y=0, color = 'black', linewidth = 0.8) # creats a black line
at y=0 for betters orientation on plot

## Definition of ax11
colax11 = 'black'

ax11 = ax10.twinx()  # instantiate a second axes that shares the same x-
axis as ax1
ax11.set_ylim(-12, 20)
ax11.set_ylabel('channel width [m], lobe width [m]', color=colax11, font-
size = lfs, backgroundcolor='lightgrey',
               labelpad=15)
```

```
ax11.tick_params(axis='y', labelcolor=colax11, labelsize = 13)
ax11.set_yticks([0,4,8, 12, 16]) # the location of the needed labels can be
set manually
ax11.set_yticklabels(["0","4","8", "12", "16"]) # the text of the needed
labels can be set manually !!!! need to be same as yticks
ax11.spines['right'].set_color(colax11)

## Definition of ax20
colax20 = 'black'

ax20.set_ylim(0,25)
ax20.set_xlabel('cross profile location and travel distance [m]',
color=colax20, fontsize = lfs)
ax20.set_ylabel('wetted perimeter [m],\nwetted area [$m^2$], velocity
[m/s]', fontsize = lfs)
ax20.tick_params(labelcolor=colax20, labelsize = 13)
ax20.grid(axis='y') # turn on only the y-axis grid lines

## Definition of ax21
colax21 = 'black'

ax21 = ax20.twinx()  # instantiate a second axes that shares the same x-
axis as ax1
ax21.set_ylim(0,250)
ax21.set_ylabel('discharge [$m^3$/s]', color=colax21, fontsize = lfs, back-
groundcolor='lightgrey', labelpad=10)
ax21.tick_params(axis='y', labelcolor=colax21, labelsize = 13)
ax21.spines['right'].set_color(colax21)


## "x-axis" grid lines
# plot lines on x axis where crossprofiles are drawn.
# therefore adjust the starting number of the range. With the if sentence
the end point of the debris flow, where no
# profile is drawn can be set as no color
for d in range(1,(len(long_para))):
    if long_para.LONGPROF_DISTANCE[d] == df_length:
        ax1.axvline(x=long_para.LONGPROF_DISTANCE[d], color = 'none',
               linestyle = '--')
        ax10.axvline(x=long_para.LONGPROF_DISTANCE[d], color = 'none',
               linestyle = '--')
        ax20.axvline(x=long_para.LONGPROF_DISTANCE[d], color = 'none',
               linestyle = '--')
    else:
        ax1.axvline(x=long_para.LONGPROF_DISTANCE[d], color = 'darkgrey',
               linestyle = '--', linewidth = 1)
        ax10.axvline(x=long_para.LONGPROF_DISTANCE[d], color = 'darkgrey',
               linestyle = '--', linewidth = 1)
        ax20.axvline(x=long_para.LONGPROF_DISTANCE[d], color = 'darkgrey',
               linestyle = '--', linewidth = 1)



### Plotting the data

## Plotting debris flow zones on ax1, ax10, and ax 20
#Create the debris flow zones in the background in dependance of the en-
tries in the zones.txt file.
for name in range(0,len(zones)):
    if zones.RULEID[name] == 7:
        global col_ero, lab_ero
        col=(247/255,74/255,38/255)
```

```
        col_ero=col
        lab_ero= 'erosion zone'
        ha=False
    if zones.RULEID[name] == 14:
        global col_ero_ass, lab_ero_ass
        col=(247/255,74/255,38/255)
        col_ero_ass=col
        lab_ero_ass= 'possible erosion zone'
        ha="|"
    if zones.RULEID[name] == 15:
        global col_trans_rock, lab_trans_rock
        col=(225/255,225/255,225/255)
        col_trans_rock=col
        lab_trans_rock='bedrock zone'
        ha=False
    if zones.RULEID[name] == 5:
        global col_trans, lab_trans
        col=(255/255,255/255,0/255)
        col_trans=col
        lab_trans='transport zone'
        ha=False
    if zones.RULEID[name] == 13:
        global col_trans_ass, lab_trans_ass
        col=(255/255,255/255,0/255)
        col_trans_ass=col
        lab_trans_ass='possible\ntransport zone'
        ha="|"
    if zones.RULEID[name] == 9:
        global col_depo, lab_depo
        col=(18/255,182/255,245/255)
        col_depo=col
        lab_depo='deposition zone'
        ha=False

    ax1.axvspan(zones.STARTPOINT[name],zones.ENDPOINT[name], facecolor=col,
        alpha=0.5, zorder=2, hatch = ha)
    ax10.axvspan(zones.STARTPOINT[name],zones.ENDPOINT[name],
        facecolor=col, alpha=0.5, zorder=2, hatch = ha)
    ax20.axvspan(zones.STARTPOINT[name],zones.ENDPOINT[name],
        facecolor=col, alpha=0.5, zorder=2, hatch = ha)

# create the colour patches of the debris flow zones for the legend
# (due to iteration processes used they can't be generated automatically)
patch_ero = mpatches.Patch(facecolor = col_ero, label = lab_ero, alpha=0.5)
patch_trans_rock = mpatches.Patch(facecolor = col_trans_rock,
        label = lab_trans_rock, alpha=0.5)
patch_trans = mpatches.Patch(facecolor = col_trans, label = lab_trans,
        alpha=0.5)
patch_trans_ass = mpatches.Patch(facecolor = col_trans_ass,
        label = lab_trans_ass, alpha=0.5, hatch = "|")
patch_depo = mpatches.Patch(facecolor = col_depo, label = lab_depo,
        alpha=0.5)

## add hatch to clarify where no sufficient data was available for measure-
ments
plt.rcParams['hatch.linewidth'] = 0.5
hat = ax10.axvspan(975,1100, fill=False, edgecolor = 'black', linewidth =
0.5, hatch = '/', alpha = 0.5, zorder=2, label = 'no sufficient data')
ax20.axvspan(975,1100, fill=False, edgecolor = 'black', linewidth = 0.5,
hatch = '/', alpha = 0.5, zorder=2)
```

```
## plot surface on ax1
lsssurf = long_sur_slo.get_group('drone_data_2019_DEM_pix4dprojectDe-
brisflowGreenland2019_dsm_heiadj_tif') #prepare data
surf, = ax1.plot(lsssurf['FIRST_DIST'],lsssurf['FIRST_Z'], color='black',
zorder=1, label = 'surface')


## plot the area of the deposition lobes on ax3. The possible deposition
lobes get hatched in blue.
for name in range(0, len(raw_depositions)):
    if raw_depositions.DEBRISFLOW_NUMBER[name] == '8_2':
        if raw_depositions.RULEID[name] == 12:
            ax3.add_patch(mpatches.Rectangle((
                raw_depositions.X_START[name],0),
                raw_depositions.X_END[name]-raw_depositions.X_START[name],
                raw_depositions.SHAPE_AREA[name], edgecolor = 'blue',
                facecolor = 'none', hatch = '/', linewidth=1.5))
        else:
            ax3.add_patch(mpatches.Rectangle((
                raw_depositions.X_START[name],0),
                raw_depositions.X_END[name]-raw_depositions.X_START[name],
                raw_depositions.SHAPE_AREA[name], edgecolor = 'blue',
                facecolor = 'none', linewidth=1.5))

# creates the patches to use in the legend
patch_depo_area = mpatches.Patch(facecolor = 'none', edgecolor = 'blue',
linewidth=1.5, label = 'Deposition lobes')
patch_depo_area_p = mpatches.Patch(facecolor = 'none', edgecolor = 'blue',
linewidth=1.5, hatch = '/', label = 'Possible deposition\nlobes')


## plots the boulder locations on ax1
for name in range(0, len(raw_boulders)):
    if raw_boulders.DF_NR[name] == '8_2':
        boulder = ax1.scatter(raw_boulders.LONGPROF_DISTANCE[name], 200,
s=100, color = 'black', zorder = 10)

mark_boulder = mlines.Line2D([], [], color='none', marker='o', mark-
eredgecolor = 'black', markerfacecolor = 'black',
                          markersize=10, label= 'boulders in channel')


## plots slope on ax2
# preparing data of slope
lsssc = long_sur_slo.get_group('slope_cal')
yhat = savgol_filter(lsssc['FIRST_Z'], 299, 1) # window size 299, polyno-
mial order 1

# plot the smoothed slope
sl, = ax2.plot(lsssc['FIRST_DIST'],yhat, color='grey', linewidth = 2, label
= 'slope', zorder=3)


## define lindewidth for parameter lines
linw = 3


## plot grey backgrounds for ax11 and ax 21 on ax10 and ax20. Therefore it
is in the background of the lines of ax10
# and ax20. Adapt the divisor according to the ration of ax10 <-> ax11 and
ax20 <-> ax 21
```

```
chan_width_bg, = ax10.plot(long_para['LONGPROF_DIS-
TANCE'],long_para['CHAN_WIDTH']/4, color = 'lightgrey',
                        linestyle = 'solid', linewidth = 15)
lobe_width_bg, = ax10.plot(long_para['LONGPROF_DIS-
TANCE'],long_para['LOBE_WIDTH']/4, color = 'lightgrey',
                        linestyle = 'solid', linewidth = 15)

discharge_bg, = ax20.plot(long_para['LONGPROF_DISTANCE'],long_para['Q']/10,
color = 'lightgrey', linestyle = 'solid', linewidth = 15)

## plot different parameter on ax10
chan_depth, = ax10.plot(long_para['LONGPROF_DISTANCE'],-
long_para['CHAN_DEPTH'], color = 'red', linestyle = 'solid', linewidth =
linw, label = 'channel depth')
chan_depth_corr, = ax10.plot(long_para['LONGPROF_DISTANCE'],-
(long_para['CHAN_DEPTH']-long_para['LEV_HEIGHT']), color = 'red', linestyle
= 'dashdot', linewidth = linw, label = 'channel depth\ncorrected')
lev_width, = ax10.plot(long_para['LONGPROF_DIS-
TANCE'],long_para['LEV_WIDTH'], color = 'green', linestyle = 'dashed', lin-
ewidth = linw, label = 'levee width')
lev_height, = ax10.plot(long_para['LONGPROF_DIS-
TANCE'],long_para['LEV_HEIGHT'], color = 'green', linestyle = 'solid', lin-
ewidth = linw, label = 'levee height')
lobe_height, = ax10.plot(long_para['LONGPROF_DIS-
TANCE'],long_para['LOBE_HEIGH'], color = 'blue', linestyle = 'solid', lin-
ewidth = linw, label = 'lobe height')

## plot different parameter on ax11
chan_width, = ax11.plot(long_para['LONGPROF_DIS-
TANCE'],long_para['CHAN_WIDTH'], color = 'red', linestyle = 'dashed', lin-
ewidth = linw, label = 'channel width')

lobe_width, = ax11.plot(long_para['LONGPROF_DIS-
TANCE'],long_para['LOBE_WIDTH'], color = 'blue', linestyle = 'dashed', lin-
ewidth = linw, label = 'lobe width')

## plot the Qmax calculation values on ax20
wet_area, = ax20.plot(long_para['LONGPROF_DISTANCE'],long_para['A'], color
= 'black', linestyle = 'dashed', linewidth = linw, label = 'max wetted\nar-
ea')
wet_peri, = ax20.plot(long_para['LONGPROF_DISTANCE'],long_para['P'], color
= 'black', linestyle = 'dotted', linewidth = linw, label = 'max wet-
ted\nperimeter')
velocity, = ax20.plot(long_para['LONGPROF_DISTANCE'],long_para['V'], color
= 'black', linestyle = 'dashdot', linewidth = linw, label = 'max velocity')

## plot Qmax on ax21
discharge, = ax21.plot(long_para['LONGPROF_DISTANCE'],long_para['Q'], color
= 'black', linestyle = 'solid', linewidth = linw, label = 'max discharge')


### definition of legend and layout
# Topographic parameter legend
leg1 = ax1.legend(handles=[hat, patch_ero, patch_trans_rock, patch_trans,
patch_trans_ass, patch_depo, patch_depo_area, patch_depo_area_p,
surf, sl, mark_boulder], bbox_to_anchor=(1.3, 1.05),
ncol=1, facecolor = 'white', fontsize= 'large', framealpha = 0, title =
'Topographic parameter', title_fontsize = 'x-large', handleheight = 2, han-
dlelength = 3)
leg1._legend_box.align = "left"

# Geometric parameter legend
```

```
leg10 = ax10.legend(handles=[chan_width, chan_depth, chan_depth_corr,
lobe_width, lobe_height, lev_width, lev_height],
bbox_to_anchor=(1.29, 1.05), ncol=1, facecolor = 'white', fontsize=
'large', framealpha = 0, title = 'Geometric parameter', title_fontsize =
'x-large', handleheight = 2, handlelength = 3)
leg10._legend_box.align = "left"

# Max channel capacity legend
leg20 = ax20.legend(handles=[discharge, velocity, wet_area, wet_peri],
bbox_to_anchor=(1.29, 1.05), ncol=1, facecolor = 'white', fontsize=
'large', framealpha = 0, title = 'Max channel capacity', title_fontsize =
'x-large', handleheight = 2, handlelength = 3)
leg20._legend_box.align = "left"

fig.suptitle('Long profile ' + debrisflo_nr, y=0.98, fontsize=25)
fig.subplots_adjust(left=0.06, bottom=0.05, right=0.78, top=0.95, wspace=0,
hspace=0.05)


### save data and plot the figure
plt.savefig(dataout)

plt.show()
```

12.4 Additional Model Parameter and Results

12.4.1 Parameter Sets of Additional Most Plausible Model Runs and Model Runs without Obstacle Polygon

		DF6 Without Obstacle Polygon	DF6 Additional Most Plausible Parameter Set	DF2_3 Additional Most Plausible Parameter Set
Input parameter	DEM used	drone DEM	drone DEM	drone DEM
	Initiation distance on long profile [m]	60	60	100
	Data resolution [m]	0.07	0.07	0.07
	Simulation resolution [m]	0.5	0.5	0.2
	Stopping criteria [%]	5	5	5
	Simulation length [s]	355	340	100
	Dump stem [s]	5	5	5
	Density [kg/m^3]	2000	2000	2000
	ξ [m/s^2]	300	300	500
	μ [-]	0.11	0.11	0.10
	Obstacle/Dam used	No	Yes	No
Release parameter	Volume released [m^3]	1600	1000	30
	Qmax [m^3/s]	47	97	1.6
	t1 [s]	3	3	1
	v [m/s]	10	10	5
	t2 [s]	68.1	20.6	35
Erosion parameter polygon 1	Erosion density [kg/m^3]	2000	2000	2000
	Erosion rate [m/s]	0.025	0.025	0.025
	Pot. erosion depth [per kPa]	0.1	0.1	0.1
	Critical shear stress [kPa]	1	1	1
	Max erosion depth [m]	0	0	0
Erosion parameter polygon 1	Erosion density [kg/m^3]	2000	2000	
	Erosion rate [m/s]	0.025	0.025	
	Pot. erosion depth [per kPa]	0.1	0.1	
	Critical shear stress [kPa]	1	1	
	Max erosion depth [m]	0	0	
Output parameter	Eroded volume [m^3]	3932	4484	55.9
	Flow volume [m^3]	5520	5473	45.5
	Calculation domain outflow volume [m^3]	12	10.6	38.6
	Volume in mapped deposition area [m^3]	3588	3551	-
	Runout length [m]	1062	1063	362

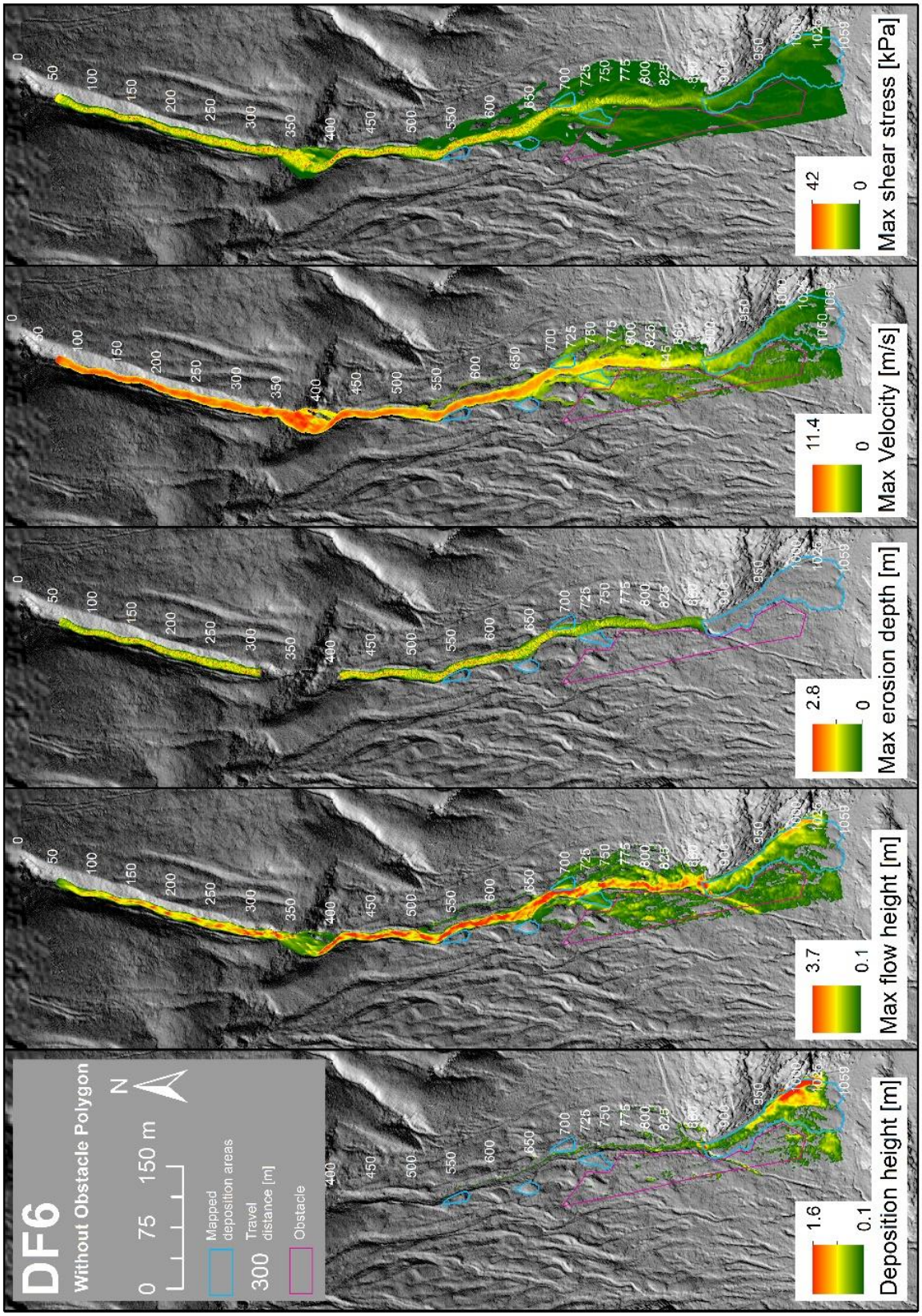

Deposition height, max flow height, max erosion depth, max velocity, and max shear stress of the most plausible simulation including erosion of DF6. The mapped deposition areas are indicated in blue. The white numbers indicate the travel distances. The pink polygon shows the obstacle polygon which is not used in this simulation run. In the background the hillshades of the drone DEM and the ArcticDEM is displayed.

12.4.2 Model Parameter without Entrainment

	Without entrainment module	DF1	DF2_3	DF6	DF8_2
Input parameter	DEM used	drone DEM	drone DEM	drone DEM	drone DEM
	Initiation distance on long profile [m]	200	100	60	50
	Data resolution [m]	0.07	0.07	0.07	0.07
	Simulation resolution [m]	0.5	0.2	0.5	0.5
	Stopping criteria [%]	5	5	5	5.7
	Simulation length [s]	175	110	360	695
	Dump stem [s]	5	5	5	5
	Density [kg/m^3]	2000	2000	2000	2000
	ξ [m/s^2]	200	300	300	200
	μ [-]	0.15	0.20	0.11	0.13
	Obstacle/Dam used	No	No	Yes	No
Release parameter	Volume released [m^3]	1100	70	5600	450
	Qmax [m^3/s]	34	3.4	97	16
	t1 [s]	3	1	3	2
	v [m/s]	6	5	10	6
	t2 [s]	64.7	41.2	115.5	56.3

Personal Declaration

I hereby declare that the submitted thesis is the result of my own, independent work. All external sources are explicitly acknowledged in the thesis.

Sursee, 23.04.2021 Manuel Studer